DEVELOPMENT OF ELECTROCHEMICAL AND COLORIMETRIC METHODS USING INORGANIC NANOMATERIALS FOR DETECTION OF BIOLOGICAL AND ENVIRONMENTAL COMPOUNDS

Miss Chanika Pinyorospathum

A Dissertation Submitted in Partial Fulfillment of the Requirements
for the Degree of Doctor of Philosophy in Chemistry
Department of Chemistry
Faculty of Science
Chulalongkorn University
Academic Year 2018

การพัฒนาวิธีเชิงเคมีไฟฟ้าและเชิงสีโดยใช้วัสดุระดับนาโนเมตรอนินทรีย์สำหรับการตรวจวัดสารเชิงชีวภาพและเชิงสิ่งแวดล้อม

น.ส.ชนิกา ภิญโญรสปทุม

วิทยานิพนธ์นี้เป็นส่วนหนึ่งของการศึกษาตามหลักสูตรปริญญาวิทยาศาสตรดุษฎีบัณฑิต
สาขาวิชาเคมี ภาควิชาเคมี
คณะวิทยาศาสตร์ จุฬาลงกรณ์มหาวิทยาลัย
ปีการศึกษา 2561

Thesis Title	DEVELOPMENT OF ELECTROCHEMICAL AND COLORIMETRIC METHODS USING INORGANIC NANOMATERIALS FOR DETECTION OF BIOLOGICAL AND ENVIRONMENTAL COMPOUNDS
By	Miss Chanika Pinyorospathum
Field of Study	Chemistry
Thesis Advisor	Professor Dr. ORAWON CHAILAPAKUL

Accepted by the Faculty of Science, Chulalongkorn University in Partial Fulfillment of the Requirement for the Doctor of Philosophy

..... Dean of the Faculty of Science

(Professor Dr. POLKIT SANGVANICH)

DISSERTATION COMMITTEE

..... Chairman

(Associate Professor Dr. VUDHICHAI PARASUK)

..... Thesis Advisor

(Professor Dr. ORAWON CHAILAPAKUL)

..... Examiner

(Associate Professor Dr. NATTAYA NGAMROJANAVANICH)

..... Examiner

(Dr. JANJIRA PANCHOMPOO)

..... External Examiner

(Associate Professor Dr. Weena Siangproh)

ชนิกา ภิญโญรสปทุม : การพัฒนาวิธีเชิงเคมีไฟฟ้าและเชิงสีโดยใช้วัสดุระดับนาโนเมตรอนินทรีย์สำหรับการตรวจวัดสารเชิงชีวภาพและเชิงสิ่งแวดล้อม. (DEVELOPMENT OF ELECTROCHEMICAL AND COLORIMETRIC METHODS USING INORGANIC NANOMATERIALS FOR DETECTION OF BIOLOGICAL AND ENVIRONMENTAL COMPOUNDS) อ.ที่ปรึกษาหลัก : ศ. ดร.อรวรรณ ชัยลภากุล

งานวิจัยฉบับนี้ประกอบด้วย 2 ส่วน ได้แก่ (1) การปฏิบัติการบนกระดาษร่วมกับการตรวจวัดทางเคมีไฟฟ้าสำหรับซี-รีแอคทีฟโปรตีนและการตรวจวัดเชิงสีสำหรับฟอสเฟตไอออน (2) การพัฒนาเทคนิคโครมาโทกราฟีและการประยุกต์ โดยแต่ละส่วนสามารถแบ่งออกเป็น 2 งาน สำหรับการปฏิบัติการบนกระดาษในส่วนแรกคือเซ็นเซอร์เคมีไฟฟ้าที่ถูกสร้างขึ้นด้วยฟอสโฟริลโคลีนบนอนุภาคทองระดับนาโนเมตรที่ถูกสะสมด้วยเคมีไฟฟ้าบนขั้วไฟฟ้าพิมพ์สกรีนคาร์บอนสำหรับตรวจวัดซี-รีแอคทีฟโปรตีน สัญญาณของสารละลายเฟอร์ไรไซยาไนด์ลดลงแบบเส้นตรงเมื่อความเข้มข้นซี-รีแอคทีฟโปรตีนเพิ่มขึ้นในช่วง 5.0 ถึง 5000 ไมโครกรัมต่อลิตร โดยขีดจำกัดการตรวจวัดจากการคำนวณเท่ากับ 1.60 ไมโครกรัมต่อลิตร ในส่วนที่สองของการปฏิบัติการบนกระดาษคือการตรวจวัดเชิงสีสำหรับฟอสเฟตไอออนบนกระดาษ โดยใช้แพลตของเงินระดับนาโนเมตรที่ดัดแปรด้วย 2-เมอร์แคปโทมีเทนซัลโฟเนต ซึ่งการเปลี่ยนแปลงสีอาศัยกลไกการต่อต้านการรวมตัวระหว่างแพลตของเงินระดับนาโนเมตรที่ถูกดัดแปรและไอออนยูโรเพียม อุปกรณ์ฐานกระดาษนี้สามารถตรวจวัดสีด้วยตาเปล่าจากการเปลี่ยนแปลงสีม่วงไปเป็นสีชมพูเมื่อความเข้มข้นฟอสเฟตเพิ่มมากขึ้น ช่วงความเป็นเส้นตรงและขีดกำจัดการตรวจวัดอยู่ในช่วง 1.0 ถึง 30 มิลลิกรัมต่อลิตรและ 1.0 มิลลิกรัมต่อลิตร ตามลำดับ สำหรับการพัฒนาเทคนิคโครมาโทกราฟีและการประยุกต์นั้น งานวิจัยส่วนแรกคือการแยกยาฆ่าแมลงที่สำคัญ 4 ชนิด ได้แก่ ไดโนทีฟูราน ไธอะมีโทแซม โคลไทอะนิดิน และ อิมิดาคลอพริด โดยใช้อัลตราไฮเพอร์ฟอร์แมนซ์ลิควิดโครมาโทกราฟีร่วมกับการตรวจวัดด้วยเทคนิคแอมเปอร์โรเมตรี การแยกเสร็จสมบูรณ์ภายใน 8 นาทีโดยใช้โครมาโทกราฟีแบบผันกลับ สัญญาณการวิเคราะห์เพิ่มขึ้นเมื่อใช้อนุภาคทองแดง-ทองระดับนาโนเมตรจากการสะสมด้วยเทคนิคเคมีไฟฟ้า พบว่าขีดจำกัดและช่วงความเป็นเส้นตรงในการวิเคราะห์ของยาฆ่าแมลงที่สำคัญทั้ง 4 ชนิดอยู่ในช่วง 0.19 ถึง 0.62 มิลลิกรัมต่อลิตรและ 1.0 ถึง 250 มิลลิกรัมต่อลิตร ตามลำดับ งานวิจัยส่วนที่สองคือการแยกกรดอะมิโนโดยใช้โครมาโทกราฟีแบบท่อเปิด สัญญาณกระแสไฟฟ้าถูกตรวจวัดบนขั้วไฟฟ้าทองแดง ซึ่งการแยกของกรดอะมิโนขึ้นอยู่กับความแตกต่างของสัมพรรคภาคโดยการแลกเปลี่ยนประจุระหว่างหมู่เอมีนจตุรภูมิบนเรซินและกรดอะมิโน การตรวจวัดสัญญาณทางเคมีไฟฟ้าเกิดจากปฏิกิริยาออกซิเดชันของทองแดงเป็นสารประกอบเชิงซ้อนระหว่างทองแดงกับกรดอะมิโน วิธีการที่พัฒนาขึ้นมีขีดการจำกัดการตรวจวัดที่ 0.42 มิลลิกรัมต่อลิตร นอกจากนี้วิธีที่นำเสนอมาทั้งหมดนั้นง่าย รวดเร็ว และมีราคาย่อมเยา โดยสามารถนำไปประยุกต์ใช้ในตัวอย่างจริง ได้แก่ สารบ่งชี้ทางชีวภาพ สิ่งแวดล้อม และอาหาร

สาขาวิชา	เคมี	ลายมือชื่อนิสิต .....
ปีการศึกษา	2561	ลายมือชื่อ อ.ที่ปรึกษาหลัก .....

5672807023 : MAJOR CHEMISTRY

KEYWORD: copper nanocomposites, silver nanoplates, chromatography, paper-based analytical devices, C-reactive protein, neonicotinoids, amino acids

Chanika Pinyorospathum : DEVELOPMENT OF ELECTROCHEMICAL AND COLORIMETRIC METHODS USING INORGANIC NANOMATERIALS FOR DETECTION OF BIOLOGICAL AND ENVIRONMENTAL COMPOUNDS. Advisor: Prof. Dr. ORAWON CHAILAPAKUL

This research comprised of 2 parts including (1) lab-on-paper coupled with electrochemical method for C-reactive protein and colorimetric detection for phosphate ions and (2) the development of chromatographic techniques and its applications. In each part, it can be classified in 2 works. The first work of lab-on-paper is the electrochemical sensor that was fabricated from phosphorylcholine assembled electrodeposited gold nanoparticles onto screen-printed carbon electrode for C-reactive protein detection. Current of ferrocyanide decrease linearly when increase C-reactive protein concentration from 5.0 – 5000 μg L^{-1}. The calculated detection limit equals 1.60 μg L^{-1}. The final part of lab-on-paper is the colorimetry on paper for phosphate ions using 2-mercaptoethanesulfonate modified silver nanoplates. The color changes rely on anti-aggregation mechanism of modified silver nanoplates and europium ions. The paper-based analytical device can use the naked-eye for detection from purple color changing to pink when increase phosphate concentration. The linearity and detection limit are in the range of 1.0 – 30 mg L^{-1} and 1.0 mg L^{-1}, respectively. For the development of chromatographic techniques and its applications, the first part is the separation of 4 important insecticides; dinotefuran, thiamethoxam, clothianidin, and imidacloprid using ultra-high-performance liquid chromatography coupled with amperometry detection. The complete separation was finished within 8 minutes using reverse-phase chromatography. The analytical signals increase when employing electrodeposited copper-gold nanoparticles. The detection limit and linear range of 4 significant insecticides were in the range of 0.19 – 0.62 mg L^{-1} and 1.0 – 250 mg L^{-1}, respectively. The second work is the separation of amino acids using open tubular liquid chromatography. The current signals were measured on copper electrode. The separation of amino acids depends on the ion exchange affinity between quaternary amine on the resin and amino acids. The electrochemical detection arises from the oxidation of copper to form complexes between copper and amino acid. The developed method has detection limit of 0.42 mg L^{-1}. Moreover, all presented methods are simple, fast, and inexpensive. The methods are applied in real samples covering food, environmental compounds, and biomarkers.

Field of Study:	Chemistry	Student's Signature .....
Academic Year:	2018	Advisor's Signature .....

ACKNOWLEDGEMENTS

First, I would like to acknowledge my funder, Thailand Research Fund (TRF) through Royal Golden Jubilee Ph. D. Program (RGJ). Without financial support, I would not be blessed with an opportunity to finish the Ph. D. program and oversea research.

I am eternally grateful for the guidance and mental support from my supervisor, Professor Dr. Orawon Chailapakul. I would like to dedicate this dissertation to her attentiveness and encouragements for her students. Also, my monumental appreciation goes to Professor Dr. Purnendu K. Dasgupta from the Department of Chemistry and Biochemistry, The University of Texas at Arlington. Throughout a year in Arlington, I was awarded with life and research experiences. I truly learned the definition of “doing a research and hard-working”.

I would like to thank my colleagues from Electrochemical and Optical Spectroscopy Center of Excellence (EOSCE), Department of Chemistry, Faculty of Science, Chulalongkorn University who always assists me during my Ph. D. study. Their useful comments and suggestions result in the completion of this dissertation. Additionally, I sincerely thank members of Dasgupta’s group (2017) that kindly provide supports during my visitation.

Ultimately, I would like to appreciate my family and friends for their love, understanding, and incredible patience for consecutive six years. Finally, I would like to mention my dogs: Jackson, Panda, and Michael, for their company throughout my writing.

Chanika Pinyorospathum

TABLE OF CONTENTS

LIST OF TABLES

LIST OF FIGURES

LIST OF ABBREVIATIONS

ºC	Degree Celsius
A	Electrode surface area
A	Ampere
AEC	Anion exchange
Ag/AgCl	Silver-silver chloride electrode
AgNP	Silver nanoparticles
AgNPl	Silver nanoplates
Au	Gold
AuNP	Gold nanoparticles
BDDE	Boron-doped diamond electrode
C	Concentration
Ca	Calcium
C_{dl}	Interface capacitance
CE	Counter electrode
CEX	Cation exchange
CLO	Clothianidin
C_m	centimeter
COP	Cycloolefin polymer
CRP	C-reactive protein
Cu	Copper
Cu^{2+}	Copper ions
CuNP	Copper nanoparticles
CV	Cyclic voltammetry
CV	Coefficient of variation
D	Diffusion coefficient
DIN	Dinotefuran
DLS	Dynamic light scattering
DP	Degree of polymerization

DPV	Differential pulse voltammetry
E	Potential
E_0	Standard reduction potential
EIS	Electrochemical impedance spectroscopy
E_p	Peak potential
Eu^{3+}	Europium ions
F	Faraday's constant
Fe^{2+}	Ferrous ions
Fe^{3+}	Ferric ions
FIA	Flow injection analysis
fmol	femtomole
FT-IR	Fourier transform infrared spectroscopy
G	gram
Gpa	Gigapascal
H	Theoretical plates height
H	Hour
H_2SO_4	Sulfuric acid
H_3O^+	Hydronium ions
HCl	Hydrochloric acid
HPLC	High-performance liquid chromatography
Hz	Hertz
I	Current
i.d.	Inner diameter
IC	Ion chromatography
IMD	Imidacloprid
k'	Capacity factor
KCl	Potassium chloride
kDa	Kilodalton
kg	kilogram
KNO_3	Potassium nitrate
L	Column length

L	Liter
LOD	Limit of detection
LOQ	Limit of quantification
M	Molar
min	Minute
mL	Milliliter
mm	millimeter
mM	Millimolar
MS	2-mercaptoethanesulfonate
MW	Molecular weight
n	Number of electrons
n	Number of repetitions
N	Theoretical plates number
NaOH	Sodium hydroxide
n_c	Peak capacity
ng	nanogram
nL	nanoliter
nM	Nanomolar
nm	Namometer
OTIC	Open tubular ion chromatography
OTLC	Open tubular ion chromatography
PAD	Paper-based analytical device
PC	Phosphorylcholine
PDI	Polydispersity index
Pi	Phosphate ions
pmol	picomole
ppm	Parts per million
psi	Pounds per square inch
R	Resistance
R	Resolution
r^2	Coefficient of determination

R_{ct}	Charge transfer resistance
RE	Reference electrode
RGB	Red-Green-Blue
rpm	Revolutions per minute
R_s	Solution resistance
RSD	Relative standard deviation
s	Second
S	Sulphur
S/cm	Siemens per centimeter
S/N	Signal-to-noise ratio
SD	Standard deviation
SEM	Scanning electron microscopy
SPCE	Screen-printed carbon electrode
SPR	Surface plasmon resonance
T	temperature
TEM	Transmission electron microscopy
THM	Thiamethoxam
t_m	Void time
t_r	Retention time
u	Flow rate of mobile phase
u-HPLC	Ultra-high-performance liquid chromatography
UV-vis	UV-Visible spectrophotometry
v	Scan rate
V	Volt
V	Volume
v_r	Retention volume
W	Peak width
WE	Working electrode
Z	Impedance
α	Transfer coefficient
µg	Microgram

µL	Microliter
µM	Micromolar
µm	Micrometer
Ω	Ohm

CHAPTER I
INTRODUCTION

1.1. Introduction

The study of analytical chemistry focusses on equipment and protocol for separation, identification, and determine the concentration of analytes. In some cases, the analysis requires a combination of two or more methods. For example, separation is responsible for the isolation and identification of target analytes, and monitoring the analytical signals are used to determine the analyte concentration. Analytical methods are classified into two categories, namely qualitative analysis, and quantitative analysis. The qualitative analysis concentrates on the identification of compounds and informs their presence or absence, but not the amount of compounds. By contrast, quantitative analysis determines the quantities of analytes those present in a substance. The analytical signals such as absorbance, conductivity, electron transfer, etc. can use for the quantitative purpose. The development of analytical methods benefits in various research fields including environmental analysis, clinical analysis, bioanalysis, forensic science, etc. The important consideration is to balance between the performance (sensitivity, selectivity, dynamic range, accuracy, precision) and the operating cost (instruments, materials, personal training, procedure time). For instance, optical and mass spectrophotometry is universal and widespread for chemical analysis. The methods can directly assess the information at an atomic level with high sensitivity; however, the complicated and costly instruments limit their applications for on-site detection and a circumstance which fast analysis is indispensable. Another interesting approach is the electrochemical method which is extremely useful as it provides both qualitative and quantitative data. The bulky instrumentations can be miniaturized into portable device that facilitate on-site applications; however, the technique is limited by the sensitivity. Fortunately, the electrode surface can be chemically modified by metal nanoparticles, and satisfactory detection limit is achieved encouraging the development of novel electrochemical methods. Additionally, color detection can employ for quick analysis of compounds and provide both qualitative and quantitative information by observing colors change and the series of color without the expensive equipment and materials. Nevertheless, the sensitivity is control by the chemical structure and interaction between the color compound and analytes. This method may offer a relatively rapid and low-cost analysis, but the performance does not meet the requirement in highly sensitive applications. Therefore, new colorimetric

methods have emerged using metal nanoparticles with exceptional optical properties as the colorimetric probe to enhance the detection capability.

Lab-on-paper is an appealing analytical method that constitutes all detection steps including sorting, mixing, and detecting in a single paper substrate. Paper is an abundant and inexpensive material suitable for the fabrication of portable and on-site detection devices that small, readily, and easy-to-use in the resource-limited area. The patterns for analytical purposes (typically reagent zone and detection zone) can be created on paper using simple fabrication methods such as inkjet printing or wax printing. Moreover, the unique characteristics of paper including the functional group, capillary force, and porosity provides the solution for grafting, transporting, and storing inside the paper substrate, respectively. The remarkable features are the consequences of the development of the analytical method on paper substrate. Lab-on-paper can be equipped with both electrochemical and colorimetric methods as the complementary technique for disposable, fast, and accurate platform of metals, environmental analytes, biomarkers, etc.

In the application of lab-on-paper to electrochemical assay, adding a part of a screen-printed electrode to the paper is effortlessly, but the hampering analytical signal is the problem. Providentially, the metal electrodeposition is associated with the electrochemical techniques offering the opportunity for the facile synthesis of metal nanoparticles onto the electrode surface. Nanoparticles can enhance the electrode active surface area and supply spacious sites for redox reactions. Gold nanoparticle (AuNP) is the most common because it is easy to synthesize, and the resulting electrodeposited nanoparticles are usually well-dispersed and homogeneously distributed. Apart from the electronic properties, AuNP can be assembled with thiol-functionally group compounds using chemisorption and a strong thiolate–Au bond is formed. Various imperative recognizing probes have been tethered onto AuNP modified screen-printed electrode and demonstrated for selective and sensitive electrochemical detection of plenty of biomolecules and disease markers. As the mentioned properties, a biomimetic of phospholipid, namely phosphorylcholine functional group polymer (PMPC-SH), was applied on AuNP surface and used for the detection of C-reactive protein in the presence of calcium ion. PMPC-SH can graft on the electrode using thiol moiety from the polymer to the AuNP modified electrode. The electrochemical signals derived from the electron transfer of the electroactive species (ferric cyanide) which inversely proportional to the concentration of C-reactive protein. Both calcium ion and ferric cyanide can be stored in the paper substrate at the reagent zone and transported to the detection zone where the electrochemical measurement was performed using

a modified electrode. This concept represents the integration of the electrochemical method and paper substrate for biomarker analysis.

Colorimetric lab-on-paper is another attractive approach for the development of an analytical method on the paper platform because it has portability, affordability, and simplicity, particularly for a rural area where rapid point-of-care diagnostic is crucial. The expertise and results analysis is not essential as the colors change is reported itself qualitatively and quantitively. Additionally, the photo can be recorded for an extensive analysis in the central laboratory. Abundant porosity in the paper allows chemicals to be collected and traveled through designed channels for the chemical reaction. The colors change is observed at the detection zone usually through the naked eye. The determination of appropriate colorimetric probe and the detection protocol are significant for colorimetric assay. Silver nanomaterials are convincing alternatives because their colors are visible and easily tunable through size and shape. An optical property of silver nanomaterials leads to plenty of diagnostic applications for detection of toxicity from the environment and numerous biomarkers. Silver nanoplates were very attracting because they offer noticeable color changes between aggregation and dispersion state. Moreover, the surface of silver nanomaterials can be modified to improve the selectivity towards the analyte ions. The reaction can perform on the paper platform and the color changes were observed with the naked eye. Because of the attraction of its properties, silver nanoplates can be applied for detection of phosphate ions using the anti-aggregation mechanism among the analyte ions, thiol-modified silver nanoplates, and aggregating agent. The color intensity is related to phosphate concentration uses for quantification of phosphate ions in real samples. Lab-on-paper using colorimetry as the detection method offers advantages such as cost, time, and resource for practical on-site detection.

A chromatographic technique is an ingenious method for isolating the analyte from its matrix and allows for different compounds in the same family to be analyzed. It is necessary to introduce the chromatographic technique for analytes' separation before measuring the analytical signal at the detector because they may possess different properties; such as N,N-dimethyltryptamine (DMT) is a potent hallucinogen, while serotonin is the neurotransmitter. The separation of individual compounds relies on the different interaction between them and the stationary phases packing in the column. The signification parts for the chromatographic method are the stationary phase and the detection. An analytical column should provide for the appropriate separation of mixtures by means of suitable interaction between the compounds and packing particles, and the condition used for the separation. Neonicotinoids family is an example of insecticides which require chromatographic separation prior to detection because their

absorbances and reduction peaks are presented at the same wavelength, and potential, respectively. Different insecticides of neonicotinoids family can separate by ultra-high-performance liquid chromatography. The detection sensitivity is improved using copper-gold nanoparticles modified on a boron-doped diamond electrode. Gold nanoparticles are common electrode modifiers because they can improve the electrical conductivity of the electrode surface. Moreover, some metals can bind with analyte using complexation which increases the analytical signal and detection sensitivity. Copper can form a strong complex with nitro or amine functional group of neonicotinoids. Therefore, the bimetallic nanoparticles of copper and gold can increase the sensitivity for electrochemical detection. Nanoparticles improves not only the detection performance, but also contributes to the separation of amino acids through anion exchange resin. Amino acids are small molecules that require nanobead resin for their separation. Nano-scale materials provide high surface-to-volume ratio and cause the analyte to associate with resins and improve the separation. Typical nanobead resins were functionalized with anion exchange resin such as quaternary amine of assorted numbers of alkyl or aryl groups, hence offers different capabilities for each resin for the separation. The development of chromatographic technique coupled with electrochemical methods using nanoparticles for assisting the detection and separation can promote the analytical assay for important insecticides and amino acids.

In this work, the development of analytical methods is classified into two main parts; lab-on-paper applications (Chapter III), and the development of the chromatographic method and its application (Chapter IV). Lab-on-paper were first developed for C-reactive protein detection employing electrochemistry as the analytical method. Next, the colorimetric paper-based device was purposed for the determination of phosphate ions using modified silver nanoplates as the colorimetric probe. Then, two chromatographic methods with electrochemical detection for insecticides and amino acids were discussed.

1.2. Objectives of the research

(1) To develop lab-on-paper coupled with electrochemical detection using phosphorylcholine functionalized gold nanoparticles electrodeposited electrode for C-reactive protein detection and colorimetric detection using thiol-modified silver nanoplates for phosphate ions detection

(2) To develop chromatographic techniques coupled with electrochemical detection using metallic nanoparticles modified electrode for neonicotinoids detection and quaternity amine nanobead resin for amino acids separation

1.3. Scope of the research

To follow the first objective of this dissertation, the patterns of lab-on-paper were designed. To obtain sensors' best performance, optimal conditions such as reagent concentration, pH, and reaction time were investigated and followed by the study of analytical performances. Afterward, effects from interferences those expected in samples were examined. Ultimately, the sensors were demonstrated for quantification of target analytes in real samples. For the second objective, the chromatographic separation was developed. Experimental conditions for the separation including mobile phase concentration, flow rate, injection volume, and pH were optimized. Next, the effect of applied potential was studied. Then, linearity, detection limit, limit of quantification, stability, and reproducibility were determined. Finally, the developed lab-on-column methods were applied to real samples.

The following chapter begins with important theory in this dissertation. Chapter III discloses sensors development on PAD for Pi and CRP. Chapter IV discusses the analytical methods for separation and detection of neonicotinoid and amino acid, respectively. Finally, the conclusions and future perspective are summarized in chapter V.

CHAPTER II

THEORY

In this chapter, the important theories of lab-on-paper, electrochemical methods, colorimetric methods, nanomaterials, and column chromatography are explained.

2.1. Lab-on-paper

Microfluidic technology receives tremendous attentions because the method development is useful and practical for wide applications. The technology relies on the management of flow (in microliter scale) in the network microchannels and develops for the miniaturized the laboratory scale into a single microfluidic device. Paper is an interesting substrate because it can filter particles or analytes from the interferences using its wettability and porosity. Lab-on-paper or paper-based analytical devices (PAD) is one of the microfluidic technologies employing paper as the substrate. Microchannel on PAD is fabricated by creating hydrophobic zone on the paper. The method is cheap, fast, and no skillful personal needed. The fabrication is also accessible in the developing country. There are several methods for the fabrication including wax printing, inject printing, photolithography, laser treatment, and plasma treatment. Reagents are dropped on PAD and retained in the cellulose fiber, then samples are added and detected at the test zone. Plenty of detection techniques are incorporated with PAD including electrochemistry, colorimetry, surface plasmon resonance, and fluorescence. The advantages of PAD are small reagents and samples consumption, inexpensive platforms, and portable.

Figure 2.1 Photo of PAD fabricated by wax-printing methods

2.2. Electrochemical methods

Electrochemistry method is a branch of analytical methods that measures current, charge, or potential from an electrochemical cell as an analytical signal. The principle was adopted for universal instruments such as potentiometric pH meter, glucose sensors, and gas sensors. However, electrochemical method is not widely used as a spectrophotometric method. It is difficult to perform automation and require routine calibration, but the instrumentation is relatively inexpensive. The method also allows for ions speciation, for example, ferro ions (Fe^{2+}) and ferric ion (Fe^{3+}) have different detection potential. Moreover, information of kinetic activity of chemicals can be studied. Principles of electrochemical method are simplified in the following sections.

2.2.1. Principles

Electrochemical methods measure analytical signal from the conductivity of dissolved ions. The signals are proportional to analytes concentration. There are two major methods in electrochemistry. First, bulk methods which the whole solutions' conductivity is measured, for example, the pH measurement using glass membrane electrode. Second is the interfacial methods which the analytical signals are derived from the phenomena occurring at the electrode interface and the solution that surrounded that electrode.

The interfacial methods are divided into static and dynamic methods. In static methods, there are no current passes between electrode; therefore, the concentration of species in the electrochemical cell remains unchanged. Potentiometry is an example of the static methods which concentration of ions is measured under static condition. The discussion of potentiometric methods can be found in section 2.2.4. Another interfacial method is dynamic methods which most of the electrochemical detection methods are developed. The classes of the interfacial methods are controlled current and controlled potential. Both methods change the concentration of species in the cell by passing current/potential to the electrochemical cell and the resulting signals are measured for their quantification. The controlled potential methods are subdivided by the means of varying or having fix potential. The method which fixes the potential and observed the current from the cell is called amperometry, while another method of variable potential is called voltammetry. The applying potential can be done by scanning the potential linearly with time or adding pulse wave while scanning. Voltammetry is considered as an important branch of electrochemistry and separately discussed in section 2.2.5. The summary of interfacial methods is shown in Figure 2.2.

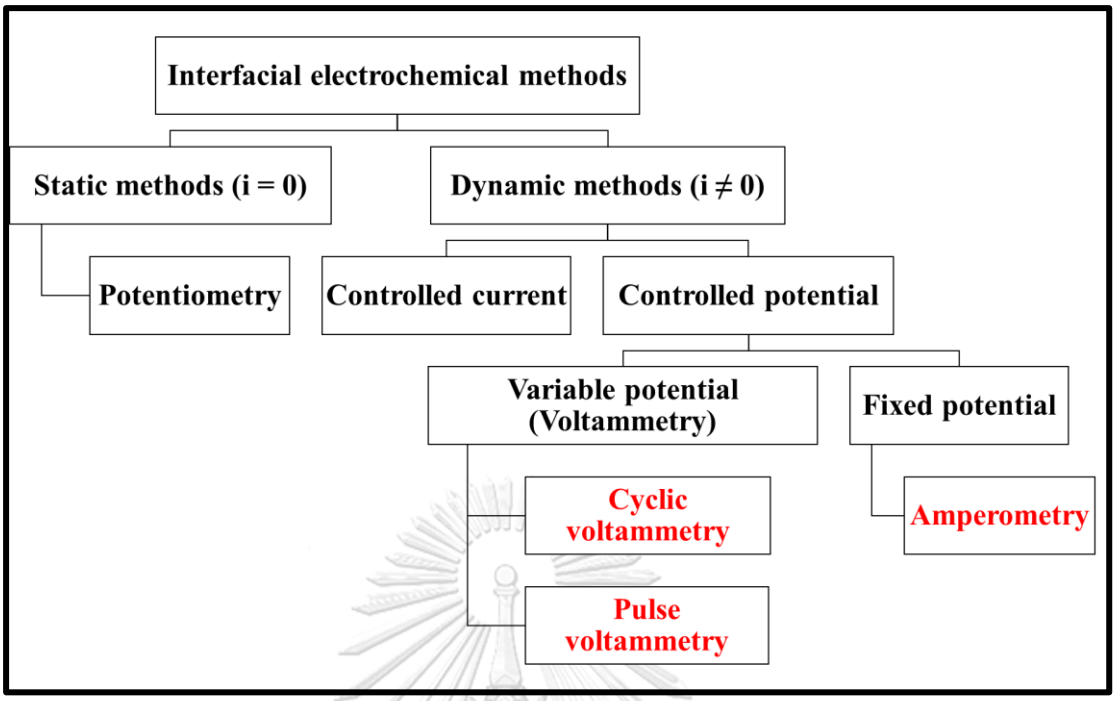

Figure 2.2 Family tree highlighting several interfacial electrochemical techniques. The specific techniques are shown in red.

2.2.2. Basic components of electrochemical instrumentations

The simplest electrochemical cell is present with two electrodes. The analytical signal (potential or current) is measured through the working or indicator electrode in which sensitive to the concentration of ion species. The analytical signal is measured with respect to a reference potential provided by a counter electrode. Another responsibility of this electrode is to complete the circuit. The ideal counter electrode should provide constant potential throughput the experiment so that the changing of current is solely resulting from the reaction at the working electrode. However, the passing of current through the electrode is fluctuating as analyte's concentrations changing in the dynamic methods. The counter electrode is replaced with two electrodes; reference electrode and auxiliary electrode, to address this problem. The constant potential is provided by the reference electrode and no current is flowed through, while the auxiliary electrode serves to complete the circuit and allows the current to flow. This configuration of the three electrodes is called a three-electrode system and widely used in the electrochemical cell of the dynamic methods with some exception when there is negligible current flow through the electrochemical cell.

2.2.3. Basic experimental designs

The electrochemical methods are designed based on Ohm's law that the measured potential (E) equals to the current (i) passing through the resistor of a circuit's resistance (R).

$$E=iR \qquad (1)$$

There are simple three experiment designs including (1) Under the static condition where there is no current flow, the potential is measured, under the dynamic conditions (2) the potential is measured while the current is controlled, and (3) the current is measured while the potential is controlled. Each of the designs required different instrumentation. The following section explains the principles and electrical circuit of different electrochemical methods.

2.2.4. Potentiometric methods

Potentiometric method measures the potential of the analyte species through the working electrode without the flow of currents. This method is useful for quantification purpose; however, the application was limited to the analysis of a few ions on metallic electrode. The discovery of glass membrane electrode in 1909 leads to the fabrication of glass pH electrode which is the breakthrough of potentiometry for quantification of H_3O^+ concentration. In this electrochemical cell, there are two reactions chamber (see Figure 2.3) connected by a salt bridge.

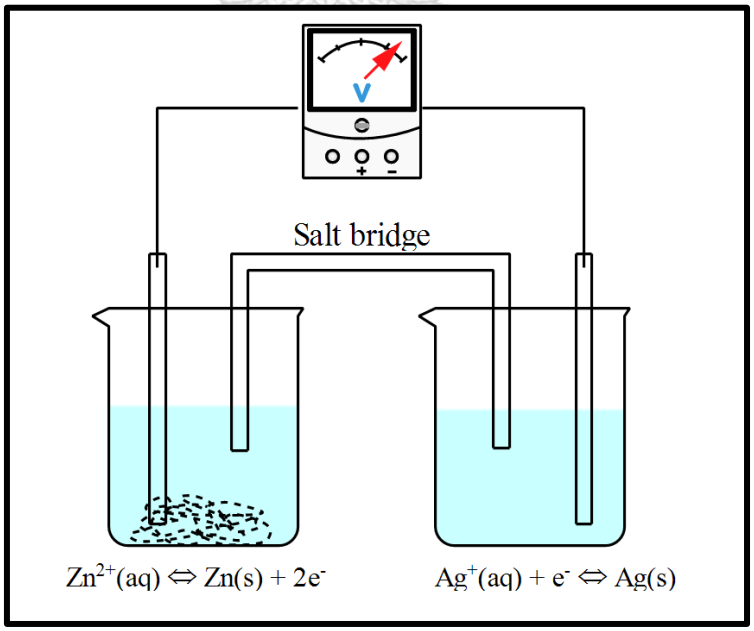

Figure 2.3 In this standard cell, the half-cells are separated; electrons can flow through an external wire and become available to do electrical work.

The first chamber designated on the left is where the oxidation is occurring at the anode and the second chamber on the right is where the reduction is occurring at the cathode. The Nernst equation below shows the mathematic expression for the relationship between oxidizing and reducing species.

$$E = E° - \frac{0.0592}{n} \ln Q \quad (2)$$

Where E is the electrode's potential

E° is the standard reduction potential

n is the number of electrons transfer

Q is the quotient of the redox reaction

The equation is valid if the experiment is carried out in typical laboratory (room temperature = 25 °C). The overall potential of the electrochemical cell (E_{cell}) equals to

$$E_{cell} = E_{cathode} - E_{anode} \quad (3)$$

Where $E_{cathode}$ is the potential at cathode

E_{anode} is the potential at anode

The simple circuit is shown below

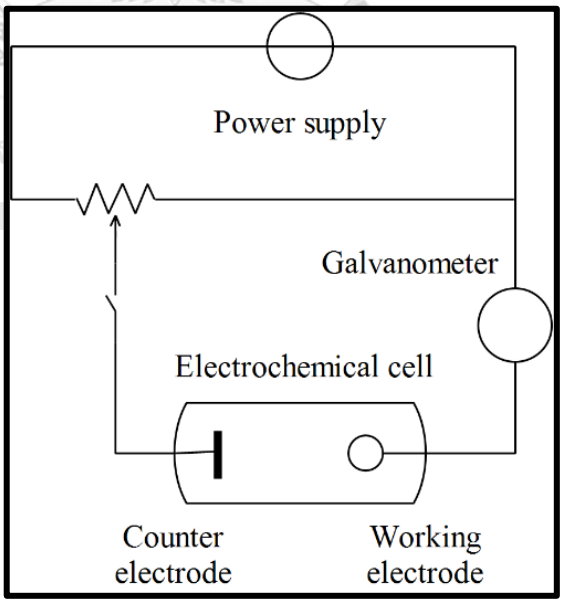

Figure 2.4 Schematic diagram of a manual potentiometer

This method applies for galvanic cell and generally combine with titration technique for determination of analyte concentration, this assay is called potentiometric titration.

2.2.5. Voltammetric methods

Voltammetry relies on the relationship between applied potential and measured current. In a three-electrode system, a time-dependent potential is given to the electrolytic cell, and the resulting current is collected. The obtained signal is concentration-dependent manner; therefore, it is suitable for analyte quantification. The working electrode of voltammetry should be easily polarized, or small such as micro-electrode. The earliest voltammetry has mercury drop as the working electrode, and the method is occasionally referred as polarography. There are two phenomena occurring when the current is flowing within the complete voltemmetric circuit; ohmic potential and polarization effect, which should be eliminated or minimized.

2.2.5.1. Ohmic potential or IR drop

Ohmic potential occurs naturally in the circuit where there is current flowing through. In the electrolytic cell, the reaction requires higher driving potential than the calculated cell potential. In galvanic cell, the cell potential is reduced to

$$E_{cell}=E_{cathode}-E_{anode}+E_{junction}-IR_{drop} \quad (4)$$

Where $E_{junction}$ is the liquid junction potential

IR_{drop} is the ohmic drop in the circuit.

The micro-scale working electrode where there is trivial flow of current, IR_{drop} is somewhat negligible.

2.2.5.2. Polarization effect

The potential obtained from the electrochemical cell is deviated from the calculated potential because of the polarization effect. There are two types of polarization including concentration polarization and kinetic polarization or overvoltage. The relationship between current and potential is non-linear after a large amount of current involved in the circuit, the phenomena is called polarization. Therefore, excess applied potential is required for redox reaction to occur. Factors that affect the polarization are size, shape, electrode material, electrolytes, temperature, convection, current quantity, and states of species in the solution. The control of experimental conditions and calibrating the system with standard can eliminate some of the factors.

Concentration polarization is occurred when the diffusion rate from the bulk solution to the electrode surface is less/more than the rate of electrochemical reduction (assuming the analyte species reduce on the electrode surface). This effect is minimized by stirring the solution

or reducing the different between concentration of the bulk and interface solution. There are three mechanisms of mass transportation.

(1) Diffusion is defined as the movement of species to balance to concentration throughout the solution. The species move from higher concentration to lower concentration and diffusion current (i_d) is occurred.

(2) Electrostatic force or migration occurs when there is charged species in the solution move to the surface of the electrode due to attraction/repulsion and generates migration current (i_m). i_m approach zero when the solution is overwhelmed with ions of electrolyte with respect to analyte ions.

(3) Any mechanical force applied to the solution can generate convection current (i_c) and reduced the effect of polarization.

The concertation of analytes is described with Nernst-Plank equation below.

$$J_{(x,t)} = -\left[D\left(\frac{\partial C_{(x,t)}}{\partial x}\right)\right] - \left[\left(\frac{zF}{RT}\right) DC_{(x,t)}\right]\left(\frac{\partial \phi}{\partial x}\right) + C_{(x,t)} V_{x\,(x,t)} \quad (5)$$

Where J is the flux

D is the diffusion coefficient

C is the concentration of the species

ϕ is the electrostatic potential

v_x is the hydrodynamic velocity

In electrochemistry, the experiment can be designed so that the measurement of current from the electrochemical cell is in concentration-dependent manner by performing in the excess ions of supporting electrolyte and quiet solution. The above equation can simplify into

$$i_t = nFAD\left(\frac{\partial C_i}{\partial x}\right)\Big|_{x=0} \quad (6)$$

Where A is the surface area of the electrode

From the equation above, the cells' current is related to the analyte diffusion or analyte concentration only.

Kinetic polarization or overvoltage is the excess voltage that provided to the electrochemical circuit so that the reaction would occur. The kinetic of the redox reaction on both cathode and anode is slow; therefore, the extra potential is added to speed up the

electrochemical reaction. There are many reasons for the overvoltage such as current density, temperature, and electrode material. The reference electrode is introduced to measure the current analogously with the working electrode. There are various of options, for example calomel electrode, hydrogen electrode, silver-silver and chloride electrode.

There are plenty of methods used for applying the potential to the electrochemical cell. In the following sections discuss only the methods employed in this dissertation.

2.2.5.3. Amperometry

When applying constant potential (more than reduction potential of the electrochemical cell) to the system, the diffusion current is directly proportional with the concentration of species. This principle employs for quantification, particularly for titration and flow-analysis detection. In flow-analysis system where the solution is continuously flow through the electrochemical cell, the current is monitored as a function of time. The total current recorded is the sum of background current (obtain from the supporting electrolyte) and current of the analyte. The total current is increased with the concentration of analytes as shown in Figure 2.5A. In chromatography, different analytes are eluted with time and the results are obtained as peaks in Figure 2.5B.

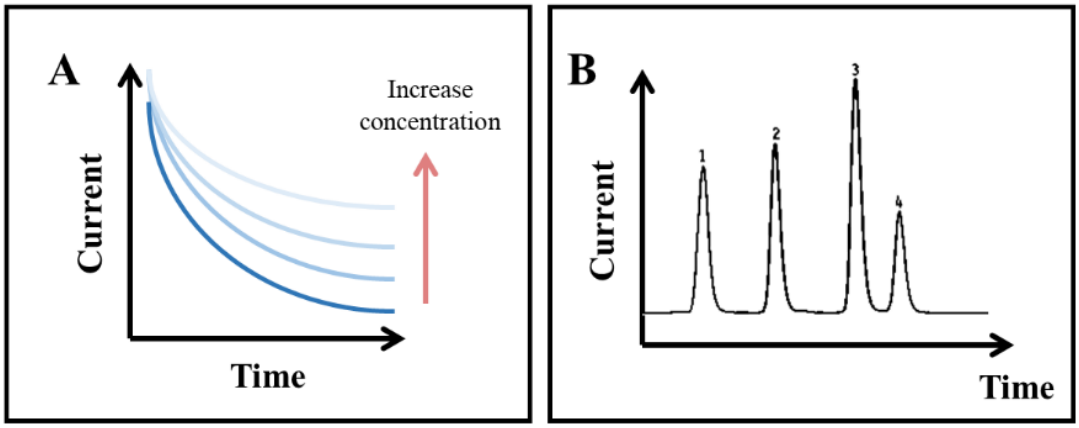

Figure 2.5 voltammograms of amperometry (A) and chromatogram using amperometry as the detection method (B)

2.2.5.4. Cyclic voltammetry (CV)

CV is used suitable for kinetic study and qualitative analysis of the electroactive species. The potential is scanned linearly from V_1 to V_2 and revered the scan (Figure 2.6A), while the current is monitored as a function of potential (Figure 2.6B). The voltammogram shows one full cycle (reversible), half cycle (quasi-reversible), or other results (i.e. irreversible) according to

the redox behavior of the species. The cyclic voltammogram in Figure 2.6B is an example of a reversible reaction. The significant parameters were peak potential (E_p) and peak current (i_p). For reduction, the peak potential and peak current is called cathodic peak potential (E_{pc}) and cathodic peak current (i_{pc}), respectively. By contrast, they are called anodic peak potential (E_{pa}) and cathodic peak current (i_{pa}) for the oxidation. In the reversible reaction, the electron transfer and the peak separation (ΔE_p) equals to

$$\Delta E_p = \left| E_{pa} - E_{pc} \right| = 2.303 \frac{RT}{nF} \quad (7)$$

Where R is the gas constant

T is the temperature

n is the number of electron transfer

F is Faraday's constant.

From the equation ΔE_p should be ca. 60 mV for one electron transfer at typical laboratory condition (T = 25 °C), and ΔE_p is greater than 60 mV in case of irreversible reaction. Using the Randles-Sevcik equation, the measured current can be related to the concentration.

$$i_p = 2.686 \times 10^5 n^{3/2} A C_o D^{1/2} v^{1/2} \quad (8)$$

Where i_p is the peak current (A)

n is the number of electrons

A is the electrode surface area (cm^2)

C_o is the concentration of species (mol cm^{-3})

D is the diffusion coefficient (cm^2 s^{-1})

v is the scan rate (V s^{-1})

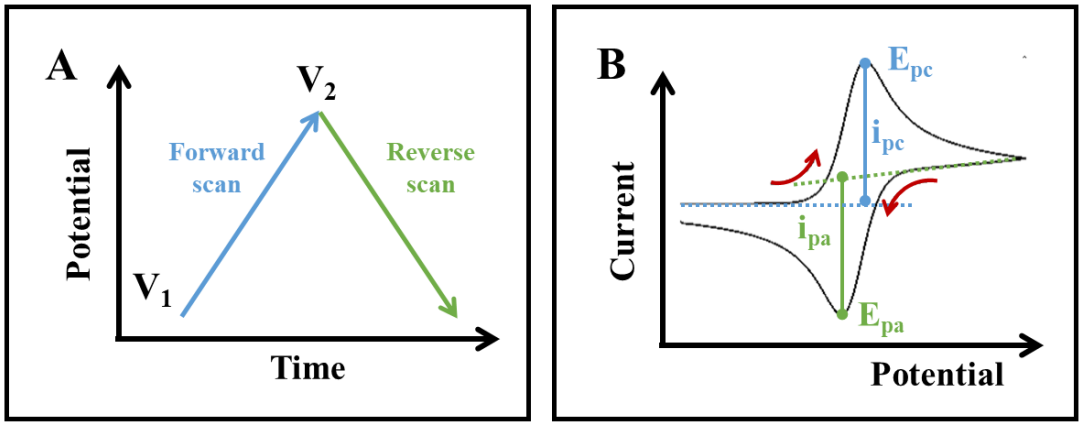

Figure 2.6 Cyclic voltammogram waveform (A) and cyclic voltammogram (B)

2.2.5.5. Differential pulse voltammetry (DPV)

In pulse voltammetry, the potential is applied as waveforms to increase speed and enhance the sensitivity. In DPV, the potential is scanned with a series of pulse (Figure 2.7A) and the voltammogram is showed as peak(s) (depend on analyte). Currents is measured before applying the pulse (1) and before the end of the pulse (2) to reduce the decay of charging current or nonfaradaic current (current that does not related with electrons transfer of the electrochemical reaction). The different of the current between these points are plot against the applied potential (Figure 2.7B).

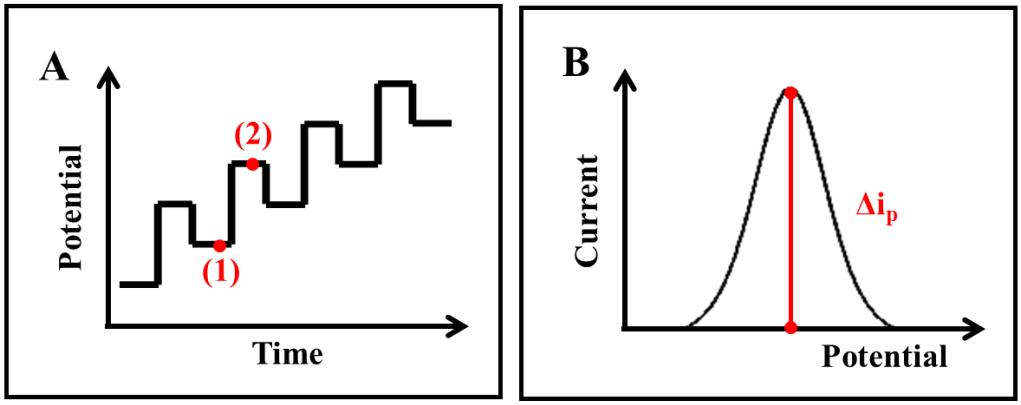

Figure 2.7 Differential pulse waveform (A) where (1) and (2) is the sampling before and after pulse, respectively, and differential pulse voltammogram (B) where Δi_p is the different currents between point (2) and (1).

The typical voltammetric circuit is illustrated in Figure 2..

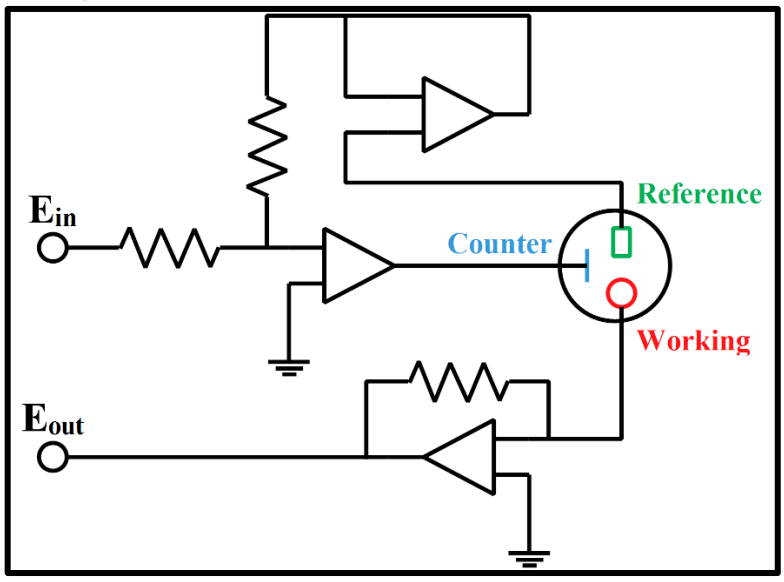

Figure 2.8 Diagram of a typical voltammetry circuit layout.

2.2.5.6. Electrochemical Impedance Spectroscopy (EIS)

Information on the internal dynamic of the system is absent from the voltammeric methods; therefore, an additional electrochemical technique is required for the investigation of electrode surface. ElS measures the resistance (impedance) on the surface of the electrode as a function of applying alternating current (AC) potential. The method is suitable for the studying of morphology after surface treatments such as corrosion and coating. Recently, it has been demonstrated as a useful technique for biosensors and other label-free assays. Impedance is the similar to resistance but account for sinusoidal behavior as well. From Ohm's law, the impedance of the system (Z) equals to

$$Z=\frac{E_t}{i_t}=\frac{E_0\sin(\omega t)}{i_0\sin(\omega t+\phi)}=Z_0\frac{\sin(\omega t)}{\sin(\omega t+\phi)} \quad (9)$$

Where Z_0 is the impedance

ϕ is the phase shift

The equation above can be represented with complex number (equation (10)) by using Eulers relationship in equation (11),

$$\exp(j\phi)=\cos\phi+j\sin\phi \quad (10)$$

$$Z(\omega)=\frac{E}{i}=Z_0\exp(i\phi)=Z_0(\cos\phi-j\sin\phi)=Z'(\omega)-Z''(\omega) \quad (11)$$

The plot of EIS is called Nyquist plot as shown in Figure 2.9A. Usually the data of EIS is represent as the semicircle in which the parameters are related to the circuit in Figure 2.9B.

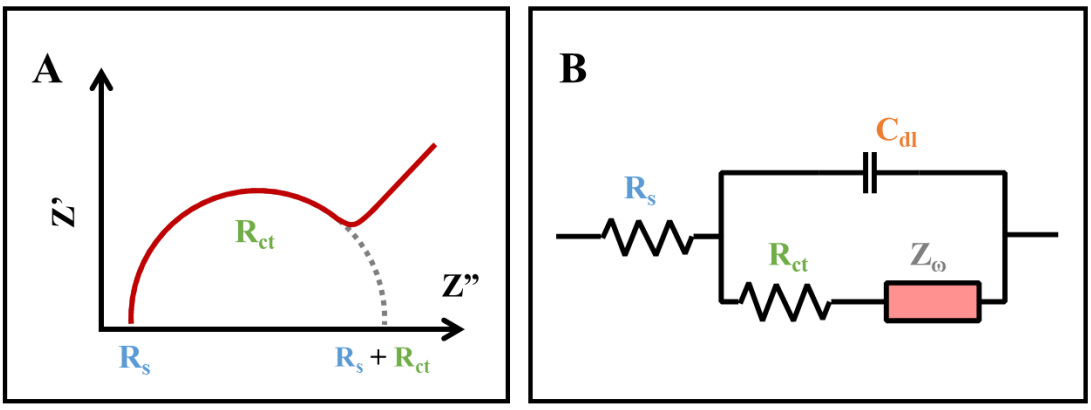

Figure 2.9 Nyquist plot (A) and the responsible circuit (B) where R_s is solution resistance, R_{ct} is charge transfer resistance, Z_ω is Warburg impedance, and C_{dl} is interface capacitance.

The conductivity of the electrode surface is inversely proportional to the semicircle diameter of Nyquist plot.

2.2.5.7. Working electrode

The current measured from the working or indictor electrode immersed in the electrochemical cell is proportional to the concentration of analyte. In this dissertation chemical modified electrodes (CME) were used, except stated, to increase the sensitivity and selectivity of the electrochemical sensors. There are three types of material employed in this work: boron-doped diamond electrode, screen-printed carbon electrode, and copper electrode. The details of CME are discussed with their applications in chapter III and IV.

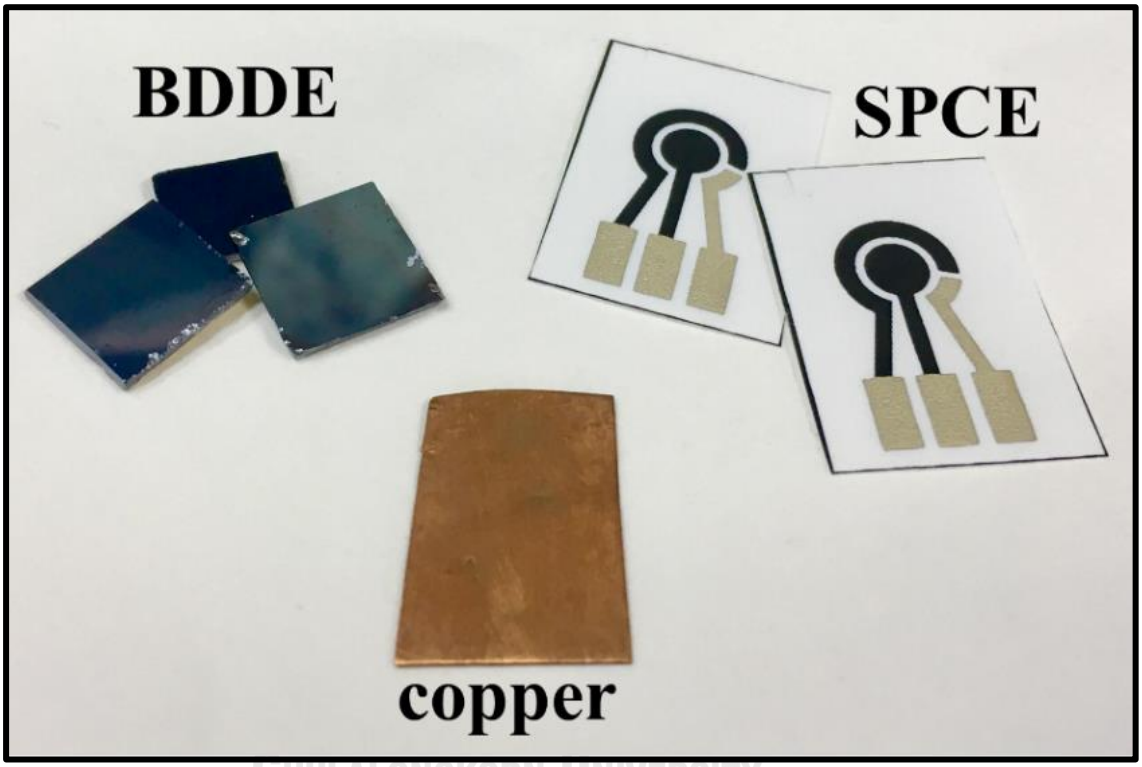

Figure 2.10 Photo of three electrodes including BDDE, SPCE, and copper.

2.2.5.7.1. Boron-doped diamond electrode (BDDE)

Diamond is the hardest gemstone known by far (~90 GPa) and it possesses high thermal conductivity and resistance to chemical corrosion. The gem can be synthesis through chemical vapor deposition (CVD) and their lattice structure can cooperate with boron for a metal-like conductivity materials known as boron-doped diamond (BDD). BDD has nanocrystalline geometry on the surface with a roughness in the nano-scale size which increase the electroactive surface area of the material. BDD has several advantages including the wide operating potential window (>2 V), low background current, and reduced fouling. Some drawbacks of BBD are such as low electrocatalytic activity; therefore, nanoparticles were modified on the surface to increase sensitivity for the electrochemical detection.

2.2.5.7.2. Screen printed carbon electrode (SPCE)

Conducting carbon is inexpensive and interesting materials for a fabrication of the working electrode for the electrochemical sensors because it contains high electrical conductivity. The structure of carbon usually has the conductivity approximately 10-12 S/cm, but with the absence of oxygen or hydrogen the conductivity can increase to ~140 S/cm. Hence, carbon being the most available element on earth is useful to produce conductive materials. Owing to the advantage of screen-printing technique, conducting carbon ink and silver/silver chloride can be screened on the substrates and used as the three-electrode system in voltemmetric methods. Substrates such as plastic, paper, and cloth are selected to reduce the production cost, moreover the fabricated electrode is portable and readily disposable. The surface of carbon is easily chemically modified by decorating high conductive material such as metal nanoparticles or increase their selectivity by grafting specific probe for analyte recognition. Effective but low-cost electrodes were applied for the electrochemical detection of various compound suggested from numerous publications in past two decades. SPCE is interesting indicator electrodes for the development of portable and disposable electrochemical sensors.

2.2.5.7.3. Copper electrode

Copper (Cu) is a transition element with very high thermal and electrical conductivity. Cu can be welded with other metal to form alloy such as brass (copper and mostly zinc (Zn)) and bronze (copper and mostly tin (Sn)) It is important elements for wire and electronics industries. The excellent electronic property of Cu leads to the fabrication of copper electrode for the electrochemical detection such as carbohydrates and amino acids. The electrochemical behavior of Cu is varied in different media, for example Cu is slightly dissolution in the anodic process to copper ions (Cu^{2+}) and some authors report the formation of copper oxides compound on the surface. Cu^{2+} can form stable complexes with amino acids through amine functional groups; therefore, it was suitable working electrode for the electrochemical detection of amino acids.

2.3. Colorimetric methods

Colorimetric method is of late attractive to researchers in different fields since it provides conveniently alternatives for semi-quantitative analysis. The color change of a product is used for the identification of the analyte species and their intensity can benefit for the quantification. Usually, the color can be observed by the naked eye, but instruments for light measurement such as spectrophotometer or colorimeter can increase the capability of the methods. Recently applications i.e. ImageJ, Color Assists, and Adobe Photoshop demonstrate by several groups that they provide reasonable sensitivity for the detection. A general example of colorimetry is red litmus paper in which the color of dyes changes to blue color and the intensity is proportional to the remaining concentration of diprotic acid present in the paper after reacts with base compound in the sample. NO_3^- detection using Griess reagent is an example of colorimetry.

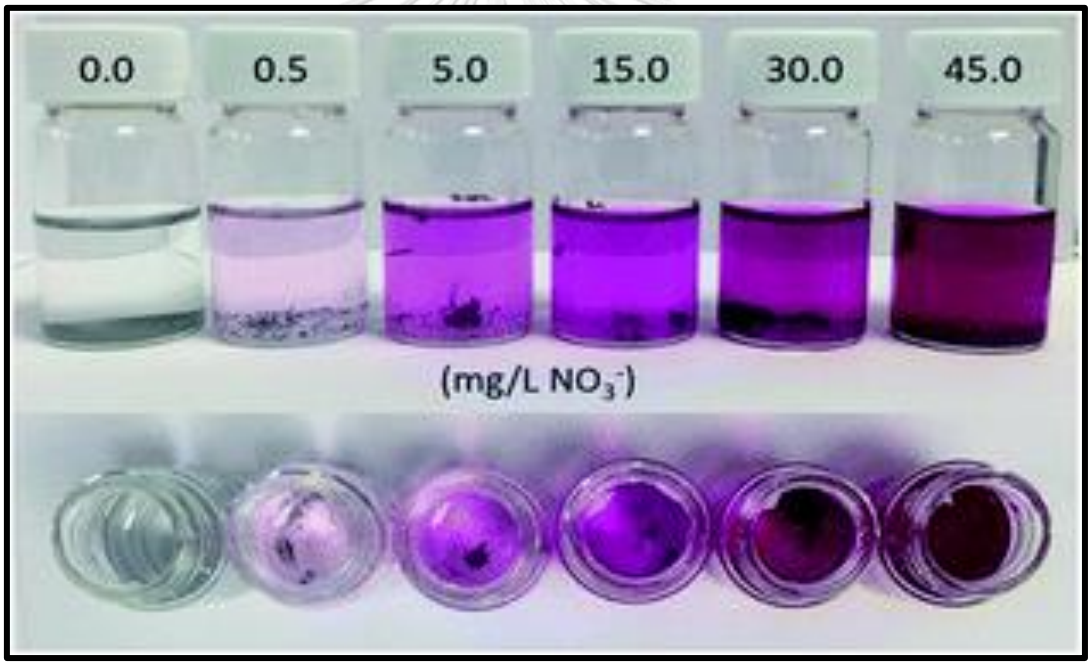

Figure 2.11 Photographic results of various NO_3^- concentration in Griess reagent [1]

2.4. Nanomaterials

Nanoparticles are particles in the size ranging from 1 to 100 nanometers. New properties derived from particles size below 100 nanometers have been applied in many fields including biomedical, optical, and electronic. Nanoparticles has a high surface area to volume ratios; therefore, they process the property of size-dependence. The number of atoms on the surface of nano-scale particles are dominant number of atoms in bulk of the material compared

with opposite situation of bulk materials. This phenomenon initiates unexpected properties [2]. There are several types of nanoparticles, Nanoparticles imparts the enhancement of conductivity to electrodes. It offers higher sensitivity detection. The electro conducting property of metal nanoparticles are derived from their small particles that exhibit greater activity. Moreover, the higher surface area to volume ratio has driven more diffusion. These are responsible for increase electrical signals. Most nanoparticles are employed as the electrocatalysts because they possess enzyme mimetic activity, such as platinum (Pt), and gold (Au). However, a good level of sensitivity is not achieved from these materials. Therefore, many researches have synthesized these materials in nano-scale to address the problem. Even though the higher electrical signal was reached, they are suffered from surface poisoning of common substances found in the sample. Nickel (Ni) and copper (Cu) have been affirmed of surface poisoning reduction and economical starting materials compared with platinum and gold. Similarly, they have been explored in nano-level and declared for enhancing property. Many attempts of metal alloys and compounds have been proposed for better sensitivity. For example, copper oxide (CuO) nanoparticles has received massive attention the substitution of enzymes, horseradish peroxidase (HRP) and glucose oxidase (GOx), because it acts as electrocatalysts on the electrode surface which assists in glucose oxidation. Nickel oxide (NiO) nanoparticles have a similar behavior of copper oxide nanoparticles and were applied in analogous practices. Furthermore, metal oxide nanoparticles are low-cost, non-toxic, chemical stable, improve electrons transfer, and strong adsorption capability. Hence, metal oxide nanoparticles are noticeably of electrode modifiers [3].

2.5. Column chromatography

Chromatography is one of the separation methods used for separating the analyte from their interferences. In lab-on-column or column chromatography, samples are injected into the stream of mobile phases and pass through the stationary phase packed inside a column. The analyte can be retained by the stationary phases using interaction such as adsorption, equilibrium partition, electrostatic interaction, and size according to the methods used for the separation. Chromatography is interesting method for separation compounds before the detection. The principles of column chromatography and two class of column liquid chromatography including high-performance liquid chromatography and ion chromatography are discussed below.

2.5.1. Principles

The general principle of separation is developed based on the different interaction between the analyte and the stationary phase. Analyte in the same family may have different affinity towards the stationary phase depended on the functional group on the analyte. In

column chromatography, the sample (or solute) is introduced at the beginning of the column as a narrow band and followed by the solvent (or mobile phases) or eluent to gradually remove the analyte off the column. Each solute is eluted individually according to its affinity with the stationary and mobile phases. The solute bands are broadening from triangular shape to Gaussian profile after they travel the column. Usually, the detector is placed at the end of the column and continuously records the analytical signal as a function of time.

There are two significant parameters for the analysis of the chromatographic peaks (see Figure 2.12). The elapsed time from the first sample introduction to the peak maximum is called the retention time (t_r). The flow rate of the mobile phases divided by the retention time gives the retention volume (V_r) which can used for the characterization of the peaks. Another parameter is the peak width at baseline (W). The peak wide is the measurement of time between two tangent lines drawn through inflection point of the chromatographic peaks. These parameters are useful for calculating the chromatographic resolution, capacity factor, column selectivity, and peak capacity.

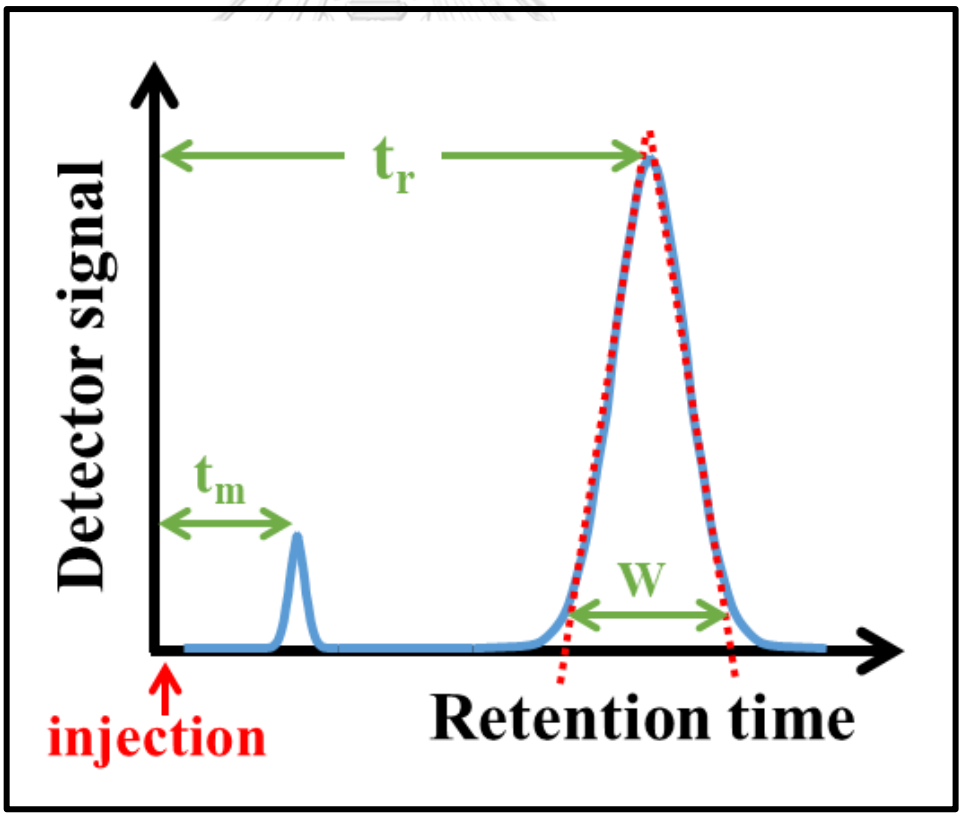

Figure 2.12 The typical chromatogram where t_m is the void time, t_r is the retention time, and W is the peak width

2.5.1.1. Chromatographic resolution

The objective of the separation is to achieve individual peaks representing one compound and resolution (R) is a parameter used to determine a degree of separation. R is calculated from two adjacent peaks (peak A and B) using t_r and W using the equation below.

$$R = \frac{t_{r,B} - t_{r,A}}{0.5(W_B + W_A)} = \frac{2\Delta t_r}{W_A + W_B} \quad (12)$$

Either increasing Δt_r or decreasing W by reducing the flow rate, increase the affinity of stationary phases, or reducing injection volume can improve the resolution of the chromatographic peaks. An acceptable R value is 1.5 meaning only 0.15% overlap of two peaks. R is useful for the development of better experiment conditions.

2.5.1.2. Capacity Factor

During the separation, the solute (S) is distributed between the mobile phase and stationary phase. The stationary phase must retain solute for the separation. Capacity factor (k') is the parameter measure the capability of the stationary phase for retaining the solute using the equation;

$$k' = \frac{t_r - t_m}{t_m} = \frac{t'_r}{t_m} \quad (13)$$

Where t_r is the retention time

t_m is the column's void time

t'_r is the adjusted retention time

2.5.1.3. Column selectivity

Two compounds, assuming A and B, are compared for the relative selectivity of a column by determining the selective factor (α) from the equation

$$\alpha = \frac{k'_B}{k'_A} = \frac{t_{r,B} - t_m}{t_{r,A} - t_m} \quad (14)$$

α equals to 1 when solute A and B eluted at the same retention time; therefore, A must always present with smaller retention time to separate a pair of solutes.

2.5.1.4. Column efficiency

In theoretical model, the chromatographic column is treated as individual sections where solutes in mobile phase partition to the stationary phase. These sections are called theoretical plate, and the number of theoretical plates (N) is attributed to the efficiency of the column. N is expressed in the equation

$$N = \frac{L}{H} \tag{15}$$

Where L is the length of the column

H is the height of the theoretical plate

The efficiency of the column is proportional to N, and inversely proportional to H, respectively. Assuming the chromatographic peaks has a Gaussian profile, H can be derived from the equation

$$H = \frac{LW^2}{16t_r^2} \tag{16}$$

Combining the equation (15) and (16), N is approximately

$$N = 5.545\left(\frac{t_r}{W_{1/2}}\right)^2 \tag{17}$$

Where $W_{1/2}$ is the width at half height of the chromatographic peaks.

2.5.1.5. Peak capacity

An estimate number of solutes that can be eluted using a chromatographic column can be calculated using the equation

$$n_c = 1 + \frac{\sqrt{N}}{4} \ln \frac{V_{max}}{V_{min}} \tag{18}$$

Where n_c is peak capacity

V_{max} is the largest volume of a solute which can be eluted and detected

V_{min} is the smallest volume of a solute which can be eluted and detected

The peak capacity predicts the maximum number of solutes that can be resolved using the analytical column.

2.5.1.6. van Deemter equation

The narrow bands of solutes are broadening when traveling through the column. It is significant to control the size of the band so that their profiles maintain the Gaussian behavior. The understanding of reasons accounted for the band broadening will results in successful separation of individual peaks. Four factors are contributed to the height of the theoretical plate (H): multiple paths (H_p), longitudinal diffusion (H_d), mass transfer in stationary phase (H_s), and mass transfer in mobile phase (H_m). The net H equals to

$$H=H_p+H_d+H_s+H_m \tag{19}$$

The equation can alternately convert to van Deemter equation:

$$H=A+\frac{B}{u}+Cu \tag{20}$$

Where term A contributes to H_p

B/u is related to H_d

Cu is derived from H_s and H_m.

The equation states the important of the flow rate of the mobile phases (u). The ideal plot between H and u is shown in Figure 2.13.

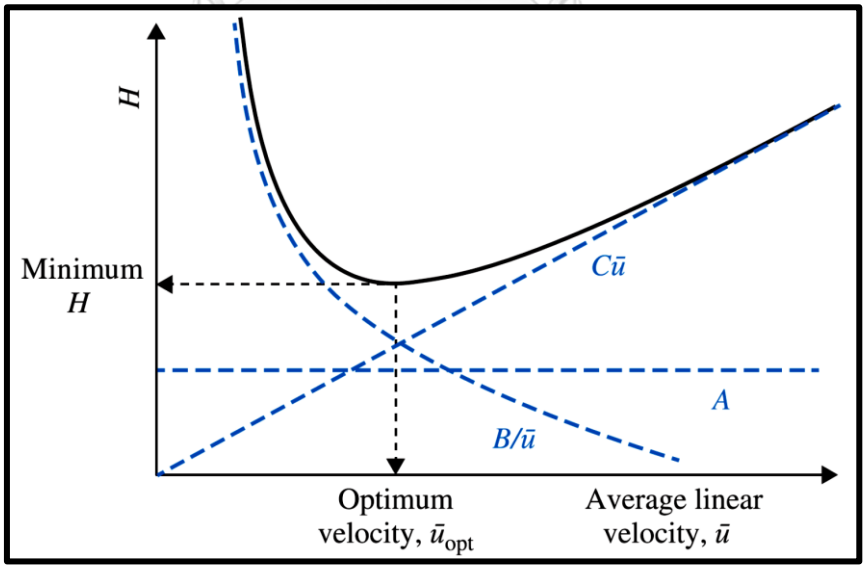

Figure 2.13 The Van Deemter plot depicts the relationship between column flow rate and peak efficiency, referred to as band broadening [4]

To improve the column efficiency for the separation, the simplest way is to consider the plot and adjusted the mobile phases' velocity to the optimum velocity.

2.5.2. High-Performance Liquid Chromatography (HPLC)

HPLC is one of the column liquid chromatography which is very effective for the separation of the analytes from the samples. The method is rapid because of the pumping system used to pressure the liquid through the column. Small particles that packed inside the chromatographic column can reduce the height of the theoretical plate and has trivial effects on the flow rate of the mobile phase. The high-pressure pump is required to force the mobile phases and solutes out/in the column. The schematic of HPLC is shown in Figure 2.14.

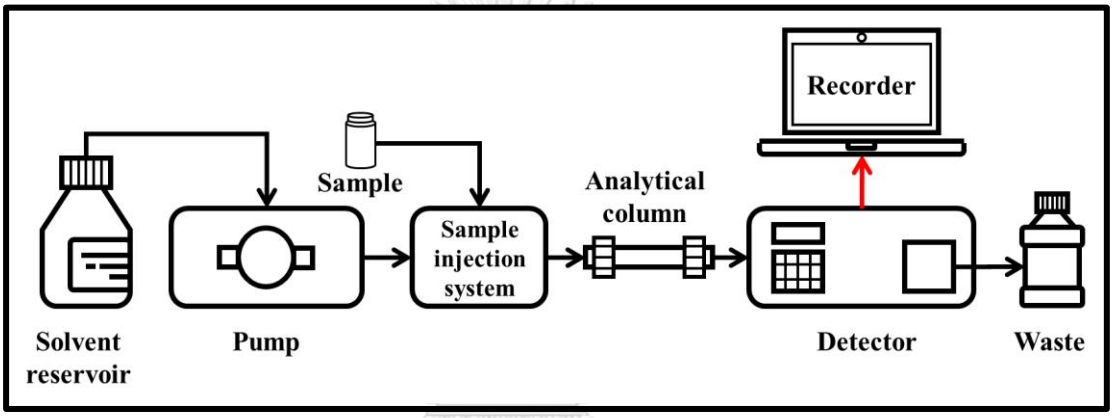

Figure 2.14 Components of typical HPLC instruments includes a pump, injector, column, detector and recorder or acquisition and display system.

2.5.2.1. Equipment

2.5.2.1.1. Solvent reservoir

The mobile phases contain in the glass or stainless-steel bottle of typical 1-2 L. The solvent reservoir must connect to degassing system to remove oxygen or nitrogen glass from the mobile phases before entering the column. The gases can interrupt the detector. There are two methods for the separation; isocratic condition (one mobile phase) and gradient condition (≥2 mobile phases) Usually, there are more than two mobile phases for the elution. The gradient elution can improve the separation of the analyte and decrease the analysis time. In some cases, more Gaussian chromatographic peaks can be obtained. The system used to control the mobile phases is called solvent programming.

2.5.2.1.2. Pump

Pump is responsible for moving the mobile phases in/out of the column. The normal operation pressure of pump is approximately 0-4000 psi depend on the pump model. The pump in HPLC can provide high precision of flow rate up to ±2%. The peak shape usually improves with the increasing flow rate because the effects from band broadening is reduced.

2.5.2.1.3. Sample injection system

Sample injection typically uses slider valve. There are manual and automatic injection. The volume of injection is varied between 2 to 100 µL.

2.5.2.1.4. Column

The stationary phases are loaded inside the glass and stainless-steel of 15-150 cm long, 2-3 mm dimeter. There are two types of stationary phases; solid particles and liquid coating. The chemical structure influences the selection of the stationary phase. High polar analytes are suitable for polar column because the polar components on the stationary phase can retain the analyte inside the column, this is called normal phase chromatography. Examples of normal phase column are silica and alumina column. By contrast, nonpolar analytes are separated by nonpolar column, this is reverse phase chromatography. Mostly, the separation uses reverse phase column such as octyl (C8) and octadecyl (C18) column.

2.5.2.1.5. Detector

The choice of HPLC detector depends on the analyte. The common detector is UV spectrophotometer because it can operate automatically without the need of calibration. In some cases, other detectors such as mass spectrophotometer, electrochemical detector, and admittance detector are required because UV spectrophotometer has insufficient sensitivity for the detection.

2.5.2.2. Ultra-High-Performance Liquid Chromatography (u-HPLC)

The principle of u-HPLC is similar to HPLC but the analysis time of u-HPLC is greatly reduced because the packing particles and the pump system. In typical HPLC, the diameter of the stationary phase is averagely 3-5 µm but <2 µm for u-HPLC. The sub 2-µm particles increase the back pressure of u-HPLC; therefore, high efficiency pump is required (pressure of ~15,000 psi). The separation of the analytes is improved because the plate count is higher, and the band broadening is reduced. The sensitivity of the methods is increased because the analyte is concentrated due to the narrower band.

2.5.3. Ion Chromatography (IC)

IC is the method uses for ionic compounds separation. Ionic samples are injected into the column fabricated from ion-exchange resin and interact with the stationary phase until displaced by stronger ions (usually the counter ions of the resin) and travelled to the end of the column for detection. The affinity of the ionic analytes and the ion-exchange resin depends on the oxidation state, hydration radius, degree of stationary phase's crosslinking, molecular weight, concentration, and temperature. The stationary phase of IC is either cation-exchange (CEX) or anion-exchange (AEX) resin. The functional group of CEX resin include mostly sulfonic acid functional group and usually the conditions for separation is acidic of pH 4. AEX resin uses quaternary amine function group; therefore, the separation is carried out in basic conditions. IC can be classified into subcategories: strong/weak CEX and strong/weak AEX. Examples of common ion-exchange resin are listed in Table 2.1.

Table 2.1 Examples of stationary phase in ion chromatography

Type	Functional group	Examples
Strong CEX	Sulfonic acid	$-SO_3-$
		$-CH_2CH_2SO_3-$
Weak CEX	Carboxylic acid	-COO-
		$-CH_2COO-$
Strong AEX	Quaternary amine	$-CH_2N(CH_3)_3+$
		$-CH_2CH_2N(CH_2CH_3)_3+$
Weak AEX	Amine	$-NH_3+$
		$-CH_2CH_2NH(CH_2CH_3)_2+$

The stationary phase can pack inside the column as small particles or coating at the surface of the column. The selectivity of the analyte to the stationary phase depends on the interaction with the ion-exchange resin. Ions possess higher oxidation state have higher affinity towards ion-exchange resin, but ions with the same oxidation number the ions with smaller hydration layer provide better exchange with the resin. In some cases, the affinity of the ions depends on both electrostatic force and Van der Waal's force (high molecular weight ions provide stronger interaction with the resin).

2.5.4. Open Tubular liquid Chromatography (OTLC)

The wall of the analytical column, for example silica column, can be hydrolyzed and functionalized with CEX or AEX. The column is carried out in open capillaries similar to gas chromatography, this is called open tubular liquid chromatography (OTLC). It is not suitable for the analytical column because the diffusion of the liquid phase is thousand times slower than the diffusion of gas and the separation cannot be obtained. Many efforts have been pursuing. Recently, OTLC has successfully developed for the separation of cations with functionalized polyolefin column using ion-exchange chromatography [5].

CHAPTER III

Lab-on-paper applications

Recently, most flow analysis systems are miniaturized into a single convenient portable device. In this chapter, two analytical method namely; electrochemistry and colorimetry were developed on paper-based analytical device. First, paper-based electrochemical sensor was fabricated for C-reactive protein detection. Thiol-terminated poly(2-methacryloyloxyethyl phosphorylcholine) was synthesized and used as a recognition material for the protein in the presence of calcium ions. The polymer was grafted onto gold nanoparticles modified screen-printed carbon electrode using gold-thiol interaction. Paper was used as substrate for storage of calcium ions and electrochemical active species ($Fe(CN)_6^{3-/4-}$). The current signals were obtained from the redox reaction of the active species. The increasing of CRP concentration is inversely proportional to the decreasing of analytical signal. Therefore, the current measurement can relate to the amount of CRP in samples. The sensor performance was exceptional with detection limit of 1.6 ng mL^{-1}. The paper-based electrochemical sensor was demonstrated for CRP detection in certified serum samples. Second, PAD was developed for Pi sensing. In this work, colorimetry was employed as the analytical method. The detection was performed on filter paper using 2-mercaptoethanesulfonate modified silver nanoplates as the colorimetric probe. Color changes from purple to pink result from the anti-aggregation of the modified AgNPls in the presence of Pi. Color shades are related to concentration; hence the semi-quantitative detection method was achieved. Pi sensor can used for monitoring soil quality with the limit of detection equals to 1.01 mg L^{-1}. Lab-on-paper demonstrates that excellent analytical methods can performed on paper substrate and they are fast, convenient, and inexpensive.

3.1. Disposable paper-based electrochemical sensor using thiol-terminated poly(2-methacryloyloxyethyl phosphorylcholine) for the label-free detection of C-reactive protein

3.1.1. Abstract

A paper-based electrochemical sensor is described that is based on the use of thiol-terminated poly(2-methacryloyloxyethyl phosphorylcholine) (PMPC-SH) that was self-assembled on a gold nanoparticle-modified screen-printed electrode (SPE). The SPE sensor was used for label-free detection of C-reactive protein (CRP). Gold nanoparticles (AuNPs) were first electrodeposited on the SPCE, followed by the self-assembly of PMPC-SH on gold. The electrochemical response of the modified SPE to CRP was measured by differential pulse voltammetry (DPV). If the CRP on the paper device is contacted with Ca (II) ions, the current (measured by using hexacyanoferrate as the electrochemical probe) decreases. The signal drops in the 5 to 5000 ng mL^{-1} CRP concentration range, and the lower detection limit (at 3 SD/slope) is 1.6 ng mL^{-1}. The use of a PMPC-modified surface also reduces the nonspecific adsorption of proteins. The sensor is not interfered by bilirubin, myoglobin and albumin. It was successfully applied to CRP detection in certified human serum. This sensor is applicable as an attractive protocol for an inexpensive, highly sensitive, and disposable material for electrochemical detection of CRP.

3.1.2. Introduction

CRP or human C-reactive protein is a nonspecific pentameric protein manufactured by hepatocytes in the liver upon stimulation by endogenous proinflammatory cytokines. The level of CRP in the circulation system increases by >1000-fold within 1-2 days due to infection, cell damage, or other inflammatory conditions compared to healthy conditions (0.8 mg L^{-1}) [6, 7]. CRP is an important risk factor for many heart diseases or cardiovascular diseases (CVD) [8, 9]. CRP is known to be present in atherosclerotic plaques and triggers the chemokine, in which later adhere the molecules to endothelial cells [10]. Thus, it is of great importance to determine the CRP level in patients for an early therapeutic treatment. The American Heart Association and the United States Centers for Disease Control and Prevention (AHA/CDC) provide the following criteria for CVD risk based on the level of CRP in human blood serum: concentrations of CRP less than 1, 1 – 3, and above 3 mg•L^{-1} represent low-risk, moderate risk, and high risk states, respectively [8, 11]. In most cases, samples from patients are sent and analyzed for the CRP concentration in clinical laboratories. Immunonephelometric or immunoturbidimetric assays are the conventional techniques for the determination of the CRP level [12]. Although these immunoassay methods are well-established and reliable, antibodies are required. Furthermore, these assays are costly, time-consuming, skillful personnel and utilize complicated instrumentation are required. Therefore, a fast, highly sensitive, selective, and simple approach for trace CRP monitoring is desired.

In the past few years, biosensors using electrochemical techniques have received attention for their portable and accessible tools for the detection of important biomarkers [13]. To achieve high selectivity and sensitivity of the measurement, various working electrodes for electrochemical sensors have been continuously developed. Metallic nanoparticles are attractive materials that have been used for the surface modification of the working electrode because they improve the electrochemical efficiency by enhancing the surface area of the electrode [14], particularly, the screen-printed electrode (SPCE), for which the size of the working electrode is limited. They show high catalytic abilities for some interested compounds [15]. Gold nanoparticles (AuNPs) are frequently utilized for this propose due to advantages including a high electron transfer and strong specific interaction with sulfur-containing compounds [16].

AuNP-modified SPCE can be assembled with paper-based analytical devices (PADs) to simplify the detection and storage of chemical reagents. Many researchers are attracted to PADs for important determinations. For example, our group has developed a dual detection (colorimetry and electrochemistry) technique for the detection of toxic environmental compounds such as heavy metals [17, 18] and biomarkers [19, 20]. With the benefits of PADs in

combination with the SPCE, electrochemical sensors can be manufactured with low cost and high throughput. Furthermore, the detection is simple, sensitive and selective. SPCEs are disposable which eliminated the problem of electrode fouling and the pretreatment of the electrode before measurement.

A single step technique for label-free CRP detection on PADs was developed. A AuNP-modified SPCE self-assembled with PADs was tethered with biomimetic polymer consisting of thiol functional groups using the interaction between sulfur and gold for the label-free detection of CRP. Generally, CRP forms a pentraxin (115 kDa) of five identical subunits or protomers (~23 kDa), which are noncovalently attached and symmetrically arranged around a pore. Each protomer has a recognition domain of a phosphorylcholine (PC) group in the calcium binding pocket [21]. In the presence of injured cells, the alleviated level of CRP in the circulating system binds with the PC receptor, then starts the classical component pathways to heal the damaged cells [22]. Specific binding between various biomimetic phospholipid structures and CRP has been reported [23]. 2-Methacryloyloxyethyl phosphorylcholine (MPC) has received great attention for this propose. Goda et al. first reported the MPC copolymer for the label-free detection of CRP using surface plasmon resonance techniques. The results showed that the binding of CRP is dependent on the local concentration of Ca^{2+} and pH of the environment [24]. MPC copolymer can be grafted on different surface such as ZnO nanowires [25] and glassy carbon electrode [26] and highly sensitive techniques including fluorescence and electrochemical impedance spectroscopy were employed for the quantification of CRP. Due to strong thiol-gold affinity, MPC bearing thiol functional group can be embedded onto the gold nanoparticles and used as recognition probe for CRP [27]. Iwasaki et al. demonstrated the utility of poly(MPC)-protected magnetic nanoparticles for the detection and collection of CRP. The analytical technique was performed by dynamic light scattering (DLS), an excellent limit of detection of this work was found at 10 nM and a good selectivity was obtained in the presence of bovine serum albumin (BSA) [28].

PMPC-SH, which contains a mercapto group, was synthesized and self-assembled onto the surface of AuNPs electrodeposited on the SPCE. The electrochemical measurement was performed using differential pulse voltammetry (DPV). The current changed upon contact with CRP in the presence of Ca^{2+} and showed a good relationship with the CRP concentration. The characterization, optimization, analytical performance, and specificity of the sensors were studied. The sensors were constructed with PADs and were convenient to be used for CRP detection. Finally, this synthetic MPC-based polymer anchored on a AuNP-modified SPCE on PADs was demonstrated to be successfully applied for detecting the CRP level in simulated body fluids.

3.1.3. Experimental

3.1.3.1. Chemicals

All chemicals and reagents used in this work are of analytical grade except when stated. Carbon and silver/silver chloride (Ag/AgCl) inks were purchased from The Gwent Group, United Kingdom for the fabrication of the SPCE. The patterns of the SPCE and PADs were designed using Adobe Illustrator CS6 v16.0.3. The screen-printed block was made by Chaiyaboon Co. Ltd. (Bangkok, Thailand). Polyvinyl chloride (PVC) used as a substrate for the fabrication of the SPCE was purchased from a local market. Potassium hexacyanoferrate (III) ($K_3Fe(CN)_6$) was purchased from Riedel-de Haën (Lower Saxony, Germany). Tris-hydrochloride (Tris-HCl), Tris-base, potassium dihydrogen phosphate (KH_2PO_4), sodium phosphate dibasic (Na_2HPO_4) was obtained from Sigma-Aldrich (St. Louis, MO, USA). 4,4'-azobis(4-cyanovaleric acid) (ACVA), 4-cyano-4-(thiobenzoylthio)pentanoic acid (CPD), hydrazine monohydrate, phosphate buffered saline pH 7.4 (PBS), dialysis membrane (3,500 Da MWCO), 2, 2, 2-Trifluoroethanol (TFE) was purchased from TCI Chemicals. 2-Methacryloyloxyethyl phosphorylcholine (MPC) was bought from NOF Corp. Potassium tetrachloroaurate (III) ($K[AuCl_4]$) was purchased from Wako Chemicals, Japan. Calcium chloride ($CaCl_2$) was obtained from May & Baker (Dagenham, England). C-reactive protein (CRP) in human serum (Certified Reference Material ERM-DA474/IFCC, Lot: 081M1600V) was purchased from Sigma-Aldrich. The amount of CRP in the samples was measured by immunonephelometric and immunoturbidimetric assays using ERM-DA470 as the calibrant. The 0.05 mM Tris-buffer consisting of Tris-HCl, Tris-base, and 0.15 mM NaCl was prepared, and the pH was adjusted by varying the composition between Tris-HCl and Tris-base. Millipore Milli-Q purified water (18.2 MΩ cm) was used throughout the experiments.

3.1.3.2. Apparatus and measurements

Electrochemical measurements were performed on an AUTOLAB PGSTAT101 (Metrohm Siam Company Ltd.) and controlled with the NOVA 2.0 software. A disposable SPCE was used and fabricated using an in-house screen-printing method. A conductive Ag/AgCl ink was employed as a pseudo-reference electrode (RE). Carbon ink was utilized to prepare the working electrode (WE) and counter electrode (CE). Electrochemical measurements of the CRP were achieved using differential pulse voltammetry (DPV) under the optimized conditions: 0.1 V amplitude and 7.5 mV step potential. In all cases, DPV was carried out at room temperature (25 ± 1 °C).

Electrochemical impedance spectroscopy (EIS) measurements were accomplished on a PalmSens4 potentiostat/ impedance analyzer (Palmsense BV, Netherland) and controlled with PSTrace software. The EIS of CRP was performed done under the follwing conditions: 5 s

$t_{equilibration}$, 0.1 MHz maximum frequency, 0.01 Hz minimum frequency, and 0.1 V E_{ac}. EIS experiments were performed at room temperature.

The surface morphology of the working electrode was studied by scanning electron microscopy (SEM) using a JSM7610 field emission scanning electron microscope (FESEM, JEOL Ltd., Japan). The high-resolution images were obtained at 15.0 kV SEI with a magnification of x10,000.

Preparation of PMPC and PMPC-SH were characterized by proton nuclear magnetic resonance (1H-NMR) spectroscopy recorded on a Varian, model Mercury-400 NMR spectrometer (USA) operating at 400 MHz using D_2O as a solvent. The number-averaged molecular weight (Mn) of synthesized PMPC was calculated from the relative ratio between the integrated peak areas of the protons from the PMPC backbone and the protons from the dithiobenzoate groups at polymer chain end

3.1.3.3. Synthesis of thiol-terminated PMPC (PMPC-SH)

PMPC with a degree of polymerization (DP) of 25 was prepared by reversible addition-fragmentation chain-transfer (RAFT) polymerization [29, 30] as follows: MPC (1.4763 g, 5.00 mmol), ACVA (9.35 mg, 33.4 μmol) and CPD (55.9 mg, 0.200 mmol) were dissolved in 5.0 mL of 2,2,2-trifluoroethanol (TFE) in a vial equipped with a magnetic bar and septum. The reaction mixture was degassed by purging with nitrogen gas for 30 min and then stirred in oil bath at 70 °C for 4 h. After polymerization, the polymer solution was purified by dialysis (MWCO 3,500 Da) against DI water for 3 days and lyophilized by a freeze dryer (model Freezeone 77520 Benchtop, Labconco, USA). To convert dithiobenzoate group at polymer chain end to thiol group for grafting onto gold surface, an aqueous solution of PMPC (5.0 mM) was treated with hydrazine (30 mol equivalents of PMPC) at room temperature for 6 h or until the polymer solution became colorless. After the reaction was completed, the reaction solution was then added to 1.2 M HCl (10 mL). The final cotton-like white solid was obtained after purification by dialysis against HCl (pH =3) for 2 days and deionized water for another 2 days at 4 °C and lyophilization.

3.1.3.4. Sample preparation

The standard stock solution of CRP was kept frozen in a freezer at -20 °C until use. The working solutions were diluted from stock solutions using Tris-buffer. The synthesized PMPC-SH (solid) was kept in a -20 °C freezer and protected from the humidity.

3.1.3.5. Fabrication of gold nanoparticles electrodeposited on a screen-printed carbon electrode (AuNPs-SPCE)

The electrode was a SPCE that can be simply fabricated at low cost. The format and preparation of the SPCE were thoroughly discussed [31]. The format consists of a reference electrode (RE), working electrode (WE), and counter electrode (CE), see Figure 3.1A. On a PVC substrate, the RE and conductive pads were printed first with Ag/AgCl ink. Second, the carbon ink was printed to form both the WE and CE. After that, the electrode was baked at 55 °C (1 h) for residual solvents removing prior to use.

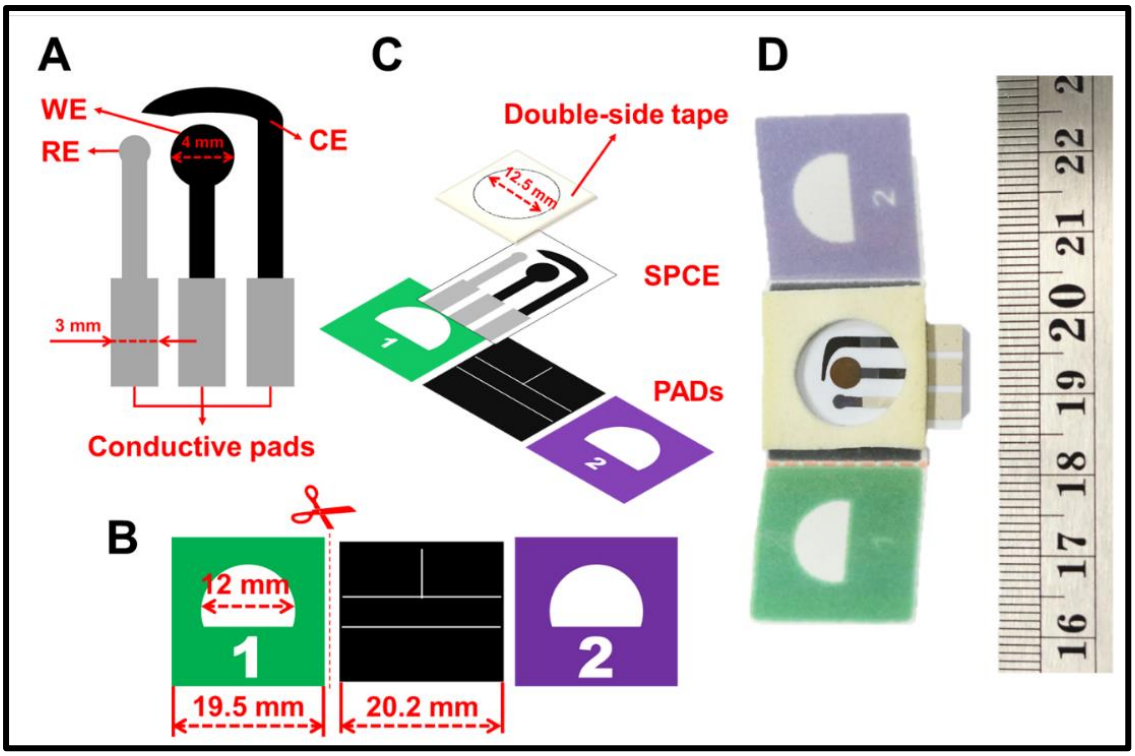

Figure 3.1 Design of devices in this work SPCE A), PADs B), the assemble of SPCE and PADs (SPCE/PADs) C), and the photo of SPCE/PADs with scale (in cm).

Gold (III) stock solution (0.1 mM) in H_2SO_4 was prepared by dissolving 0.0377 g of potassium tetrachloroaurate (III) ($K[AuCl_4]$) in 1 mL 0.2 M H_2SO_4. For other gold (III) concentrations, the solution was diluted from the stock solution. For WE modification by AuNPs, 30 µL of gold (III) solution (5 mM) was dropped onto the surface of the three electrodes followed by applying a constant potential of -0.4 V (vs. Ag/AgCl) for 200 s without stirring the solution. Then, the electrode with the AuNPs electrodeposited on the SPCE (AuNPs-SPCE) was completely rinsed with distilled water and dried under N_2 gas before use. For electrode characterization, AuNPs on WE were studied using SEM and EIS.

3.1.3.6. Fabrication of paper-based analytical devices (PADs) for AuNPs-SPCE

PADs were fabricated by the wax printing method. First, the design in Figure 3.1B was depicted using Microsoft Power Point. The designs were printed onto Whatman No.1 filter paper using a wax printer (Xerox ColorQube 8570DN). The paper was then baked inside the oven at 150 ℃ for 2 min, and 2 mm thick double-side tape was punctured with a 1 cm diameter hollow hole puncher. After that, the AuNPs-SPCE was placed in the middle of the paper and attached above with the punctured double-side tape described previously (see Figure 3.1C for more information about device assembly). The PADs consist of three parts, first is the middle of the PADs in which the SPCE was placed. Second, a green flap (label with 1) was used for the storage of Ca^{2+} and dropping the sample. Third, a purple flap (label with 2) was used for the storage of $K_3Fe(CN)_6$ for the detection using the PADs.

3.1.3.7. Preparation of CRP sensors and DPV measurement

Figure 3.2A shows the schematic for the preparation of PMPC-SH self-assembled onto the AuNPs-SPCE. The copolymer of PMPC-SH contains a thiol functional group, which can react with gold using the favorable sulfur-gold interaction. The solution of PMPC-SH was prepared by dissolving precipitated PMPC-SH in Tris-buffer solution at a pH of 6. Next, 5 µL of the solution was dropped onto the surface of the working electrode and left at room temperature for 1 h. Then, the electrode was thoroughly washed with Tris-buffer twice to remove the excess PMPC-SH on the electrode surface. These electrodes were termed PMPC-SH/AuNPs-SPCE, and the current obtained from them was subtracted from the current during the detection of CRP. The devices were kept in a desiccator at room temperature.

For the detection of CRP, PADs were employed. Prior to the measurement, 100 µL of 10 mM Ca^{2+} was dropped in the middle of the channel of the green flap and left to dry at room temperature for approximately 10 min. Next, the same volume of 4 mM $[Fe(CN)_6]^{3-/4-}$ prepared in 0.1 M KNO_3 was dropped in the channel of the purple flap and left to dry. To detect CRP, the green flap was folded to the middle, and 100 µL of sample was dropped and left for incubation. After 1 h, the green flap was removed, and the electrodes were washed with Tris-buffer solution twice to remove the excess. The electrodes in this step were termed CRP/PMPC-SH/AuNPs-SPCE. Then, the purple flap was folded to the middle and 100 µL of 0.1 M KNO_3 was dropped and left for 10 min to allow the solution of $[Fe(CN)_6]^{3-/4-}$ to permeate to the surface of the electrodes. Finally, the current was measured by DPV techniques using an applied potential in the range of -

0.3 – 0.5 V. The total analysis can be performed within 1.5 h. The procedure for CRP detection on PADs is summarized in Figure 3.2.

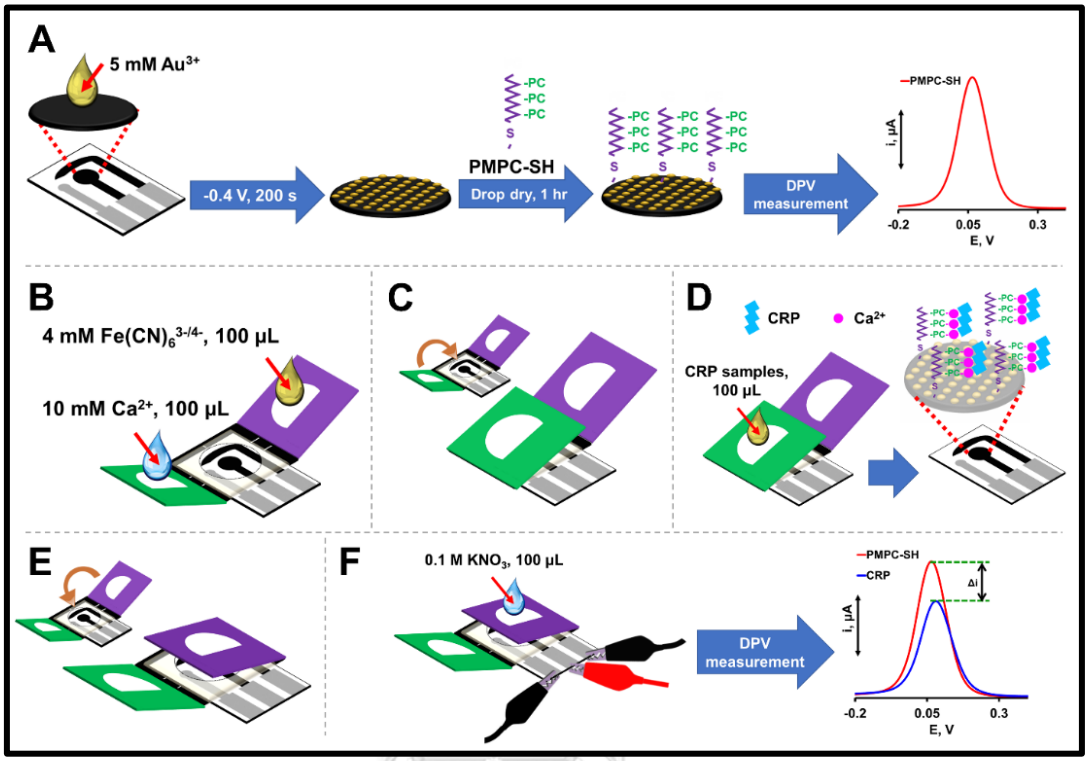

Figure 3.2 Preparation of PMPC-SH/AuNPs-SCPE/PADs for CRP detection using DPV

3.1.4. Results and discussion

3.1.4.1. Synthesis and characterization of PMPC and PMPC-SH

MPC was characterized by Proton nuclear magnetic resonance (^{1}H-NMR). Figure 3.3 illustrates ^{1}H-NMR spectra of the synthesized PMPC before and after reduction. As shown in A, the characteristic peaks of MPC repeating unit were clearly observed. By calculating the relative peak ratio between the peak integration of $H_{c,\,d,\,e}$ and $H_{f,\,g,\,h}$ from ^{1}H-NMR spectrum of PMPC, the observed molecular weight (MW) was 8,547 which was close to the targeted MW (targeted MW is 7661) indicating well-controlled characteristic of RAFT polymerization. After reduction (Figure 3.3B), the signal of aromatic protons of dithiobenzoate group ($H_{f,\,g,\,h}$) disappears confirming that the terminal dithiobenzoate groups were cleaved and converted to thiol groups.

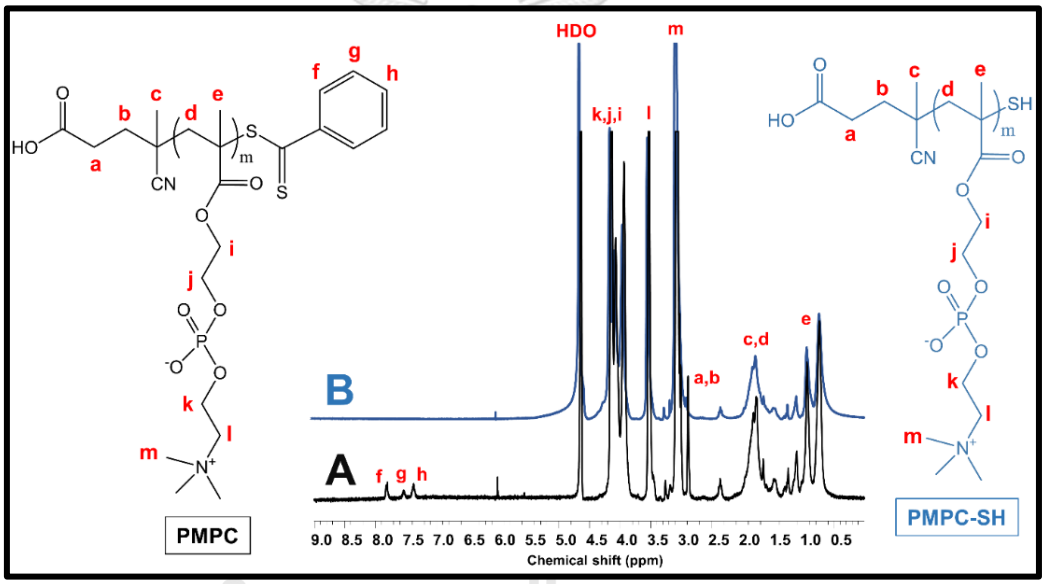

Figure 3.3 ^{1}H NMR spectra of PMPC-SH (B) compared to PMPC (A).

3.1.4.2. Characterization of the modified electrode

Gold nanoparticles were electrodeposited from gold (III) solution onto the surface of the SPCE for the self-assembly of PMPC-SH. The presence of AuNPs on the electrode surface after the electrodeposition step was studied by SEM technique. The unmodified carbon electrode showed no presence of AuNPs (Figure 3.4A), while AuNPs distributed homogeneously throughout the electrode surface were observed (Figure 3.4B) after the electrodeposition of AuNPs. From the size distribution curve (Figure 3.4C), the average particle size was 56.17 nm with a PDI of 0.082. The results indicated that the deposited AuNPs were affixed onto the electrode surface with a uniform manner.

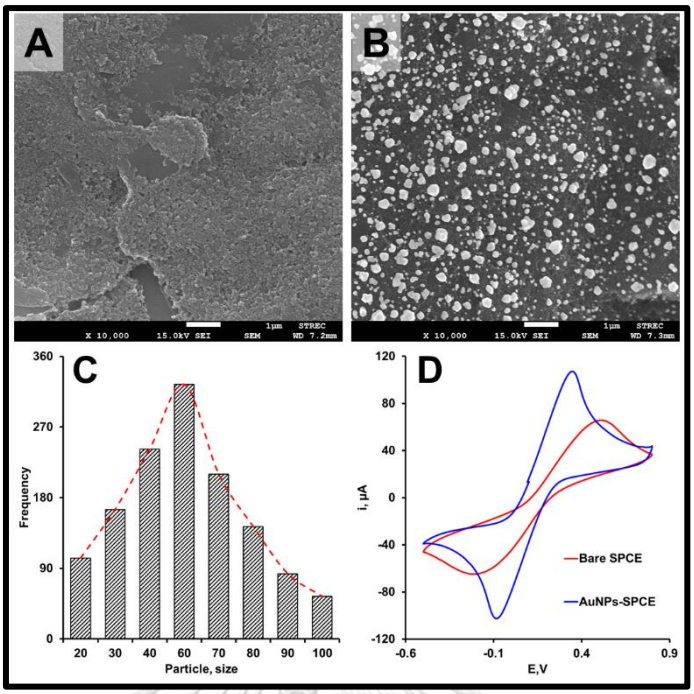

Figure 3.4 Characterization of AuNPs-SPCE: SEM images of the carbon material (A), and AuNP-modified carbon electrode (B); particle distribution (C); and CV of the bare SPCE compared to the AuNPs-SPCE using 5 mM $[Fe(CN)_6]^{3-/4-}$ in 0.1 M KNO_3 as redox probe at a scan rate of 100 mV/s (D).

The nearly monodisperse distribution of gold nanoparticles can significantly increase the electroactive surface area. The currents obtained from AuNPs-SPCE and bare SPCE were compared. As seen in Figure 3.4D, the AuNPs-SPCE exhibited a higher current for $[Fe(CN)_6]^{3-/4-}$ detection with respect to the bare SPCE. The effective surface areas (A) of these electrodes were derived from the calculation of the Randles-Sevcik equation: $i_p = 2.69 \times 10^5 \, A \, D^{1/2} \, n^{3/2} \, \nu^{1/2} \, C$, where D is the diffusion coefficient of $[Fe(CN)_6]^{3-/4-}$, C is the concentration of $[Fe(CN)_6]^{3-/4-}$, and n is the number of involved electrons. The slope obtained from a plot of the peak current versus the square root of the scan rate (ν) was employed for the evaluation of the electroactive surface. The experiments were studied using cyclic voltammetry (CV) at various scan rates in a 5.0 mM $[Fe(CN)_6]^{3-/4-}$ solution containing 0.1 M KNO_3. The results showed that the peak currents (i_{pa}) of the SPCE (Figure 3.5A and B) and AuNPs-SPCE (Figure 3.5C and D) proportionally increased with increasing $\nu^{1/2}$. For the SPCE and AuNPs-SPCE, the electroactive surface areas were calculated to be 0.0272 ± 0.0014 cm^2 and 0.0657 ± 0.0033 cm^2, respectively using Randles-Sevcik equation. In summary, the electroactive surface area was increased by 42% for the AuNPs-SPCE. The results imply the increase of the surface area, which can increase the sensitivity of the detection.

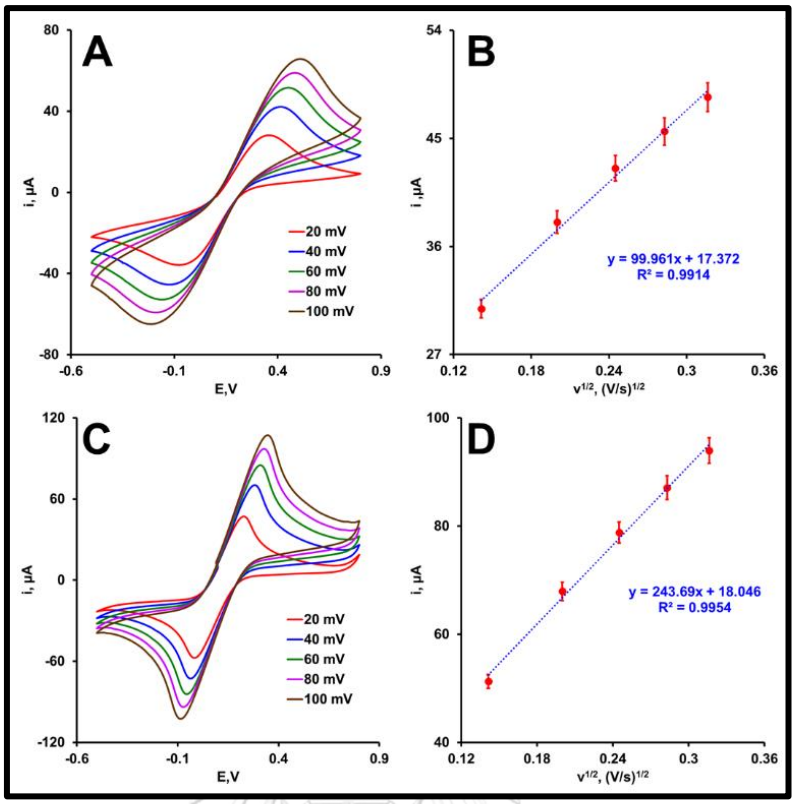

Figure 3.5 Study of the electroactive surface area of the bare SPCE A) and AuNPs-SPCE B) using CV with various scan rates of 20 to 100 mV/s. Plots between square root of scan rate (V/s)$^{1/2}$ and current (µA) of bare SPCE C) and AuNPs-SPCE D).

3.1.4.3. Electrochemical detection of the CRP using the sensors

To confirm the successful preparation of this sensor, the EIS technique was employed. This characterization technique studies the changes of the material's impedance including surface-modified electrode. The electron-transfer kinetics of the redox probe in the solution ($[Fe(CN)_6]^{3-/4-}$) at the electrode interface control the electron-transfer resistance (R_{ct}) which is illustrated by semicircle diameters at high frequency. The electrodes including the SPCE, AuNPs-SPCE, PMPC-SH/AuNPs-SPCE, and CRP/PMPC-SH/AuNPs-SPCE were studied and the results are shown in Figure 3.6A. The signal from the bare SPCE (red line) was nonlinear with a higher R_{ct} of 4.92 kΩ in comparison to the AuNPs-SPCE (blue line) which had a R_{ct} of 0.57 kΩ at high frequencies. This is due to the enhancement of electron-transfer kinetics by AuNPs deposited on the SPCE. After PMPC-SH was self-assembled on the AuNPs-SPCE, a R_{ct} of 1.03 kΩ was observed (green line). This augmentation of R_{ct} can be ascribed to the hindrance of the electrode surface by PMPC-SH, which reduced the accessibility for the $Fe(CN)_6^{3-/4-}$ redox couple. After the CRP was added in the presence of Ca^{2+}, the R_{ct} increased to 2.25 kΩ (gray line). This indicates that an interaction between CRP and PMPC-SH occurred.

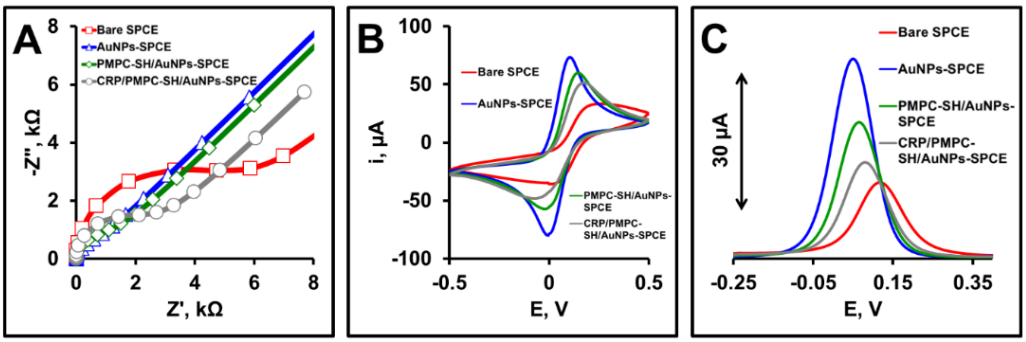

Figure 3.6 EIS (A), CV (B), and DPV (C) of 10 ng mL^{-1} CRP detection steps on PMPC-SH/AuNPs-SPCE/PADs

The detection of CRP was measured by the change in the current (ΔI) obtained from an electrochemical redox species ($[Fe(CN)_6]^{3-/4-}$) before and after the PMPC-SH/AuNPs-SPCE interacts with CRP in the presence of Ca^{2+}. The current difference ($\Delta I = i_{blank} - i_{CRP}$) increased after the addition of CRP. This is because the target analyte interacted with the PC group of PMPC-SH and remained on the surface of the WE. Therefore, the R_{ct} on the surface of the electrode was increased and decelerated the kinetics of the electron transfer at the surface [32]. The i_{CRP} was affected and decreased compared to the blank signal, which led to the increase of ΔI. The results obtained from EIS demonstrated that the R_{ct} of CRP greatly increased to 2.25 kΩ (previously described). Together with the discussion of the PMPC-SH/AuNPs-SPCE characterization, the results suggested that the electrode can be used for CRP detection. EIS results (Figure 3.6A) corresponded with the results performed using cyclic voltammetry (CV) as shown in Figure 3.6B.

Differential pulse voltammetry (DPV) was used as an analytical technique because it can provide higher sensitivity (the current is sampled before the change in potential; thus, the effect of the charging current is decreased) [33]. It is also convenient to perform DPV analysis on a portable potentiostat suggesting its practicality for on-site detection in the future over the impedance spectroscopic method developed by our previous work [34]. Similar trends were observed using DPV (in Figure 3.6C) when compared with those found from EIS and CV analysis as previously described. From the results, the anodic current of AuNPs-SPCE is significantly higher than that of the bare SPCE. This is attributed to the enhancement of electron transfer by increasing the electroactive surface area. The oxidation potential of the AuNPs-SPCE was also shifted to approximately 0.05 V, suggesting that AuNPs facilitate the electron transfer of the redox probe. After the self-assembly of PMPC-SH on the surface of AuNPs, the current decreased, and the potential shifted further. A similar phenomenon was observed after the addition of CRP. ΔI before and after the addition of analytes using DPV for the current measurement can be used for the detection and quantification of CRP.

3.1.4.4. Optimization of variable parameters

Two PMPC-SH having different degree of polymerization (DP), DP50 and DP25 were used. The DP reflects a number of MPC repeating unit per chain of PMPC. As seen in Figure 3.7A, both PMPC-SH systems can similarly bind with CRP; except that the ΔI of the two systems were different. Interestingly, ΔI obtained from PMPC-SH DP25 was higher. This is because PMPC-SH with DP50 is principally twice longer in length than that with DP25 which should yield thicker layer of self-assembled PMPC layer and thus hindered the transfer of the electrons (the resistance is higher) on the interface of the electrode. From the results, the PMPC-SH of DP25 was therefore selected for further studies.

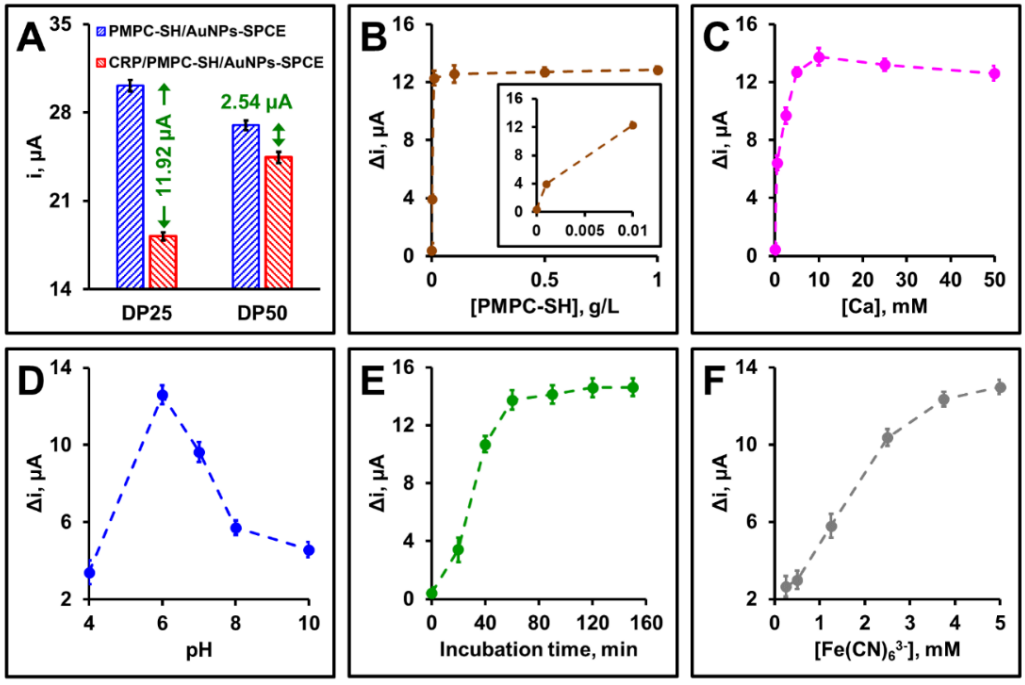

Figure 3.7 Optimization of important parameters for CRP detection using the PMPC-SH/AuNPs-SPCE/ PADs: DP of PMPC-SH (A), concentration of PMPC-SH (B), concentration of Ca^{2+} (C), pH (D), incubation time (E), and concentration of $[Fe(CN)_6]^{3-/4-}$(F).

PMPC-SH was tethered on the surface of the electrode and used for the detection of CRP. The phosphorylcholine functional group (PC) was responsible for reacting with the CRP at the CRP binding site in the presence of Ca^{2+}. PMPC-SH was distributed on the surface and allowed to assemble on the surface of the AuNPs-SPCE. To cover the surface of the electrode, the amount of PMPC-SH was optimized. The important parameters were 10 mM Ca^{2+}, 100 ng·mL^{-1} CRP and the DP of PMPC-SH of 25. Concentrations of PMPC-SH was varied as follows: 0, 0.001, 0.01, 0.1, 0.5, and 1 g·L^{-1}. The results are shown in Figure 3.7B. In this plot, ΔI increased for PMPC-

SH concentrations in a range of 0 – 0.01 g•L^{-1}, and then, saturation was reached. This outcome suggested that the PMPC-SH self-assembly corresponds to a Langmuir isotherm. Even when the PMPC-SH concentration was increased beyond 0.01 g•L^{-1}, ΔI remained unchanged. This indicated that a PMPC-SH concentration of 0.01 g•L^{-1} was certainly enough to attain a well-assembled PMPC layer, and the excess was entirely washed out from the electrode surface. Hence, the optimal concentration of PMPC-SH was 0.01 g•L^{-1} and was employed for the study of the analytical performance.

The CRP-Ca^{2+} interaction described by Christopeit et al. showed that the CRP-PC affinity is dependent on the concentration of Ca^{2+} [35]. There are reports of hypercalcemia and acidosis at sites of inflammation, infection, or tissue damage for the activation of CRP [36, 37]. Two free Ca^{2+} are involved in the binding between CRP and the PC group of lipid bilayers [38, 39]. For biomimetic synthetic PMPC-SH, Ca^{2+} showed low ($K_{D, low}$ = 0.03 mM) and high ($K_{D, high}$ = 5.45 mM) affinity towards CRP. The results also demonstrated a clear sigmodal shape, which represents two different behaviors of Ca^{2+} interaction with CRP. Therefore, the effects of Ca^{2+} concentration was therefore studied. For this experiment, concentrations of Ca^{2+} ranging from 0 mM to 50 mM were chosen. The results (in Figure 3.7C) indicated that the minimum concentration of Ca^{2+} that gives the highest ΔI is 10 mM. The total concentration of Ca^{2+} on the working electrode was 5 mM, which also corresponds to the $K_{D, high}$ of other reports. The affinity between amino acids such as glutamate, glutamine, aspartate, and asparagine on CRP towards Ca^{2+} is varied by pH. CRP sensor was demonstrated that at biological pH (~7.4), the best performance was achieved.

The self-assembled monolayers (SAMs) of thiol are pH dependent. SAMs were quite stable under acidic conditions; however, SAMs easily changed their binding in basic solutions. Kong et al. studied the effects of pH on the thickness of alkanethiol compounds assembled on a gold surface and found that the thickness of the compounds decreased with the increase of the pH [40]. Therefore, the pH of the solution for the self-assembly of PMPC-SH was also investigated. The crucial parameters for this experiment were 0.01 g L^{-1} PMPC-SH, 10 mM Ca^{2+}, and 100 ng mL^{-1} CRP. Phosphate buffer with different pH values were prepared including those with pH values of 4, 6, 7, 8, and 10. The results are shown in Figure 3.7D. As expected, ΔI decreased with increasing the pH above 6; however, ΔI at pH of 4 is considerably lower than that at pH of 6. This can be due to the desorption (or detachment) of the ligands considering protonation of the ligands by proton (H^+) [41]. Hence, the optimal condition for the self-assembly of PMPC-SH is at pH of 6 and this pH was used for all the experiments to follow.

The PMPC-SH was self-assembled on the AuNPs-SPCE by the thiol functional group for CRP detection. The incubation time between the polymer and the electrode was optimized. For

this, four different incubation times of 20, 40, 60, and 90 min were evaluated. The concentrations of the PMPC-SH, Ca^{2+}, and CRP used were 0.01 g•L^{-1}, 10 mM, and 100 ng mL^{-1}, respectively. As can be seen in Figure 3.7E, the minimum incubation time of PMPC-SH that can be used is 60 min at which the ΔI began to increase. Less than 60 min was not long enough for PMPC-SH to complete its SAM formation on the surface of the electrode, as the ΔI values became smaller. The period of 60 min was therefore considered as the optimal incubation time at which high ΔI values were obtained with proper reproducibility.

CRP detection was measured indirectly from the electron transfer of $[Fe(CN)_6]^{3-/4-}$ from the interface of the functionalized electrode. The concentration of the redox probe was optimized for high sensitivity for this sensor. To perform this experiment, 0.25, 0.5, 1.25, 2.5, 4, and 5 mM concentration of $[Fe(CN)_6]^{3-/4-}$ were dropped on PADs, and their currents were measured using DPV. In Figure 3.7F, it can be observed that the values of ΔI increased until a fixed value was reached. From a concentration above 4 mM, saturation of the current was produced, and therefore, the optimal concentration established to determine the calibration plot of CRP was 4 mM $[Fe(CN)_6]^{3-/4-}$

To produce the optimal CRP sensing system, important parameters expected to alter the performance of the sensor including the DPV parameters, deposition time for AuNPs, DP of PMPC-SH, concentration of PMPC-SH, pH, concentration of Ca^{2+}, incubation time, and concentration of $[Fe(CN)_6]^{3-/4-}$ were optimized. The first optimized parameter was the deposition time for AuNPs. Gold (III) solution (5 mM) was prepared in 0.2 M H_2SO_4 and electrodeposited onto the surface of the SPCE by applying constant potential at -0.4 V (vs Ag/AgCl). The deposition time was varied between 30 and 700 s. The results showed that the current was increased with increasing the deposition time from 30 to 200 s and was slightly decreased after 200 s (Figure 3.8A). This is due to the formation of larger AuNP agglomerates with long high deposition time (as shown in Figure 3.8), which decreased the electroactive surface area of the electrode and resulted in the depletion of the current [42]. Therefore, a deposition time of 200 s was chosen for the next experiments.

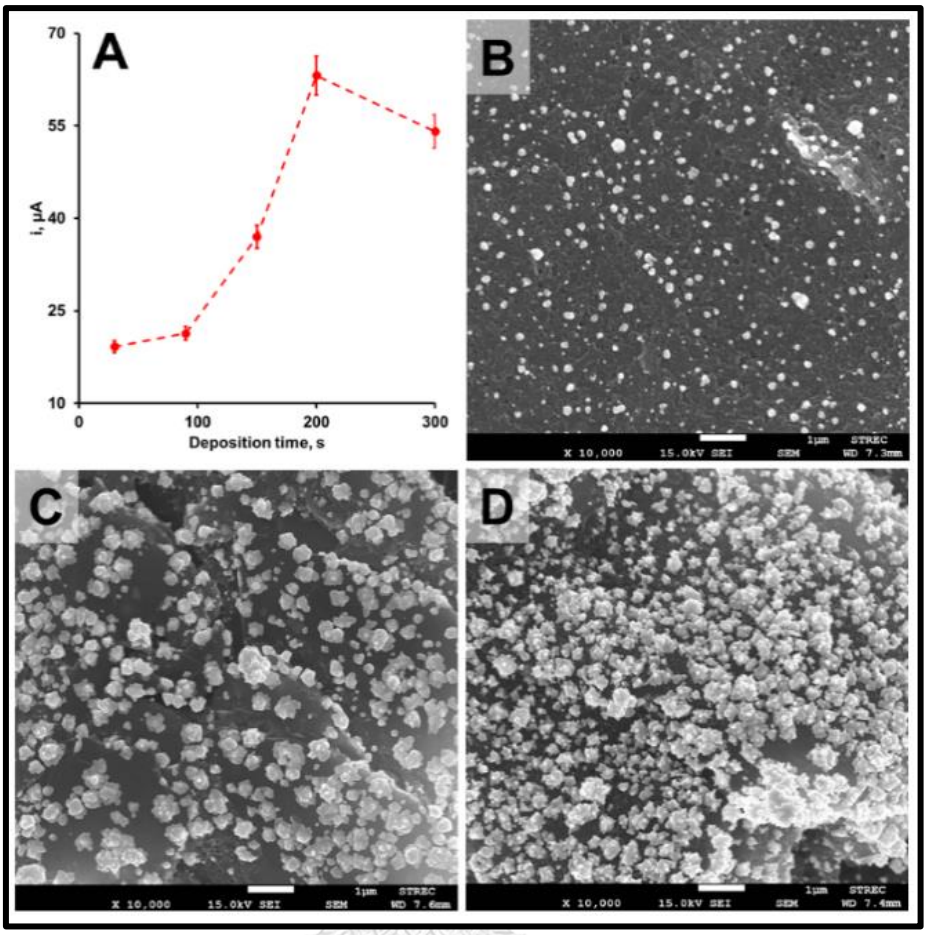

Figure 3.8 Study of the deposition time versus current A) and characterization of the AuNPs-SPCE evaluated by SEM using varied deposition time: 30 s, 200 s, and 700 s.

3.1.4.5. Analytical performance

The analytical performance of the sensor was evaluated with different concentrations of CRP. For this, the concentrations of CRP employed were in a range of 5 – 5000 ng•mL^{-1}. The optimal concentrations of PMPC-SH and Ca^{2+} as well as the incubation time were 0.01 g•L^{-1}, 10 mM, and 60 min, respectively. The PMPC-SH interacts with CRP through the PC binding site of the CRP pocket in the presence of Ca^{2+}. The results are shown in Figure 3.9A. In this representation, the current decreased with the increase in the concentration of CRP. This is because of the effect on the kinetics of the electron transfer reaction by $[Fe(CN)_6]^{3-/4-}$, which is delayed at the interface of the electrode, mostly due to the steric hindrance presented by the (PMPC-SH)-CRP formed. To evaluate the detection limit (LOD), sensitivity, and linear response range, a calibration plot was constructed. In this calibration plot (Figure 3.9B) differences in the current between the current of the blank and analytes (ΔI) were plotted versus the concentration of CRP. The linear relationship (R = 0.9969) between the ΔI and the concentration of CRP is according to the equation ΔI =

5.5096 log [CRP] + 19.408. All the measurements were performed with *n* = 3 replicates. The detection limit, 1.55 ng·mL^{-1}, was estimated as 3 times the standard deviation (*n* = 3) of the blank and the sensitivity (5.5096) is the slope of the calibration plot, with all of these in label-free conditions and uninvolved of the immunoassay which is the significant advantage of this work over other works presented by our group [43, 44]. In addition, a calibration plot with a linear range of 5 – 5000 ng·mL^{-1} CRP was obtained. The comparison of the analytical performance between this sensor and other sensors is presented in Table 3.1. In addition, the repeatability and stability of the CRP electrochemical sensors were investigated. Three different concentrations of CRP including 10, 100, and 1000 ng·mL^{-1} of five different sensors were measured for currents. %RSD of 1.36%, 0.99%, and 1.06% were obtained, respectively. The senior achieved a great stability (RSD < 1.34) after 8 weeks. Thus, this device exhibits the excellent potential for CRP detection with a good performance.

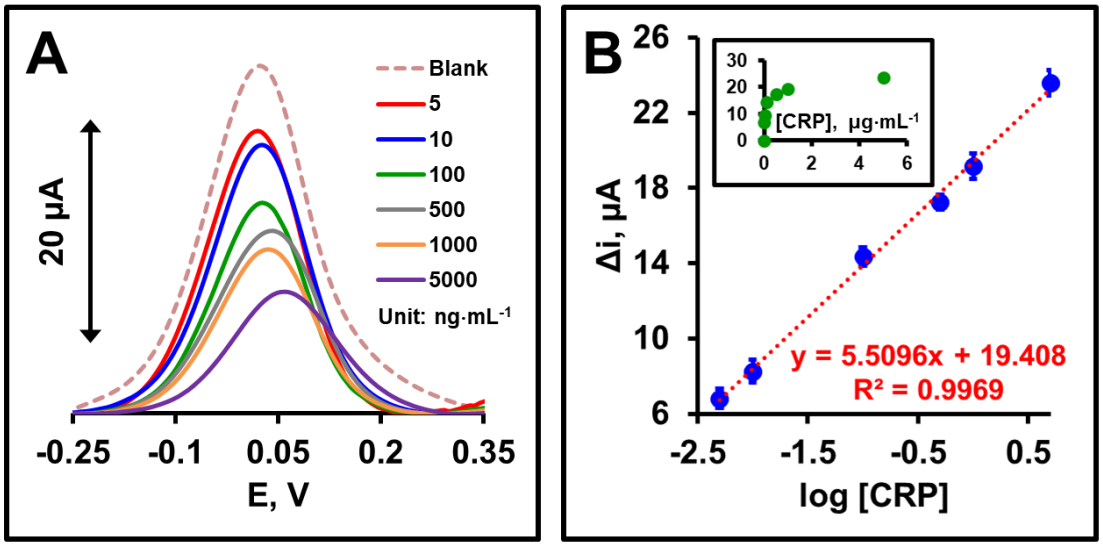

Figure 3.9 DPV plots for CRP detection with increasing CRP concentrations (A). Calibration curve vs logarithm of CRP concentration (B). Each value corresponds to replicated experiments (n = 3).

Table 3.1 Comparison of the analytical performance of other CRP sensors with the developed method

Materials	Substrate	Technique	Limit of detection (ng mL^{-1})	Linear dynamic range (µg mL^{-1})	Immunoassay approach	Ref.
anti-CRP	AuNPs/graphene/SPCE	EIS	15	50 – 100x10^3	Yes	[31]
Goat anti-human CRP polyclonal antibody	Gold electrode	EIS	20.24	0.058 – 5.75	Yes	[33]
anti-CRP	AuNPs/SPCE	Amperometry	17	0.047–23.6	Yes	[34]
Poly[MPC-co-BMA-co-MEONP]	Fe_3O_4 NPs	DLS	1.15 x 10^3	0 – 69	No	[19]
cytidine 5'-diphosphocholine sodium salt dihydrate-choline	Carbon screen printed paper-based electrochemical impedance device	EIS	1	0.005 – 500	No	[23]
PMPC-SH	AuNPs-SPCE/PADs	DPV	1.55	0.005 – 5	No	This work

3.1.4.6. Application in the analysis of CRP in human serum samples

An efficient electrochemical sensor must have a good selectivity. The impact of interferences can be studied from the value of the ΔI in the presence of other proteins. To show that the proposed sensor can detect CRP specifically in real serum samples, selectivity experiments were performed. The proteins studied were bilirubin, myoglobin, and albumin, proteins abundantly found in a real serum sample. The procedure used in this investigation follows identically to that previously reported [44] except for displacing proteins in the last step of the experiment. The concentration of the protein used in these selectivity assays was 1000 ng mL^{-1}, except 100 ng mL^{-1} for CRP. The concentrations of PMPC-SH and Ca^{2+}, as well as the incubation time were those optimized in the previous sections. The results are shown in Figure 3.10A. The results demonstrated that other proteins insignificantly influenced CRP detection. This is because PMPC-SH is resistant to the adsorption of nonspecific protein [45-47] but can be used for synthetic receptors for CRP. The antifouling property is another remarkable advantage of using biomimetic MPC polymer for a CRP sensor.

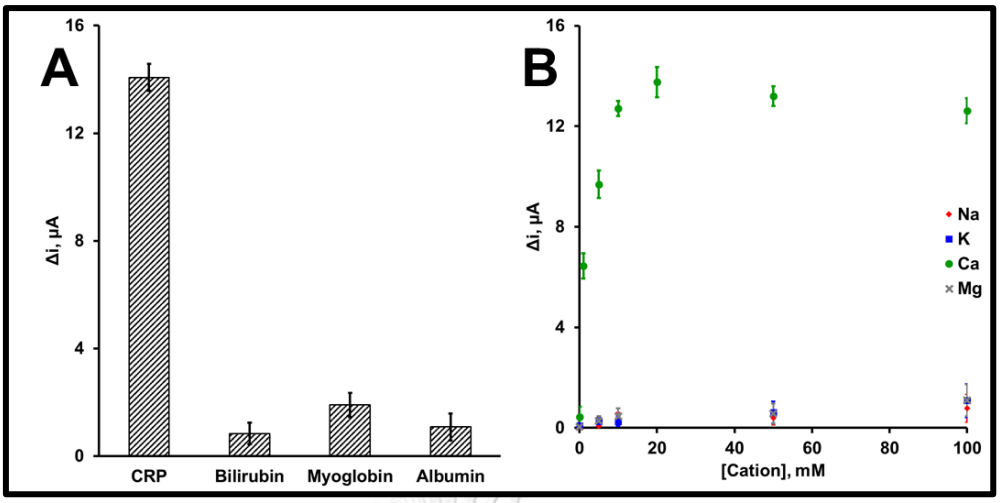

Figure 3.10 Selectivity of PMPC-SH for CRP (100 ng mL^{-1}) in the presence of bilirubin, myoglobin, and albumin at 1000 ng mL^{-1} (A). The effects of cations including Na^+, K^+, Ca^{2+}, and Mg^{2+} on the PMPC-SH/AuNPs-SPCE CRP sensor. Error bars are obtained based on three independent measurements.

In another pentraxin family such as serum amyloid P, which has 50% homology to CRP, there are reported binding sites for Ca^{2+} [48-50]. There are possibilities of different divalent cations that can be occupied the inside Ca^{2+} binding sites [51]. However, these ions have a lower affinity for the binding sites compared to Ca^{2+} leading to a weaker interaction with CRP. Even so, the physiological presence of these cations in the circulation system as well as the interactions of these cations are concentration dependent. Therefore, the effects of different cations on the developed sensors were studied. The concentrations of these ions are much higher than the relevant concentrations that have been observed in blood. From the results in Figure 3.10B, high ΔI values between the PC binding site and Ca^{2+} were obtained, whereas other ions including Na^+, K^+, and Mg^{2+} (other ions such as Mn^{2+}, Cu^{2+}, and Zn^{2+} are present in very low concentrations [52, 53]) have demonstrated much lower ΔI values. This phenomenon may be attributed to the induction of Ca^{2+} for the conformational change of CRP, which results in a more compact protein as well as decrease of the hydrodynamic radius of the protein [54]. Hence, our proposed CRP sensors can selectively detect CRP without influence from any physiological components.

CRP sensor was applied for CRP detection in a certified CRP reference material prepared in certified serum of human to demonstrate the feasibility of CRP sensor in real sample applications. The certified CRP sample was first diluted to the desired concentration using Tris-buffer, then determined for their anodic currents by DPV and recurred for their exact concentration by the external standard calibration. $T_{calculated}$ of the results from this method and

the label values equals to 0.01 which lower than t-value of 2.13. The statistical data suggests that this electrochemical CRP sensors agrees with the certified number calculated from serum sample at 95% confidence interval by a pair t-test. The analysis was done in triplet replications (n = 3), and the relative standard deviation was excellent (RSD ≤ 5%). Therefore, our method for CRP detection can be used as a novel and respectable sensor for the sensitive and fast analytical method of this inflammation marker.

Table 3.2 Comparison of the obtained results between the proposed method and standard CRP detection methods

[CRP]			T-test	
Standard method	Proposed method	%Recovery	$t_{critical}$	$t_{calculated}$
5.15	4.97 ± 0.57	96.60		
2.58	2.74 ± 0.88	106.46		
0.52	0.49 ± 0.18	95.95	2.13	0.10
0.10	0.10 ± 0.01	101.33		
0.00	ND	-		

3.1.5. Conclusions

The label-free detection of CRP with PMPC-SH self-assembled on a AuNPs-SPCE constructed with PADs was achieved. The gold nanoparticles exhibited good dispersion with an average size of ~60 nm. The surface area of the working electrode increased by 2.5-fold after the electrodeposition of AuNPs. PMPC-SH comprised of the thiol functional group was synthesized and anchored onto the AuNPs on the SPCE using sulfur-gold interactions. CRP can react with PMPC-SH using the PC binding site in the presence of Ca^{2+}. The CRP quantification was obtained from different electron transfers of $K_3Fe(CN)_6$ due to the formation of (PMPC-SH)-CRP compounds on the working electrode surface. The current change was inversely proportional to the CRP concentration. The study showed a dependency of only the Ca^{2+} concentration among other cations. Important parameters including the degree of polymerization, concentration of PMPC-SH, concentration of Ca^{2+}, and pH, were optimized. The sensor was highly sensitive with a limit of detection in the $ng{\cdot}mL^{-1}$ (1.55 $ng{\cdot}mL^{-1}$) range and a wide linear dynamic range (5 – 5000 $ng{\cdot}mL^{-1}$). The sensor was successfully applied to selectively and specifically detect certified CRP samples. The results from this method agreed with the concentration of the certified reference material. PMPC-SH tethered onto a AuNPs-SPCE on a PADs can serve as a useful, rapid, and inexpensive tool for the detection of inflammation and the control of CRP levels in plasma without the use of immunogenic substances.

3.2. Colorimetric sensor for determination of phosphate ions using anti-aggregation of 2-mercaptoethanesulfonate-modified silver nanoplates and europium ions

3.2.1. Abstract

A new, distinctive, and inexpensive colorimetric sensor for the detection of phosphate ions (Pi) performed on paper-based analytical devices (PADs) based on the anti-aggregation of 2-mercaptoethanesulfonate (MS)-modified silver nanoplates is proposed. An aggregation of MS-AgNPls due to the electrostatic interaction between the negatively charged sulfonate group on MS-AgNPls and europium ions (Eu^{3+}) causes a color change. Conversely, the color of MS-AgNPls remains unchanged in the presence of premixed Eu^{3+} with Pi because of the higher binding affinity that Eu^{3+} has towards Pi, leaving the AgNPls dispersed. An apparent color change from brown to red with the increasing amount of Pi can be observed by the naked eye on PADs and can be used for quantification by the measurement of color intensity using ImageJ software and determined with the color comparator. The aggregation and anti-aggregation of MS-AgNPls were characterized by TEM, UV-vis spectroscopy, and FT-IR to confirm the mechanism. This method can detect Pi in the range of 1 - 30 mg L^{-1}, with a detection limit of 0.33 mg L^{-1} (3SD/slope) and a limit of quantification equal to 1.01 mg L^{-1} (10SD/slope). The optimum parameters, including pH, MS and Eu^{3+} concentrations, reaction time, and interference effects, were studied. This method can be applied with the detection of Pi in real samples collected from soils, and the results agree with those of the standard method (UV-vis spectroscopy).

3.2.2. Introduction

Agricultural products are largely influenced by the quality of the environment, especially the soil [55, 56]. Phosphorus (P) is one of the most important elements found in soil and necessary for the development of plants. It helps the production of roots, strengthens the stem, promotes the growth of the flowers and fruits, and increases other elements' fixation, such as nitrogen [57]. The deficiency of phosphorus will lead to the slow development of seeds and other products [58-60]. This deficiency can be improved by adding excessive phosphorus fertilizer. However, redundant levels of phosphorus will harm the environment and cause eutrophication [61]. Therefore, the quantification of phosphorus in soil is important.

Currently, there are various methods, such as electrochemistry [62, 63], spectroscopy [64], and fluorometry [65], for P analysis. These methods provide high sensitivity and accuracy; however, sophisticated instruments and tedious sample preparation are required. Additionally, the experiments need to be performed in laboratory, which is unsuitable for cost-limited and on-site monitoring. Since their introduction in 2010 by Martinez et al., paper-based analytical devices (PADs) have emerged as a promising technology to address the growing need for simple, quantitative, and point-of-care assay platforms [66]. PADs have been used in various applications ranging from clinical diagnosis [67, 68] to environmental monitoring [69, 70] due to their low cost, ease of use, portability, and disposability [71, 72]. The fiber network of paper provides the ability for reagent storage. Additionally, the exposure to vase toxic chemicals to the researcher/user can be greatly reduced, because PADs require only a few microliters of sample and reagents. Colorimetric detection is the most common detection method in PADs due to its relatively simple operation and visual observation. The color change observed is proportional with analyte concentration and allows for direct analysis by the naked eye, digital camera or smartphone, with no personal scientific skill needed.

Colorimetric sensors based on principles of aggregation, anti-aggregation, or etching of noble metal and carbon nanoparticles, such as silver, gold nanoparticles, carbon nanodots, and graphene quantum dots, in the presence of target analytes are attractive to many researchers because of their selectivity, sensitivity, and simplicity [73, 74]. Among the noble metal nanoparticles, it is well known that silver nanoparticles (AgNPs) give the strongest surface plasmon resonance (SPR). AgNPs' physical and chemical properties are tunable by changing size and shape, and they are highly stable in the dispersion stage and biocompatible [75, 76]. Therefore, the studies have concentrated on detection of various biological and environmental markers using different shapes of AgNPs. For example, Chen et al. have developed triangular silver nanoplates (AgNPls) for H_2O_2 sensing. In that work, AgNPls was etched from triangle to

round shape in the presence of H_2O_2 and the absorbance at 670 nm was significantly decreased. The color change can be observed from blue to mauve [77]. AgNPls have higher ratio of lateral dimension to thickness and dominate an extreme degree of anisotropy. Therefore, a high tunability of their localized SPR is favor and maximum electromagnetic-field enhancement is created [78].

Recently, the colorimetric sensors based on anti-aggregation have been developed to enhance the sensitivity and selectivity of detection of target analytes [79, 80]. The key concept is based on the modification of nanoparticles' surfaces with specific binding ligands, such as oleylamine [81], cysteamine [82], and amino acids [83]. The addition of an aggregation agent can induce the aggregation of nanoparticles via crosslinking between the ligand and aggregation agent. In the presence of the target analyte, which has higher binding affinity with the aggregation agent than that of the ligand modifier, the target analyte will form complexes with the aggregation agent, leading to the redispersion of nanoparticles. Therefore, in this work, the detection of P is developed based on this concept. The aggregation agent used in this work is the europium ions (Eu^{3+}), because it is well-known that Eu^{3+} can strongly bind with phosphate ions (Pi) using the self-assembly of a ternary complex [84]. This advantage increases the selectivity of detection.

To the best of our knowledge, a simple, fast and cost-effective colorimetric sensor for the detection of Pi by the anti-aggregation of modified AgNPls on PADs has not been reported. In this work, we have developed a rapid, highly sensitive, and selective, PADs for detect and quantify the concentration of Pi in soil and water. The assay employed 2-mercaptoethanesulfate (MS) and Eu^{3+} as the surface modification ligand on AgNPls and aggregation agent, respectively. The color changes from purple to pink can be observed by naked eye and established in concentration dependent manner. Moreover, they were measured for the concentration using ImageJ software and color comparator developed in this work. The mechanisms were investigated by TEM, UV-vis spectroscopy (UV-vis), and FT-IR; and proposed. The optimal conditions, including pH, concentration of MS and Eu^{3+}, and reaction time were studied. Prior applying the sensors to real samples, the effect of interferences from metal ions and anions were investigated. Finally, the sensor was used with real samples and compared with conventional methods for Pi detection.

3.2.3. Experimentals

3.2.3.1. Chemicals and instruments

2-Mercaptoethansulfonic acid (MS), sodium orthophosphate (Na_3PO_4), ammonium molybdate ($(NH_4)_2MoO_4$), Trizma® hydrochloride, and Trizma® base were purchased from Sigma-Aldrich (St. Louis, MO, USA). Copper (II) sulfate ($CuSO_4$), sodium dihydrogen-orthophosphate 1-hydrate ($NaH_2PO_4.H_2O$), and L-ascorbic acid were obtained from BDH (BDH, England). Potassium sulphate (K_2SO_4) and sodium sulphate (Na_2SO_4) were obtained from Univar (Auckland, New Zealand). Iron (II) sulfate heptahydrate ($FeSO_4.7H_2O$), disodium hydrogen phosphate anhydrous (Na_2HPO_4), sodium hydrogen carbonate ($NaHCO_3$), and sodium hydroxide (NaOH) were purchased from Merck (Darmstadt, Germany). Sodium chloride (NaCl) was obtained from Carlo Erba Reagents (Carlo Erba, France). Europium ions (Eu^{3+}) were purchased as a liquid from SCP Science (SCP, Canada). Standard Zn^{2+} solution was acquired from BDH (Darmstadt, Germany). Silver nanoplates (AgNPIs) were obtained from the Sensor Research Unit, Faculty of Science, Department of Chemistry, Chulalongkorn University, Thailand. All chemicals were used as received without purification procedure. All chemicals were prepared in 25 mM Tris buffer pH 7 following the recipe from Sigma-Aldrich.

AgNPI images were captured for its anti-aggregation using an H-7650 transmission electron microscope (TEM) (Hitachi Model, Japan). The functional groups of MS and MS/AgNPIs were observed with an FT-IR spectrophotometer (Nicolet 6700, USA). A UV-vis spectroscopy system (Hewlett-Packard 8453E, Germany) was used for studying the AgNPIs' mechanism and validating the phosphate ion (Pi) amount in real samples. DLS was performed on Nanoparticle Analyzer model SZ-100, Horiba Scientific, Kyoto, Japan.

3.2.3.2. Synthesis and surface modification of AgNPls

AgNPIs were received from the Sensor Research Unit, Department of Chemistry, Faculty of Science, Chulalongkorn University as a gift [85]. They were synthesized by using a chemical reduction method. Concisely, $AgNO_3$ was stirred with $NaBH_4$ vigorously using homogenizer in a starch solution (2%(w/v)) which used as stabilizer of AgNPls. The yellowish solution of AgNPs were obtained and further undergone size conversation by reacting with H_2O_2 (1 mL H_2O_2: 10 mL AgNPs). The mixture was further stirred for 10 min to complete the shape transformation process. The finished AgNPls have pink color. For surface modification of AgNPls, the solution was diluted 2-fold and 4 mM of MS was added to the solution (10 µL MS: 990 µL AgNPls). Then, it was incubated under vibration (VTX-3000L Mixer, Ususio, Japan) for 2 hours at room temperature. MS-AgNPls obtained were characterized using UV-vis spectrometer and FT-IR.

3.2.3.3. Design and fabrication of PADs

In this work, PADs were fabricated employing wax printing method. First, PADs were designed using Adobe illustrator CS4 software. Each PADs have a circular shape surrounded by limiting area (wax). The dimensions of PADs are labeled in Figure 3.11. Next, the pattern was printed using wax printer (Xerox ColorQube 8570DN) onto Whatman No. 1 filter paper (A4 size). The wax area limits the flow of solutions (hydrophobic), while detection area was hydrophilic. Then, the paper was baked inside the oven at 150 °C for 1 min. After that PADs were cut out, and 180 PADs were obtained per a paper of A4 size. Finally, before PADs were ready to use, the tape was placed on one-side of PADs to prevent the leakage from the back. The whole fabrication process could be finished in 2 min.

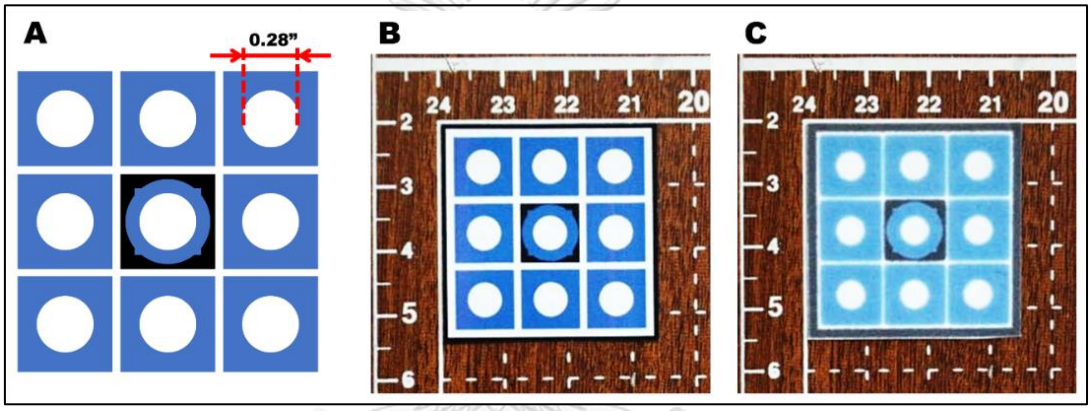

Figure 3.11 PADs designed used in this work labeled with size of a circle (inch) A), PADs before B) and after C) baked inside the oven at 150 °C for 1 minutes.

3.2.3.4. Colorimetric sensing of Pi on PADs

Prior to Pi detection, PADs (Figure 3.12) were prepared by dropping 0.5 µL of Eu^{3+} and MS-AgNPls to detection zone, respectively. For comparison, mixtures of Eu^{3+} and MS-AgNPls were dropped in the control zone. Next, PADs were allowed for chemicals to dry. Then, 1.0 µL samples of Pi were dropped on the same spot. The solution will be limited inside the detection zone. The reactions were completed within 3 min, and finally the color changes can be observed by the naked eye. For determination of color intensity, PADs were captured with a digital camera (Canon 1000 D1, Japan) and ImageJ software (National Institutes of Health, USA) was used for the analysis. The color intensity (red mode from RGB) of different detection spots was collected. In this experiment, the color changes were observed together with a blank (the control zone). The intensity in this work is reported as delta color intensity ($\Delta I = I_{analyte} - I_{blank}$). In addition to ImageJ, the color comparator was used for a quantification of Pi. The color changes were coerced to

nearest color chart and noted for the indicated concentration. Three results obtained from UV-vis, ImageJ, and color comparator were studied.

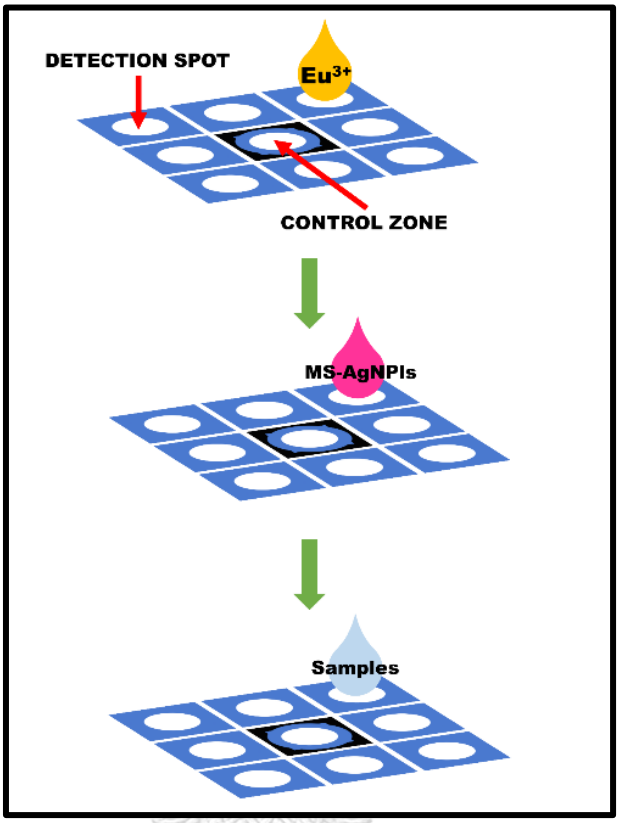

Figure 3.12 The design of PADs and their important positions including control zone and detection zone. The chemicals were dropped before PADs was used for Pi detection; 0.5 µL Eu^{3+} was dropped and 0.5 µL MS-AgNPls were dropped at detection zone, respectively

3.2.3.5. Real sample preparation

Soil samples, including organic matter, topsoil, and subsoil, were collected at different depths. Soil from organic matter was collected from the surface, whereas topsoil and subsoil were obtained at 20 centimeters and 50 centimeters below. The collected samples were left to dry for a week. Various concentrations of Pi were spiked into 2-gram soil samples and were adjusted to a volume of 20 mL in a conical flask with Tris buffer. The mixtures were incubated using an orbital shaker incubator (Ratek, Australia) at 180 rpm for 30 minutes and transferred into centrifuge tubes to perform centrifugation (Hettich Universal 320R, UK) at 5000 rpm for 30 minutes. Finally, the extracted solution was collected by filtering the supernatant through 0.45 µm nylon filter membranes. Water samples were used without extraction. The spiked samples were validated by the molybdenum blue method and compared with the proposed method.

3.2.4. Results and discussion

3.2.4.1. Characterization of MS-AgNPls

The synthesis of AgNPs was done by a chemical reduction method and were undergone shape transformation by H_2O_2 to create AgNPls (pink color). Then, MS-AgNPls were prepared by adding various concentrations of MS into AgNPls and incubating for 2 hours. To confirm the modification of MS onto the AgNPls, MS-AgNPls were characterized. First, the UV-vis results in Figure 3.13A show the SPR characteristic peak of AgNPls at 520 nm. The sharp and tall peak can demonstrate that the MS-AgNPls were monodispersed [86, 87]. Moreover, there is a slightly redshift of the SPR peak of the MS-AgNPls (blue line) from AgNPls (red line) because the plasma oscillation frequency around the AgNPls was decreased in the formation of MS-AgNPls [88]. Second, the shape and size of MS-AgNPls were characterized with TEM. From the TEM images in Figure 3.13B, MS-AgNPls have a circular shape with good dispersion. The size of the MS-AgNPls is 50 nm and similar to another literature review that they usually gives the UV-vis spectral peak at approximately 500 - 550 nm [89]. The results from TEM are thereby related with those from UV-vis. Third, FT-IR spectra was investigated for MS modification on the surface of the AgNPls. The spectrum of MS-AgNPls in Figure 3.13C (blue color) was compared with MS spectrum (red color). From the results, there are similarities of peaks between 1,000 – 1,700 cm^{-1} where the stretching modes of -C-H, -COO-, or -COOH occur. This result can be ascribed to the fact that MS was assembled on the surface of the AgNPls [90]. However, there are outstanding differences between the spectra. First, the characteristic peak of thiol (-S-H) at 2,550 cm^{-1} from MS is absent from MS-AgNPls [91, 92]. This demonstrates that -S-H bonds were cleave to form Ag-S bonds. During the formation of MS-AgNPls, the hydroxyl peak (-O-H) at 3,500 cm^{-1} of MS-AgNPls was wider compared to that of MS alone. It is possible that molecules of water were produced in the modification process of MS onto AgNPls [93]. In summary, the characterization results from three techniques were agreed. Thus, MS-AgNPls were successfully prepared.

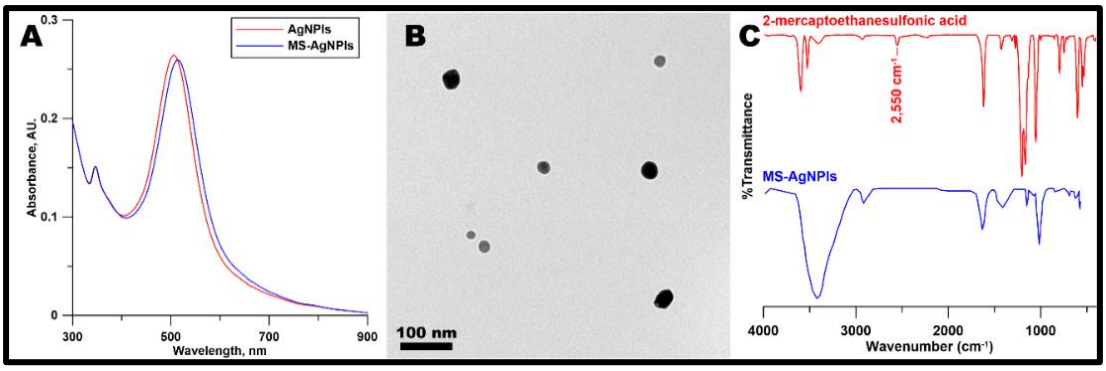

Figure 3.13 The characterization of unmodified AgNPls (red line, (a)) and MS-AgNPls (blue line, (b)) using UV–vis A), TEM images of well-dispersed MS-AgNPls B), FT-IR spectra of MS (red line, (a)) and MS-AgNPls (blue line, (b)) C (For interpretation of the references to colour in this figure legend, the reader is referred to the web version of this article)

3.2.4.2. Colorimetric detection of Pi based on the anti-aggregation of MS-AgNPls in the presence of Eu^{3+} (in the solution)

From the literature review, many publications demonstrated the cation-induced aggregation of metal nanoparticles modified surface. Aggregation agent (cations) could induce the aggregation by forming complexes with nanoparticles. In this work, modified AgNPls were obtained by bonding MS to the surface of AgNPls using Ag-S bonds and MS-AgNPls were yielded. They showed an SPR band at 500 nm (Figure 3.14 (red line)) and appeared pink (Figure 3.14, inset (a)). The MS-AgNPls were highly dispersed and randomly distributed due to the electrostatic repulsion of the negatively charged sulfonic group of the ligand. In the addition of Eu^{3+} to the MS-AgNPls solution, the color of MS-AgNPls solution changed from pink to purple (Figure 3.14, inset (b)). A new absorption band at 750 nm and a decrease in the intensity of the SPR band at 500 nm were observed as shown in Figure 3.14 (blue line). Further investigation was done by TEM (see Figure 3.14B), which showed that MS-AgNPls formed irregular and large clusters. Therefore, the addition of Eu^{3+} ions to a solution of MS-AgNPls resulted in the aggregation of MS-AgNPls. For Pi detection, the samples were added and allowed to incubate for 1 min. The color of MS-AgNPls solution changed from purple to pink as shown in inset Figure 3.14A (c), indicating the aggregated MS-AgNPls dispersed. TEM images (Figure 3.14C) also supported the anti-aggregation process. Moreover, the results from UV-vis in Figure 3.14A (green line) show the SPR peak at 500 nm of MS-AgNPls in the presence of Pi were similar to MS-AgNPls alone (red line), and the SPR peak at 750 nm cannot be observed. This phenomenon is corresponding to the TEM results that the MS-AgNPls are in the dispersion stage. Other evidences from dynamic light scatter (DLS) [94], shown in Figure 3.15, agrees with TEM and UV results. The zeta potential was shifted in the presence of

Eu^{3+} in MS-AgNPls solution (red line), while the peak potential and the size distribution of MS-AgNPls in the presence of both Eu^{3+} and Pi (green line) were similar MS-AgNPls alone (blue line). These are attributed to aggregation and anti-aggregation, respectively. The results suggest that Pi ions had stronger affinity with Eu^{3+} ions than with MS-AgNPls. Therefore, Eu^{3+} ions and Pi ions took the role of aggregation and anti-aggregation reagents, respectively. The changes in the solution color, induced by the competitive interactions of Eu^{3+} with MS-AgNPls and Pi ions, allowed the colorimetric detection of Pi ions by the naked eye. The mechanism is illustrated in Figure 3.16.

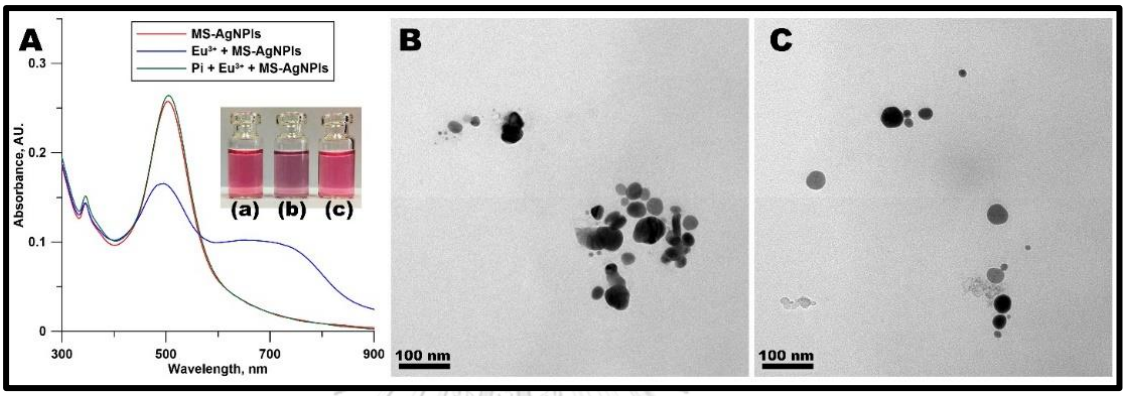

Figure 3.14 UV–vis studied in the solution of A) of MS-AgNPls (red line (a), inset (a)), 10 mg L^{-1} Eu^{3+} and MS-AgNPls (blue line (b), inset (b)), and 5 mg L^{-1} Pi, Eu^{3+}, and AgNPls (green line (c), inset (c)). TEM images of colorimetric detection of Pi based on anti-aggregation of MS-AgNPls in the presence of Eu^{3+} B), and in presence of both Pi and Eu^{3+} C) under the same conditions (For interpretation of the references to colour in this figure legend, the reader is referred to the web version of this article).

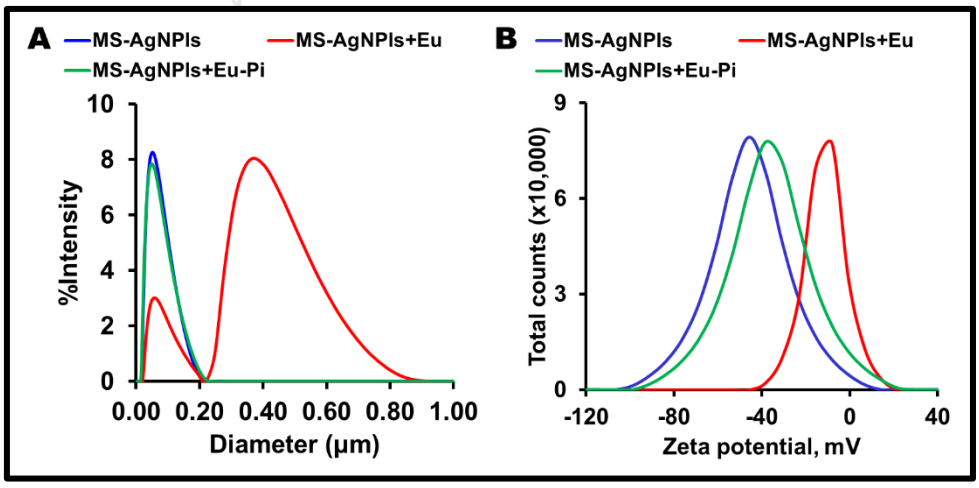

Figure 3.15 Dynamic light scattering (DLS) A) and zeta potential analysis B) of the MS-AgNPls (blue line), MS-AgNPls+Eu (red line), and MS-AgNPls+Eu-Pi (green line).

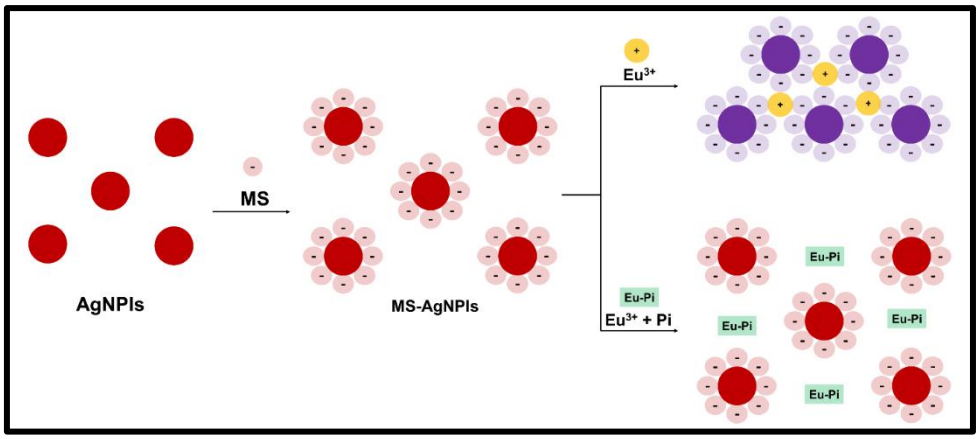

Figure 3.16 The proposed mechanism for colorimetric detection of Pi based on anti-aggregation of MS-AgNPls in the presence of Eu^{3+}.

3.2.4.3. Colorimetric detection of Pi based on the anti-aggregation of MS-AgNPls in the presence of Eu^{3+} (on PADs)

After the preparation and characterization of the MS-AgNPls, the interaction between MS-AgNPls in the presence of Eu^{3+} and for the sensing of Pi was investigated. The reaction was performed on PADs and observed by the naked eye, and the color intensity of the detection spot was measured using computer software (ImageJ). To compare the changes, three reactions were compared together, including the solutions containing MS-AgNPls and Tris buffer, MS-AgNPls and Eu^{3+}, and MS-AgNPls and premixed Eu-Pi. The results on PADs are shown in Figure 3.17A. The original color of MS-AgNPls are pink and remain the same color after Tris buffer was added. After adding Eu^{3+} into the solution of MS-AgNPls, the color of the solution changed from pink into purple. In contrast, in the addition of Eu-Pi into the MS-AgNPls, the color of the solution is unchanged. The color changes are clearly observed by the naked eye. PADs can be measured for their color intensity to achieve a quantitative measurement. The color intensity was obtained by drawing a circle in the ImageJ and measuring the red intensity from the RGB stack. The color intensities of red, blue, green, average, and gray portions are compared in Figure 3.17B. The color intensity was calculated as the difference of color intensity (ΔI), which is derived from the subtraction of the color intensity obtained from detection spot of the blank (the solution containing MS-AgNPls and Eu^{3+}) from the analyte (MS-AgNPls and Eu-Pi). From the results, it appears that the red intensity gives the highest difference between the detection spot of MS-AgNPls and Eu-P, and MS-AgNPls and Eu^{3+}. Therefore, the red channel was selected for quantitative analysis in this work. Moreover, in this work a color comparator (Figure 3.17C) was developed using the calibration curve for the detection Pi. The color charts with their

concentration (1 – 30 mg L^{-1}) labelled inside the box were printed onto A4 paper. The middle of the device was used to place PADs. The color comparators were not printed together with PADs using wax printer, because the color of the comparator can be altered upon heating PADs inside the oven. At least six color comparators were obtained from a single print. Furthermore, the color comparators can be reused once finished the analysis because they were not contaminated. The semiquantitative analysis of the proposed method for Pi sensing was simpler and faster without the needs of computer or smartphone.

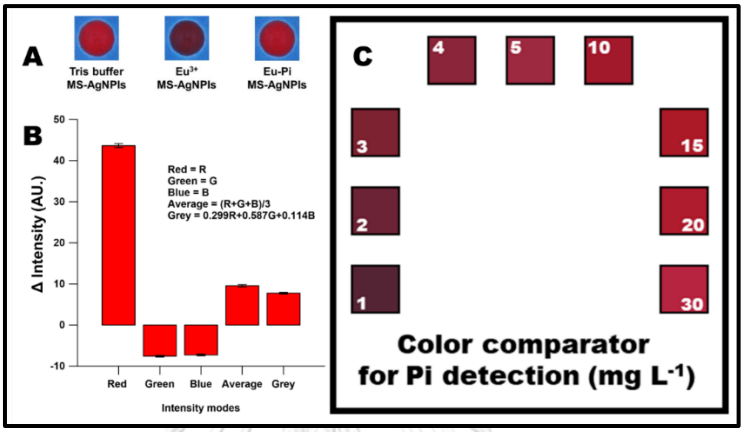

Figure 3.17 Colorimetric detection of Pi performed on PADs A), plot between intensity modes (red channel, green channel, blue channel, average intensity, and gray intensity) and the color intensity determined using ImageJ B), and the color comparator developed based on calibration curve (1 – 30 mg L^{-1}) in this work C).

3.2.4.3. Optimization of important parameters

To achieve the best analysis performance for Pi detection, the parameters of colorimetric assay including pH, concentration of Eu^{3+}, concentration of MS, and reaction time were optimized. Since, pH is the most important because it involves in the protonation and deprotonation of Pi, and the complexing of Eu^{3+}. Therefore, the effect of pH was study first as shown in Figure 3.18A. It can demonstrate that pH has affects the reaction of MS-AgNPls. The ΔI of detection spots at lower pH (than 7) is increased and reached the maximum at pH 7. In the acid condition the ΔI is increased with pH because Pi is more deprotonated ($H_2PO_4^-$ and HPO_4^{2-}) and more of Pi is available for interact with Eu^{3+}. However, the ΔI was decreased suddenly when the reaction was performed in the basic condition. This is due to the hydroxide can form complex with Eu^{3+} and precipitate the Eu ions from the solution. Hence, there is less Eu^{3+} in the solution to induce the aggregation of MS-AgNPls. The ΔI in basic solution is decreased as the pH

increased. The highest ΔI is occurred at pH 7, therefore the solutions in this work was adjusted to pH 7.

Next, the concentration of MS and Eu^{3+} were studied. The concentration of MS was varied from 0 – 8 mM and concentration of Eu^{3+} was 0 – 50 ppm (*Note*: ppm = mg L^{-1}). In this study MS was used to modify the surface of AgNPls so that the AgNPls will have the negative charges and Eu^{3+} was used to induce the aggregation of the MS-AgNPls. Therefore, these two parameters were studied together because they may interfere with each other. From the results in Figure 3.18B, the ΔI of the solutions are closed to zero when there was no MS modified on the surface of the AgNPls demonstrating that MS-AgNPls remain dispersed. It is due to the absent of negatively charged MS which cannot be aggregated in the addition of Eu^{3+}. The phenomenon is occurred according with when there was no Eu^{3+} added into the solution of MS-AgNPls. Consequently, the MS-AgNPls was dispersed and color intensity of the blank and analyte is almost equal. In the addition of MS and Eu^{3+}, the ΔI increase demonstrating that there is a significant difference between the color intensities of the blank and analyte. It can be indicated that the reactions were occurred. Interestingly, the increase of MS concentration results in the self-aggregation of the MS-AgNPls which leads to the decrease of the sensitivity. At MS equals to 4 mM gives the highest ΔI possibly because it gives the suitable surface modification of AgNPls. For the concentration of Eu^{3+}, 10 ppm is the best condition because it is limited by the concentration of Pi. The aggregation of MS-AgNPls was caused by the remnant of the Eu^{3+} after the reaction with Pi. In case of adding excess Eu^{3+} in the fix concentration of Pi compare with adding the equivalent amount of Eu^{3+} and Pi, the aggregation of the excess is higher and results in decreasing of the ΔI. According to the plots in Figure 3.18B, ΔI is decrease with the increase concentration Eu^{3+}. To achieve highest sensitivity for this sensor, the appropriate amount of Eu^{3+} must be compromised between giving the aggregation of the MS-AgNPls and providing the low detection limit of Pi. From comparing the ΔI obtained from various concentration of Eu^{3+}, it was selected at 10 ppm. In the next experiments, conditions of the reaction were pH 7, 4 mM MS, and 10 ppm Eu^{3+}.

Finally, the optimal reaction time was studied. The same PADs consisting of three detection spots (MS-AgNPls, MS-AgNPls and Eu^{3+}, and MS-AgNPls and premixed Eu-Pi) was measured for the ΔI at and 1-minute interval. The solutions were only dropped on PADs without mixing. Thus, the solutions required time for completely diffuse together and the color changed was stabilized. The results were shown in Figure 3.18C. From the results, the ΔI was increased sharply between 0 – 3 minutes and has no significant difference afterwards. Therefore, 3 minutes was selected as the optimal reaction time. Based on the above results, the optimal parameters

were pH 7, 4 mM MS, 10 ppm Eu^{3+}, and the reaction time 3 minutes. These conditions were used in the further experiments.

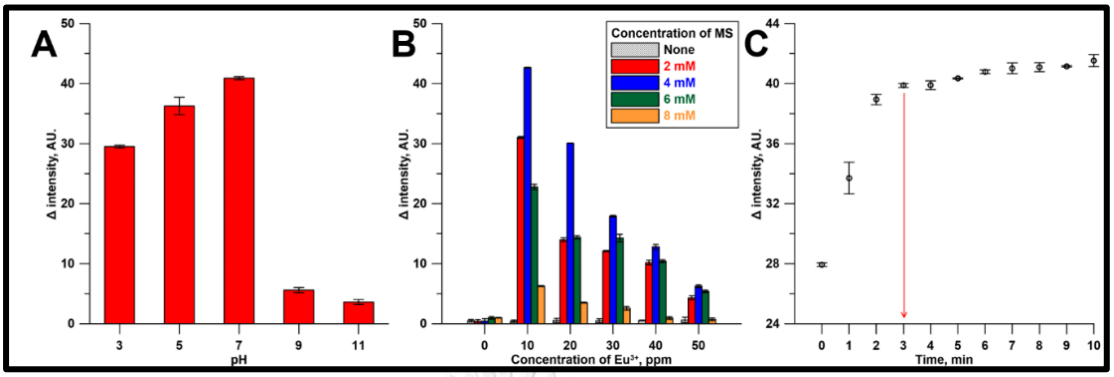

Figure 3.18 The study of optimal parameters including pH A), concentration of MS and Eu^{3+} B), and reaction time C), that could affect the performance of the colorimetric sensors for Pi detection.

3.2.4.4. Analytical performance

Under the optimized conditions, the performance of this Pi sensor was investigated by adding various concentrations of Pi into the reaction. The changing of color intensity was observed with the naked eye and measured with ImageJ. The results are illustrated in Figure 3.19. The ΔI is increased with the increase in the concentration of Pi. The calibration curve is plotted on the logarithmic scale (Figure 3.19A, inset (b)) and the linear range for Pi detection was found to be in the range of 1 – 30 mg L^{-1} Pi. The linear fitting equation is ΔI = 9.1331 * log [Pi] + 1.8292, with a coefficient of determination (R^2) equal to 0.9934. The detection limit (LOD) of the sensor ($3SD_{blank}$/slope) is calculated as 0.33 mg L^{-1}, and limit of quantification (LOQ, $10SD_{blank}$/slope) equals to 1.01 mg L^{-1}. The developed detection method of Pi is a semiquantitative method because the color change can be observed by the naked eye and the color intensity can be used for quantification of the Pi. Table 3.3 shows the performance of this sensor compared with other works; this developed method is comparable to others. Moreover, this method is more simple, cost-effective, portable and rapid. The stability of Pi sensors was studied every month for 12 months. Excellent stability was obtained for Pi detection (%RSD = 0.43 - 1.99 %). To evaluate the reproducibility of the developed method, seven sensors were employed. Pi detection was tested at concentrations of 1, 5, 30 mg L^{-1}. % RSD of 1.24%, 1.42%, and 0.29% were achieved, respectively. The results demonstrated that this assay has remarkably stability and reproducibility.

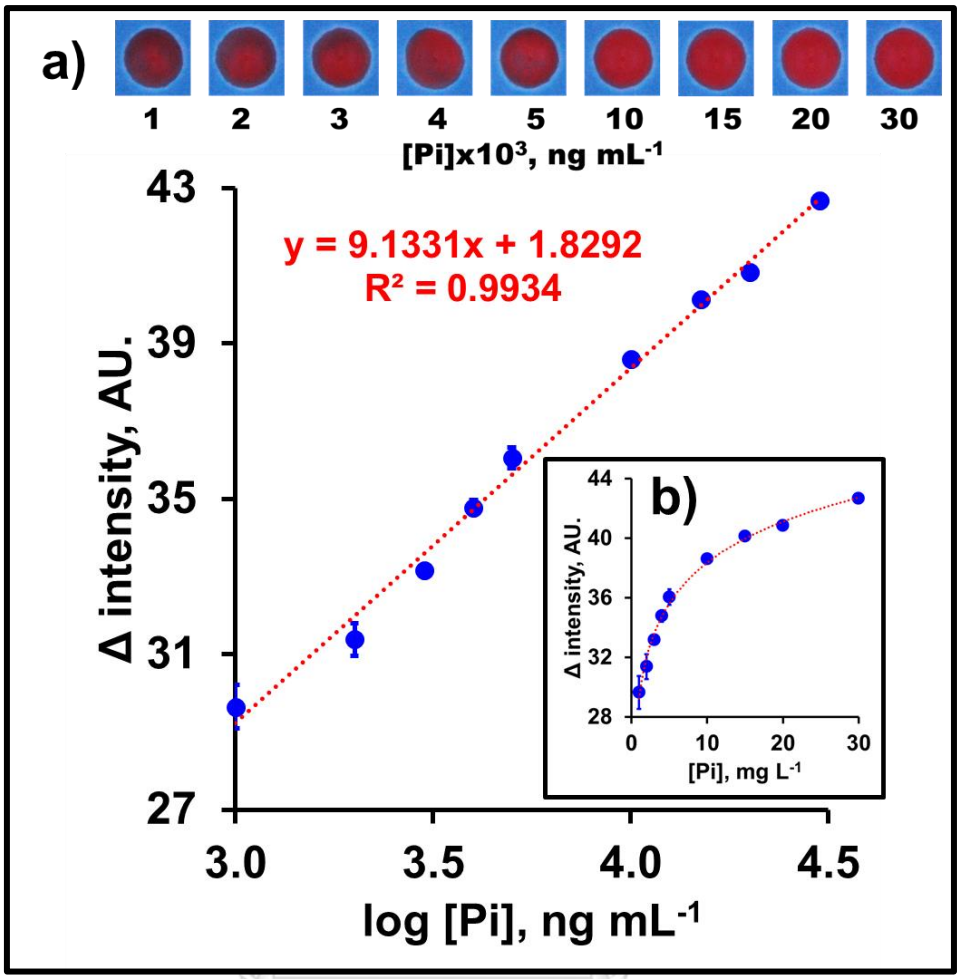

Figure 3.19 Calibration plot between ΔI and logarithmic of various Pi concentrations (mg L^{-1}) under optimal conditions; the photographic results performed on a single detection spot for Pi detection on PADs (inset (a)), and plot between ΔI and Pi concentration (mg L^{-1}) (inset (b)).

Table 3.3 Brief summary of sensing performances of different sensors for Pi detection

Colorimetric sensor	Linear range	Detection limit	Reference
MA-AuNPs	47.5 ng L^{-1} – 2.85 mg L^{-1}	7.22 ng L^{-1}	[95]
Rhodamine B-phosphomolybdate complex	0 – 665 ng mL^{-1}	47.5 ng mL^{-1}	[96]
$[Zn_2(H\text{-bpmp})]^{3+}$	0 – 47.5 mg L^{-1}	0.95 mg L^{-1}	[97]
$(NH_4)_2MoO_4$	9.5 – 950 mg L^{-1}	-	[98]
MS-AgNPls	1 – 30 mg L^{-1}	0.33 mg L^{-1}	This work

3.2.4.5. Selectivity and interference study

Selectivity is another important factor in colorimetric detection. Therefore, the effects of the detection of Pi towards other cations and anions were investigated. The cations and anions which were expected to be found in soil, including Na^{+}, K^{+}, Mg^{2+}, Ca^{2+}, Fe^{2+}, Fe^{3+}, Ni^{2+}, Co^{2+}, Cu^{2+}, Cd^{2+}, Pb^{2+}, Cl^{-}, HCO_3^{-}, CO_3^{2-}, and SO_4^{2-}, were studied. Figure 3.20A and Figure 3.20B shows the selectivity of the colorimetric assay for Pi detection. Most of the interfering ions cannot cause significant changes in the ΔI. Only Pi can interrupt the aggregation of MS-AgNPls by the complexation with Eu^{3+}, causing the color change from dark purple to pink. This can be observed by the naked eye. In addition, the influence of other ions on the anti-aggregation of MS-AgNPls by Pi was investigated (as shown in Figure 3.21). The experiments were performed in the mixture of Pi and other ions. The effects of cations were higher than anions because they can possibly react with MS-AgNPls using electrostatic force. However, Eu^{3+} prefer to engage with the oxygen donor atoms than that from other ions and molecules [99]. Therefore, Eu^{3+} interacts with MS-AgNPls and Pi more than other cations. Even though other cations were present in samples, most of the aggregation were strongly induced by Eu^{3+}. Hence, the detection of Pi using Eu^{3+}-induced aggregation of MS-AgNPls can perform without interferences from cations. In the case of anions, they show trivial effects on the reaction, which can be ignored. From these results, the sensors can be applied to the detection of Pi in soil and water effectively.

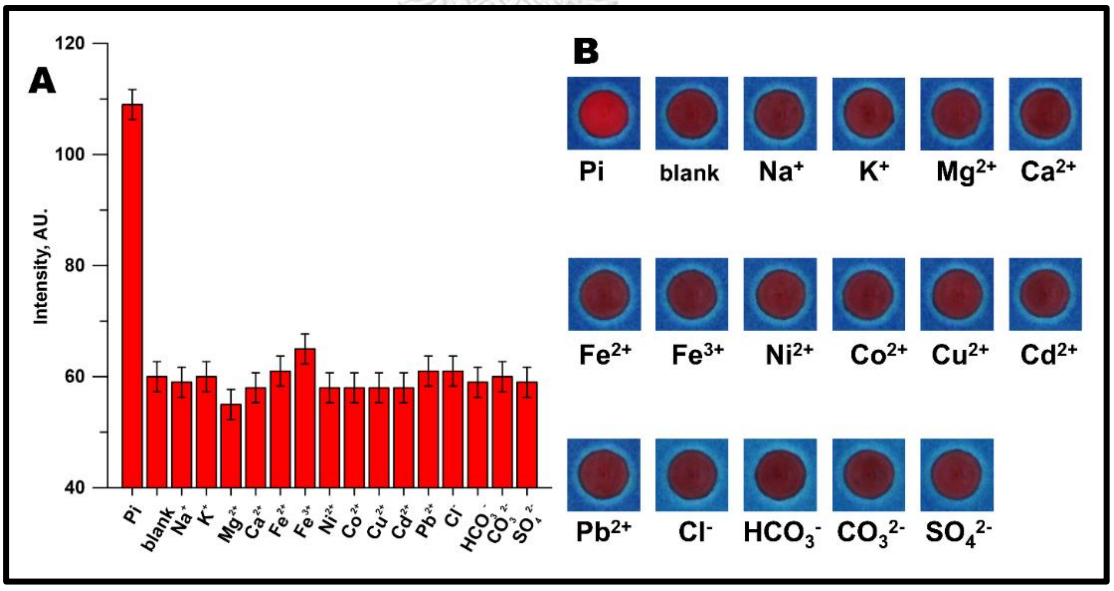

Figure 3.20 Color intensity A) measured from photographic results on PADs B) for the interference study of Pi detection in the presence of various ions. The concentrations of chemicals used in this study were 5 mg L^{-1} Pi, 200 mg L^{-1} interfering ions, and 10 mg L^{-1} Eu^{3+}. All chemicals were prepared and used under optimal conditions.

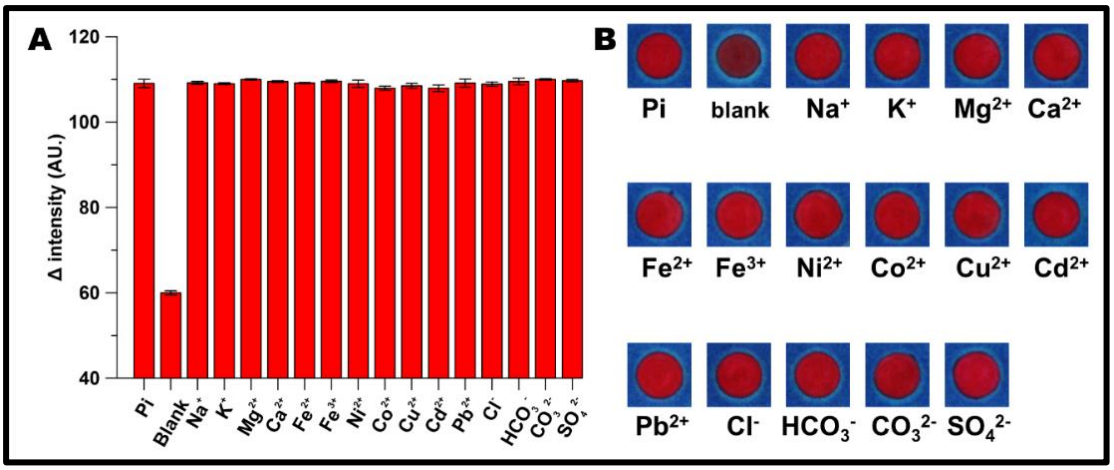

Figure 3.21 Color intensity A) measured from photographic results on PADs B) for the interference study of Pi detection in the presence of various ions. The concentrations of chemicals used in this study were 5 mg L^{-1} Pi, 200 mg L^{-1} interfering ions, and 10 mg L^{-1} Eu^{3+}. All chemicals were prepared and used under optimal conditions.

3.2.4.6. Real samples analysis

Samples in this work were collected from three different agricultural area in Thailand. Nutrients are dispersed in soil, and those close to the roots are absorbed and consumed in plants. Phosphorus, for example, is scattered throughout because of many factors, particularly water and can be dissolved in water and penetrate downwards because of water run-off. Therefore, water sampling from nearby area were also investigated. The percentage recoveries of Pi detected in soil samples were investigated by spiking different concentrations of Pi (mg L^{-1}) into the samples. The results are summarized in Table 3.4. The recoveries of the proposed method were found to be in the range of 91.2% and 98.7%, respectively. Additionally, the results obtained from our proposed sensor and standard UV-vis using molybdenum blue assay were compared. The good relationship between both methods was demonstrated (paired t-test at the 95% confidence level gave $t_{calculated}$ (0.467) below $t_{critical}$ at t = 1.701). This result indicated that the proposed method is capable of application in real soil samples.

Table 3.4 Comparison of performance and %recovery values for soil and water spiked with various concentrations of Pi between the standard method and the proposed method (n = 3)

Sample + Spike (mg L^{-1})	Measured concentration (mg L^{-1}) $\bar{x}$ ± SD (%Recovery)	
	Standard method	Proposed method
Water[a]	1.350 ± 0.034	1.343 ± 0.081
Soil[a]	1.208 ± 0.068	1.206 ± 0.016
Soil[a] + 5	6.021 ± 0.014 (96.3)	5.926 ± 0.077 (94.4)
Soil[a] + 10	11.08 ± 0.075 (98.8)	10.55 ± 0.077 (93.5)
Soil[a] + 20	21.08 ± 0.065 (99.3)	20.88 ± 0.004 (98.3)
Water[b]	1.059 ± 0.015	1.026 ± 0.057
Soil[b]	0.906 ± 0.049	0.864 ± 0.030
Soil[b] + 5	5.854 ± 0.007 (99.0)	5.705 ± 0.068 (96.8)
Soil[b] + 10	10.88 ± 0.035 (99.8)	10.73 ± 0.093 (98.7)
Soil[b] + 20	20.81 ± 0.081 (99.5)	20.13 ± 0.029 (96.3)
Water[c]	4.060 ± 0.007	4.028 ± 0.033
Soil[c]	3.455 ± 0.046	3.352 ± 0.036
Soil[c] + 5	8.201 ± 0.099 (94.9)	7.911 ± 0.085 (91.2)
Soil[c] + 10	13.44 ± 0.081 (99.9)	12.81 ± 0.003 (94.6)
Soil[c] + 20	23.35 ± 0.048 (99.5)	22.80 ± 0.053 (97.2)

[a], [b], and [c], indicate three different agricultural area where samples were collected for Pi detection.

In addition to the measurement of color intensity, color comparator was developed using the calibration plots and used for determination of Pi concentration. The colorimetric sensors were distributed to 30 volunteers to performed Pi detection with the color comparator and the results were reported in Table 3.5. Most of the population (more than 80%) disclosed the concentration correctly. The number of percentages is high at low concentration (1 – 2 mg L^{-1}) because the color from PADs was closed to 1 mg L^{-1} on the color comparator. However, the false identification was raised around 3 – 5 mg L^{-1} and 10 – 15 mg L^{-1}. This is attributed to those color with a complication to differentiate by the naked eyes. In this range, the intensity measurement and the developed calibration curve will be significant. The results were adequate to suggest the well-condition of Pi in the environment. PADs could be disposed of immediately after the analysis. Furthermore, the reaction required only a trace of chemicals compared to other methods. The total cost of the process performed on the paper device was 0.2 cents (US

currency), which is an extremely low cost with respect to the conventional method. Hence, the proposed platform possesses the capability for fast screening and high-throughput on-site phosphorus monitoring in resource-constrained settings.

Table 3.5 Photographic results of colorimetric Pi detection performed on PADs and concentrations of Pi evaluated using the color comparator developed from the calibration plot

Sample + Spike (mg L^{-1})	Photographic results	Estimated [Pi], mg L^{-1}	User conclusion (n=30)*
Water[a]		1 – 2	96.7%
Soil[a]		1 – 2	96.7%
Soil[a] + 5		5 – 10	83.3%
Soil[a] + 20		20 – 30	93.3%
Water[b]		1 – 2	96.7%
Soil[b]		1 – 2	96.7%
Soil[b] + 5		5 – 10	80.0%
Soil[b] + 20		20 – 30	90.0%
Water[c]		4 – 5	83.3%
Soil[c]		3 – 4	80.0%
Soil[c] + 5		5 – 10	86.6%
Soil[c] + 20		20 – 30	96.7%

[a], [b], and [c], indicate three different agricultural areas where samples were collected for Pi detection.

* User conclusion defines the %populations who indicate [Pi] within the "estimated [Pi]" correctly.

3.2.5. Conclusion

In this work, the determination of phosphorus in soil by a colorimetric method based on the anti-aggregation of MS-AgNPls was developed. The reaction involved the competition between Eu^{3+} and Pi for MS-AgNPls. The mechanism was characterized by TEM, UV-vis, and FT-IR. The results demonstrated that MS was bonded to the surface of AgNPls via Ag-S interaction. Moreover, the cation-induced aggregation was achieved by using Eu^{3+} as the aggregation agent. It was found that Pi can compete with MS-AgNPls for the binding to Eu^{3+}, and redispersed MS-AgNPls. The reaction can be monitored by the naked eye and quantify by determination of color intensity using ImageJ and color comparator. The proposed method was performed on PADs for the first time, which comprised the advantages of simple, rapid, and inexpensive instrumentation. The optimization conditions were 4 mM for MS, 10 ppm for Eu^{3+}, and 3 minutes for incubation time. Under the optimized conditions, the linearity of Pi detection on PADs was in the range of 1-30 mg L^{-1}. LOD and LOQ were as low as 0.33 mg L^{-1} and 1.01 mg L^{-1}, respectively. Interferences, including both cations and anions, were studied. The results show that there are no interfering effects from cations and anions. Finally, this method was applied in real samples and showed satisfactory results that agreed with those of the conventional method.

CHAPTER IV

The development of chromatographic techniques and its applications

In this chapter, lab-on-column couple electrochemical method was developed for neonicotinoids and amino acids. First, ultra-high-performance liquid chromatography was used for separation of four important neonicotinoids (dinotefuran, thiamethoxam, clothianidin, and imidacloprid) and detected on copper-gold nanoparticles electrodeposited on boron doped diamond electrode. The bimetallic nanoparticles modified electrode catalyst the electrochemical reduction and increase the electroactive surface area. Current signals were monitored by amperometry. The developed method was applied for neonicotinoid analysis in vegetable and honey samples with satisfactory results. Second, amino acids were separated by open tubular ion chromatography and detected using copper micro-electrode. The charges and size of amino acids provide difference affinity towards the anion-exchange resin (PA10) nanoparticles coated sulfonated electrode. Twelve amino acids were separated using the developed chromatographic method. The currents were monitored from oxidation of copper to copper ions and complexation between copper-amino compounds. Highly sensitive analytical method was successfully demonstrated for amino acids detection.

4.1. Cu-Au nanoparticles modified boron-doped diamond electrode coupled with ultra-high-performance liquid chromatography for amperometric detection of insecticides

4.1.1. Abstract

In this work, a novel electrochemical sensor using bimetallic nanoparticles of Cu and Au electrodeposited on boron doped diamond (BDD) electrode was developed for the detection of four significant insecticides (*Dinotefuran*, *Thiamethoxam*, *Clothianidin*, and *Imidacloprid*) after separation by ultra-high-performance liquid chromatography (u-HPLC). The fabricated nanocomposite modified BDD electrode was investigated for the morphology by scanning electron microscopy (SEM) and electrochemical impedance spectroscopy (EIS). u-HPLC methodology was performed in reverse-phased C18 column with an isocratic condition. The separation was accomplished through a mix of 7% acetonitrile and 0.01 M Britton Robinson buffer (pH 6.4) as a mobile phase. By the differential pulse voltammetry (DPV), CuNPs/AuNPs/BDD electrode enhances anodic peak currents of the insecticides substantially in compare with the bare BDD electrode. Under optimal conditions for amperometry (-1.6 V vs Ag/AgCl), wide linear dynamic range of insecticides was varied from 0.004 -1 mM (1.0 – 250 mg L^{-1}). Moreover, an excellent detection limit (3SD/slope) as low as 0.75 µM (0.19 – 0.62 mg L^{-1}) was achieved. Finally, this method was successfully applied for the measurement of concentration of insecticide compounds in the honey and vegetable samples with the percent recovered in the range of 97.40% - 101.92%. Thus, this electrochemical sensor based on Cu and Au nanocomposite modified BDD electrode couple with u-HPLC can rapidly, selectively, and sensitively detect important insecticides.

4.1.2. Introduction

Insecticides have a strong influence in agricultural industry as they help protect the food from nuisance pests and preserve food quality. Even though the use of these compounds can minimize the cost of food production, their residues are harmful to human and require a scrutinized inspection. One of the popular insecticides is the group of neonicotinoids introducing in early 1990s [100], the compound consists of nitro group and several N-containing ring. It is renowned as the most effective chemicals for controlling biting insect pests such as aphides, whiteflies, and some micro lepidoptera by attacking the nicotinic acetylcholine receptor (nAChR) and paralyzed the insects' central nervous system [101, 102]. Upon contamination to crops, these compounds can be transported to all parts of plant including pollen or nectar which bees and other pollinating insects collect and consumed [103]. Consequently, many plants are likely to absorb the insecticides easily through the reproduction process. For that reason, the use of neonicotinoids is questioned by the European Food Safety Authority (EFSA) [104]. Since 2013 some neonicotinoids including thiamethoxam, clothianidin, and imidacloprid were restricted [105]. European Union has designated maximum residue limit (MRLs) of acetamiprid in tea should be less than 100 μg kg^{-1} [106]. Japan also set the MRLs of imidacloprid in milk and chicken at 20 μg kg^{-1} [107]. Currently, more countries are considered the toxicity of insecticides seriously.

Various analytical approaches have been useful for detection of neonicotinoids such as UV-visible spectrometry [108], mass spectrometry [109], capillary electrophoresis [110], and etc. However, those assays are either offers high sensitivity with tedious laboratory practice or simple, unfortunately low sensitivity. Among others, electrochemical methods are convincing because it can offer remarkable sensitivity with simple, fast, and cost-effective detection [111]. Moreover, this technique can be coupled with flow analysis such as liquid chromatography, flow injection, and on-chip devices [112]. Chromatography is the most powerful method for separation utilizing the appropriate column, particularly when the plenty of mixtures were determined simultaneously. Nowadays, a commercially available system namely ultra-high-performance liquid chromatography or u-HPLC using sub 2 μm particle size and high-pressure pump (>10,000 psi) are successful for the isolation of the complex samples [113]. Moreover, the method is automatic, high-throughput, and provide high reproducibility. Therefore, u-HPLC was employed for the separation of neonicotinoids before detection by the electrochemical method.

The common analytical method in the electrochemistry is voltammetry. There are three electrodes employed in voltammetry, but the most significant electrode is the working electrode. The sensitivity of the detection relied chiefly on the conductivity of the material that used for a fabrication. A boron-doped diamond (BDD) electrode has proved to be a competent

electrode in substitution to other electrodes such as glassy carbon electrode or platinum electrode. Its good characteristics including wide detection potential window (≥ 3.5 V), high reproducibility, low surface absorption property, and stability to corrosive draw attentions for several applications [114-116]. In 2016, Brahim, M. B., et al. have published BDD for imidacloprid detection using square-wave voltammetry as analytical techniques [117]. The detection baseline was stable and allowed for the detection limit as low as 8.60 μM. To improve the sensitivity of the electrode, plenty of researches have demonstrated the use of metal electrodeposited electrode for the detection of insecticides. Lezi, N., and Economou, A. have developed sputter bismuth on disposable screen-printed electrode for the detection of neonicotinoids [118]. It was found that the capacitive current was increased and the current of the analyte was elevated accordingly. The detection limit was approximately 0.04 – 0.07 μM. In addition to metal, the nano-sizes particles were considered a great conductor with catalytic property as demonstrated by numerous of publications. Our group also reported gold nanoparticles modified BDD for the detection of arsenic ions [119], and gold-platinum nanoparticles for the determination of glucose [120]. The results reflect the catalytic features of the metal nanoparticles in which enhance reaction and enlarge the electroactive surface area of the electrode. Despite the good properties of the metal nanoparticles, there is no reports of the metal nanoparticles for the neonicotinoid's detection. Therefore, this work interested in the metal nanoparticles modified electrode for the detection of important neonicotinoids.

In this study, the bimetallic nanoparticles comprising of copper nanoparticles (CuNPs) and gold nanoparticles (AuNPs) were electrodeposited on BDD electrode (CuNPs/AuNPs/BDD) for the detection of four insecticides (dinotefuran, thiamethoxam, clothianidin, and imidacloprid) after the separation by u-HPLC in reverse phase mode. The redox reaction of the analytes has been described. The modified electrodes were characterized by scanning electron microscope (SEM), electrochemical impedance spectroscopy (EIS), and cyclic voltammetry (CV). Various conditions for electrode modification, u-HPLC separation and amperomtric detection were optimized. Under optimal conditions, different concentrations of analytes were injected into u-HPLC and measured for the current signal for constructing the calibration curve. Finally, u-HPLC coupled amperometry developed in this work were applied for the determination of neonicotinoids in real vegetable and honey sample.

4.1.3. Experimental

4.1.3.1. Chemicals

Four insecticides including dinotefuran, thiamethoxam, clothianidin, and imidacloprid were purchased from The LGH Labor GmBH (Augsburg, Germany). Britton Robinson buffer (BRB) is consists of boric acid, acetic acid, sodium hydroxide (Merck, Darmstadt, Germany), and phosphoric acid (Carlo Erba Reagents, Barcelona, Spain). BRB at different pH were adjusted by mixing different proportions of the chemicals. Potassium tetrachloroaurate (III) ($K[AuCl_4]$) was purchased from Wako Chemicals, Japan. Copper (II) sulfate ($CuSO_4$) was obtained from BDH (BDH, England). The metal ions solutions were prepared in 0.2 M sulfuric acid (H_2SO_4). Potassium hexacyanoferrate (III) ($K_3Fe(CN)_6$) was purchased from Riedel-de Haën (Lower Saxony, Germany) and prepared in 0.1 M potassium chloride (KCl) for a characterization of the electrodes. Millipore Milli-Q purified water (18.2 MΩ cm) was used throughout the experiments. All chemicals and reagents used in this work are of analytical grade except when stated. A chromatographic grade acetonitrile was obtained from Merck, Darmstadt, Germany and employed as organic solvent for u-HPLC experiments.

The standard solutions of insecticides at different concentrations were diluted with acetonitrile : Milli-Q water (50:50) from the stock solutions (10 mM) prepared in the same solvent. The solutions were filtered through with 0.22 µm nylon membrane before use in all u-HPLC experiments. The standard solutions were kept in the amber vial to protect the insecticides from the light degradation.

4.1.3.2. Electrodes

The boron-doped diamond (BDD) electrode (0.75 × 2 cm) was employed as the working electrode. A platinum (Pt) wire and Ag/AgCl were used as an auxiliary and reference electrode, respectively. CuNPs/AuNPs/BDD were prepared by electrodeposited metallic nanoparticles step-wisely. First, an applied potential at -0.4 V were constantly applied to the BDD immersed in the solutions of gold solution (5 mM) for 30 seconds to reduce Au^{3+} to Au^0. Next, the AuNPs modified BDD electrode was thoroughly rinsed with deionized water and blow with N_2 gas until dry. Then, CuNPs were electrodeposited by applying fixed current of -225 µA to the AuNPs/BDD electrode for 90 seconds immersed in $CuSO_4$ solution (5 mM). Cu^0 nanoparticles were obtained because of an electrochemical reduction of Cu^{2+} on the electrode. After that, the surface of CuNPs/AuNPs/BDD were stabilized by performing cyclic voltammetry from 0 to 1 V for 20 cycles (0.1 V/s) in 0.1 M NaOH to prevent spontaneous oxidation of copper due to oxygen [121]. Finally, the bimetallic modified electrode was rinsed and dry as previously mention. The solution was

continuously stirred with a magnetic stir bar during the electrodeposition step. The surface morphology of CuNPs/AuNPs/BDD was studied by scanning electron microscopy (SEM) using a JSM7610 field emission scanning electron microscope (FESEM, JEOL Ltd., Japan). The high-resolution images were obtained at 5.0 kV SEI with a magnification of x10,000. Electrochemical impedance spectroscopy (EIS) measurements were performed on a PalmSens4 potentiostat/impedance analyzer (Palmsense BV, Netherland) and controlled with PSTrace software. The EIS was accomplished under the following conditions: 5 s $t_{equilibration}$, 0.1 MHz maximum frequency, 0.01 Hz minimum frequency, and 0.1 V E_{ac}. EIS experiments were carried out at room temperature.

4.1.3.3. Electrochemical measurement

Chronoamperometric experiments were studied with a CHI 660B electrochemical workstation (CH Instruments, Austin, TX). The detector in this work is a three-electrode system. The working electrode were as prepared CuNPs/AuNPs/BDD (geometric area = 0.3 cm^2). The reference and counter electrode were Ag/AgCl and stainless-steel tube, respectively. The modified electrode was stood in the middle of the flow cell where the reduction occurs. The channel between the inlet/outlet and the electrode are separated by a thick silicon rubber gasket (~1 mm). The processing of current signal was done using CH instrument potentiostat 1232A.

4.1.3.4. u-HPLC instrumentation

Chromatographic separations were performed using a KinetexTM core-shell C18 column (2.6 µm particle size, 50 mm x 4.6 mm i.d., Phenomenex Inc., CA, USA) with a reversed-phase mode. The u-HPLC pump model is LC-20ADXR (Shimadzu Corporation, Japan), with a 0.1–100 mL loop autosampler (SIL-20 A). Data obtained from the UV-visible detector (SPD-M20A) were obtained at a wavelength of 265 nm and analyzed with LC solution software (Shimadzu Corporation, Japan). The separation conditions were: 7% acetonitrile (organic solvent) mixed with 93% 0.01 M BRB pH 6.4, flow rate 1 mL min^{-1}, injection volume 7 µL, run time 10 min, and detection potential -1.6 V (vs. Ag/AgCl). C18 column was incubated in the oven which set at a temperature of 37 °C. The UV-visible detection cell was fixed at the same condition. All experiments were performed in three replications. The schematic of the instrumentation is presented in Figure 4.1.

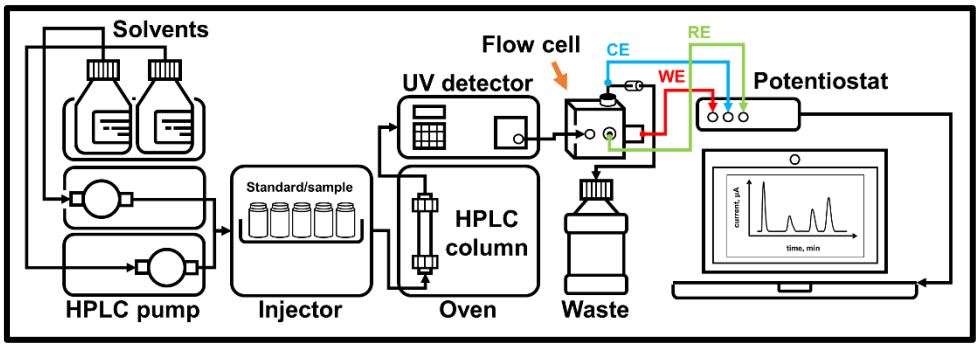

Figure 4.1 Schematic of u-HPLC consisting of solvents deliver, 2 pumps, sample injector, analytical column, UV-vis and electrochemical detector, wastebottle, and data acquisition unit. WE, CE, and RE are working, counter, and reference electrode, respectively.

4.1.3.5. Sample preparation for u-HPLC

A water spinach, kale, and two types of honey were purchased from local markets of Bangkok.

Vegetable samples: Acetonitrile of a volume 40 mL was added to chopped dry sample (10 g) and blended mechanically for 3 minutes by a juice blender. The mixtures were then centrifuged (4000 rpm) for 30 min until a clear solution was obtained. Next, the supernatant was filtered through a Buchner funnel with 0.2 µm filter and transferred to round bottom flask to evaporate the organic solvent using rotary vacuum evaporator. The residue was re-dissolved in 1 mL of acetonitrile and deionized water (50:50) fortifying with neonicotinoids used in this work and filtered through 0.2 µm (nylon membrane). Three samples were prepared accordingly and added with various concentrations of neonicotinoids; 0.04, 0.2, and 0.4 mM. Finally, the solutions were directly injected into the u-HPLC system. The concentrations of the analytes were determined using the standard addition method and compared with the blank sample prepared with the same procedure.

Honey samples: 1 g of honey was dissolved completely in 2 mL of deionized water by agitation with the shaker for 5 min, after 6.5 mL of acetonitrile was added. The mixtures were centrifuged (4000 rpm, 30 min) to separate the organic and aqueous phase. Next, the supernatant was evaporated under N_2 gas until 100 µL was remained and spiked with neonicotinoids. After that the solutions were adjusted to desired concentrations of analytes and made up to 1 mL with acetonitrile:water (50:50). Finally, the solution was filtered through 0.2 µm nylon membrane before injection the u-HPLC system.

4.1.4. Results and discussion

4.1.4.1. Characterization of CuNPs/AuNPs modified BDD electrode

The surface morphology of the electrodes was investigated by field emission scanning electron microscopy (FESEM) and electrochemical impedance spectroscopy (EIS). Figure 4.2A displays a typical BDD electrode surface comprising of crystal faces or grains with different conductivity as a result from partly accumulated boron dopant [122]. After AuNPs electrodeposited on BDD, it is clearly observed that flower-like structure of AuNPs were isolated evenly among numerous tiny nanoparticles regardless of BDD edges as shown in Figure 4.2B. For CuNPs/BDD results (Figure 4.2C), CuNPs were smaller than AuNPs and non-uniformly presented on the grains of BDD. This is attributed to the high conductivity of boron concentration at the fringe position [123]. The distribution of the CuNPs/AuNPs bimetallic nanoparticles materials deposited BDD in Figure 4.2D contrasts with CuNPs/BDD that the nanoparticles were homogeneously dispersed throughout the electrode surface because CuNPs can grow on both the conductive site of the diamond layer and AuNPs [124]. This result suggests that AuNPs is responsible for the negative charges on the electrode surface in which Cu^{2+} can be reduced to Cu^{0} preferably [120]. Moreover, the study of an elemental mapping (see Figure 4.2(a)-(-d)) agrees with the results from FE-SEM that the AuNPs and CuNPs were uniformly distributed on the electrode surface. Thus, there are a significant amount of nanocatalysts electrodeposited on the electrode surface.

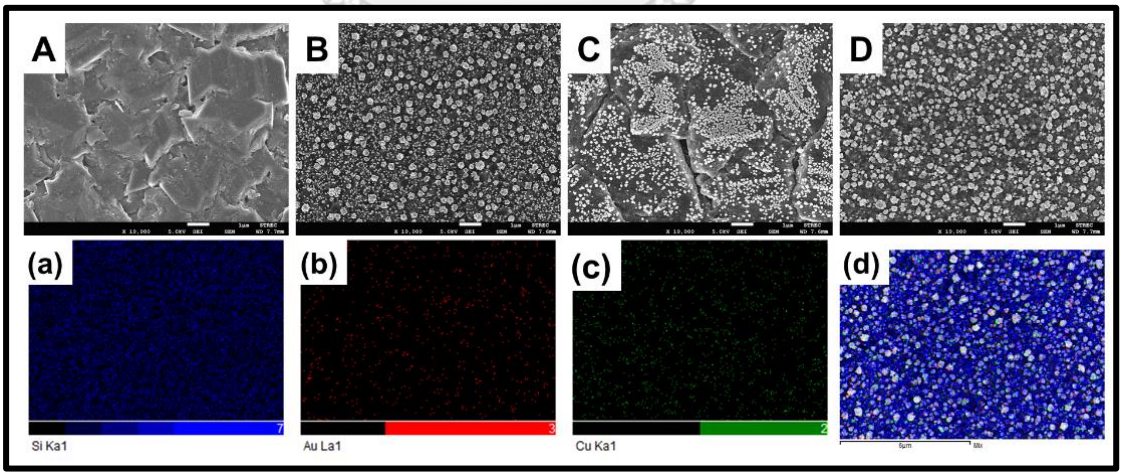

Figure 4.2 SEM images of bare BDD (A), AuNPs/BDD (B), CuNPs/BDD (C), and CuNPs/AuNPs/BDD (D); and their elemental mapping BDD (a), AuNPs/BDD (b), CuNPs/BDD (c), CuNPs/AuNPs/BDD (d). The color represents silicon (blue color), gold (red color), and copper (green).

The conductivity from different electrodes were studied by EIS techniques and their Nyquist plots are shown in Figure 4.3A. From the curve, the charge transfer resistance or R_{ct} of $Fe(CN)_6^{3-/4-}$ can be identified from the diameter of the semicircle. R_{ct} equals to 120, 1.92, 2.10, and 0.96 kΩ of BDD, AuNPs/BDD, CuNPs/BDD, and CuNPs/AuNPs/BDD, respectively. Surprisingly R_{ct} of metal nanoparticles modified electrode was much lower than BDD indicating that the nanoparticles can facilitate the electrons transfer of the electroactive species to the electrode interface. This phenomenon assures that the enhancement of the conductivity derived from gold and copper nanocatalyst electrodeposited on the electrode surface. Additionally, CuNPs/AuNPs/BDD demonstrated the high conductivity compared with others electrode. Hence, the outstanding sensitivity can be achieved with bimetallic nanoparticles modified electrode.

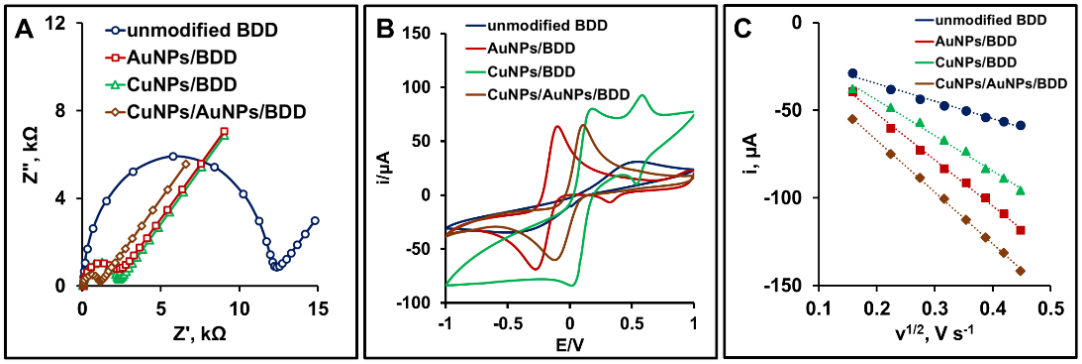

Figure 4.3 Nyquist plots (A), cyclic voltammogram (B), and plots between square root of scan rate ($v^{1/2}$, $V\ s^{-1}$) and current (μA) of unmodified BDD (blue line), AuNPs/BDD (red line), CuNPs/BDD (green line), and CuNPs/AuNPs/BDD (brown line). Testing solution is 5 mM $Fe(CN)_6^{3-/4-}$ in 0.1 M KCl.

The electroactive surface area of metallic nanoparticles modified electrode were studied with a cyclic voltammetry. To estimate the area, each electrode was employed for the measurement of current at different scan rates in the presence of $[Fe(CN)_6]^{3-/4-}$. This active species was involved in this experiment because they possess fast electron transfer characteristic and the number of electron transfer is known (n=1). Figure 4.3C shows the cyclic voltammograms of BDD, AuNPs/BDD, CuNPs/BDD, and CuNPs/AuNPs/BDD at different scan rates. The equivalent cathodic and anodic peak are observed; therefore, the electrochemical reaction is reversible. The Randles-Sevcik equation (Equation (21)) was employed for the determination of the active surface area:

$$i_p=(2.99x10^5)\alpha n^{3/2}ACD^{1/2}\nu^{1/2} \quad (21)$$

Where i_p is the peak current (A)

D is the diffusion coefficient of $[Fe(CN)_6]^{3-/4-}$ ($7.60x10^{-6}$ cm^2 s^{-1} in 0.1 M KCl)

C is the concentration of $[Fe(CN)_6]^{3-/4-}$ (mol cm^{-3})

n is the number of involved electrons in the reaction

α is the transfer coefficient (0.5)

ν is the scan rate (V s^{-1}).

From the plot between i_p and $\nu^{1/2}$, the electroactive area of the electrodes is calculated to be 0.1703, 0.4465, 0.3447, and 0.5010 mm^2 for BDD, AuNPs/BDD, CuNPs/BDD, and CuNPs/AuNPs/BDD, respectively. Thus, the electroactive surface area of the electrode was increased accordingly after modification with CuNPs, AuNPs, and CuNPs/AuNPs, respectively.

4.1.4.2. Redox behavior of modified electrodes towards neonicotinoids

Several groups have reported the electrochemical detection of neonicotinoids, particularly imidacloprid and thiamethoxam based on hanging mercury electrode [125, 126], silver amalgam electrode [127], and glassy carbon electrode [128]. In this work, the redox reaction of four insecticides was studied on CuNPs/AuNPs/BDD electrode. The voltammograms were evaluated using cyclic voltammetry. From CV in Figure 4.4, the redox reaction of all neonicotinoids is irreversible as only cathodic current was presented when scanning a full cycle and the result is corresponding to other reports [129]. Since unmodified BDD electrode offers limited sensitivity and in this case is unsuitable for the following experiments because the peak current is low. CuNPs/AuNPs/BDD was employed for other studies (see Figure 4.5). Under optimized CV conditions, the reduction potential vs. Ag/AgCl of dinotefuran (DIN), thiamethoxam (THM), clothianidin (CLO), and imidacloprid (IMD) were -1.73, -1.63, -1.49, and -1.46, respectively. There is a single reduction peak from THM, CLO, and IMD; while the two peaks were observed from DIN. According to the literature reviews, there are two reductions of the insecticides occurring step-wisely. First, the nitro group is reduced to hydroxylamine employing four electrons, and further reduced to amine group after accepting other two electrons [126]. However, the second step is obscured by the hydrogen evolution [130]. It can be concluded that the results in this study agrees very well with others.

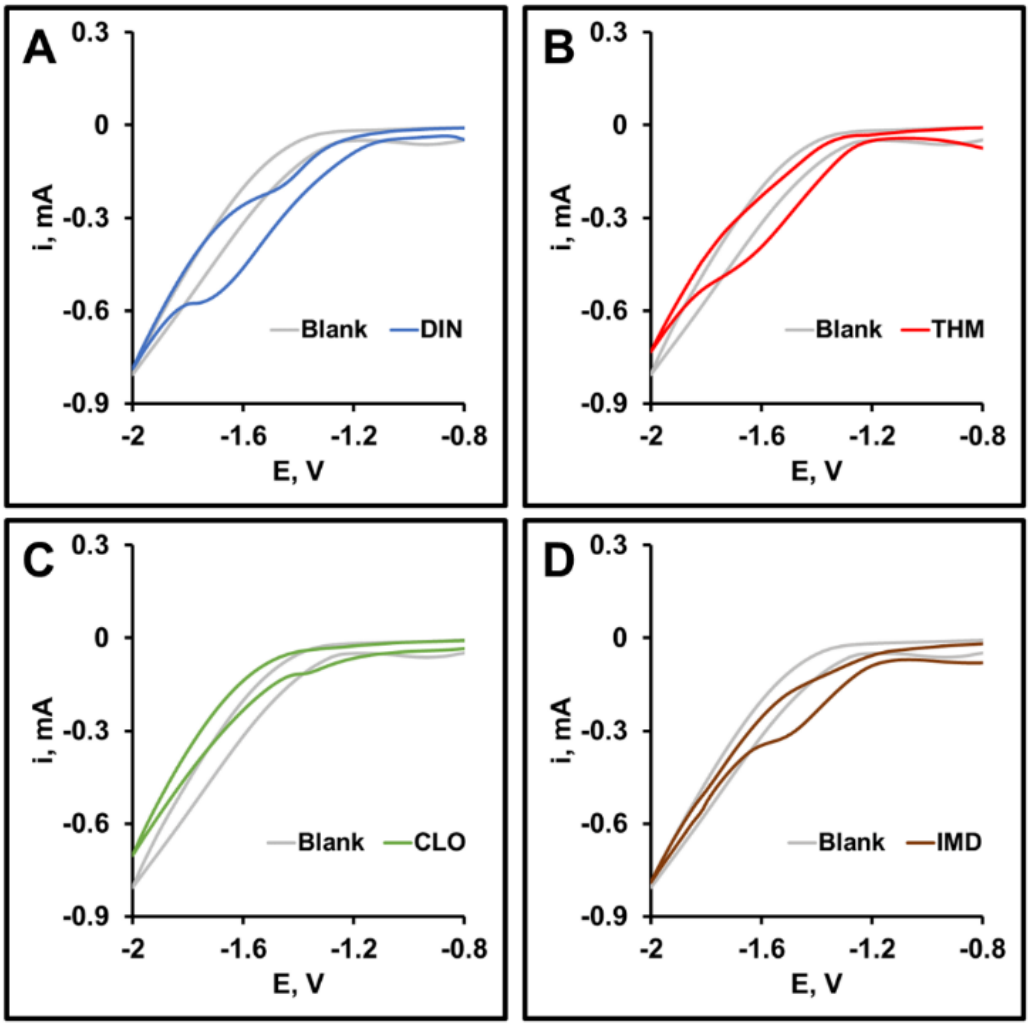

Figure 4.4 Cyclic voltammogram of 5 mM DIN (A), 4 mM THM (B), 1.25 mM CLO(C), and 2 mM IMD (D) on unmodified electrode. The solution was prepared in 90% BRB buffer pH 7 : 10% acetonitrile and it was used as blank (grey line) for this study.

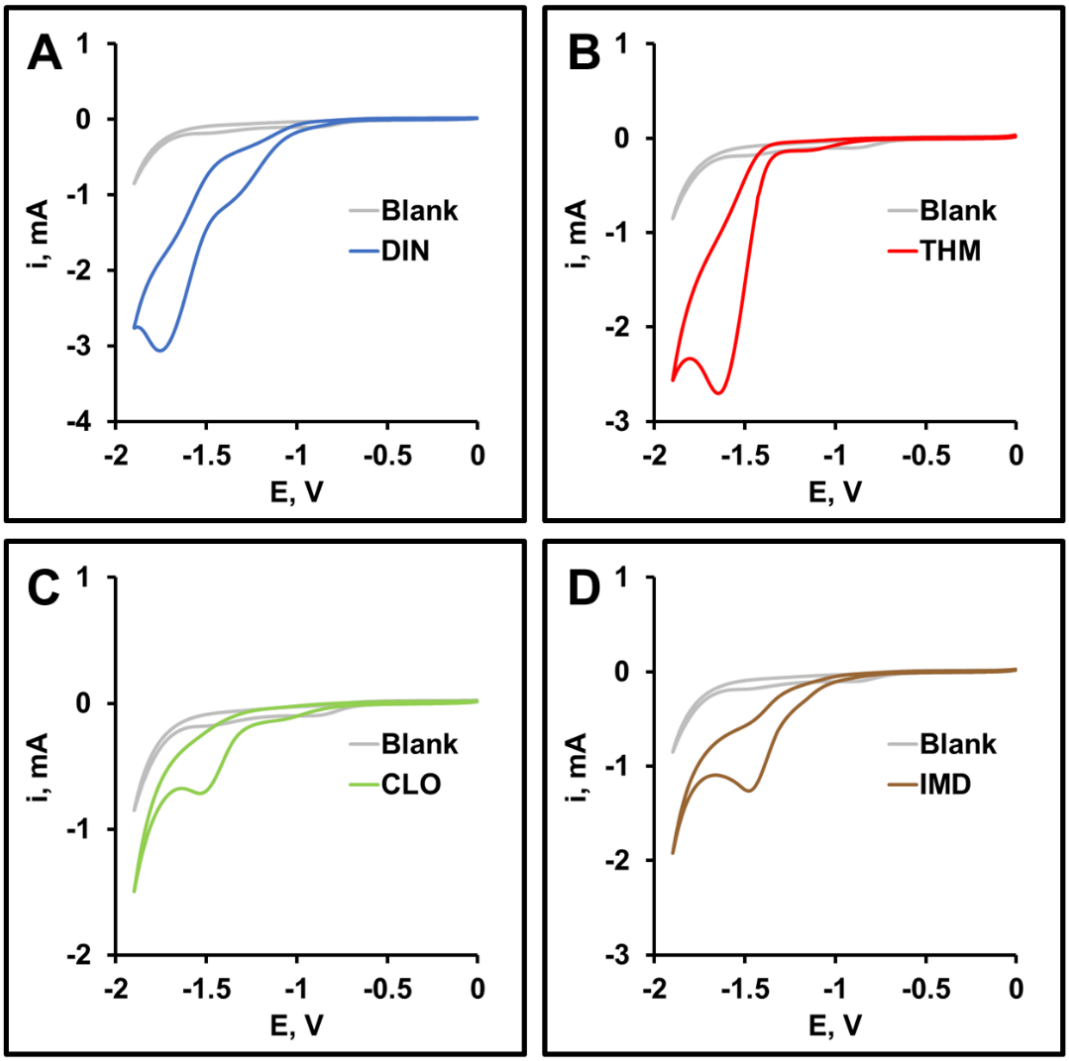

Figure 4.5 Cyclic voltammogram of 5 mM DIN (A), 4 mM THM (B), 1.25 mM CLO(C), and 2 mM IMD (D) on CuNPs/AuNPs/BDD electrode. The solution was prepared in 90% Britton-Robinson buffer pH 7 : 10% acetonitrile and it was used as blank (grey line) for this study.

4.1.4.3. Method optimization

4.1.4.3.1. Electrode modification

Variable parameters that can influence the analyte detection signal were optimized. First, the parameters that affects the modification of BDD electrode by electrodeposition techniques including applying potential (0 to -0.8 V) and current (0 to -350 µA), deposition time (0 to 300 s), and concentration of the metal ions (1 to 10 mM) were investigated. In this work, metal nanoparticles were deposited orderly. According to the literature review, AuNPs should be priory accumulated on the electrode because it favors other nanoparticles to be attracted by providing

the negatively charged. It was found that AuNPs were formed after -0.3 V was applied to the electrode (see Figure 4.6). -0.4 V was selected as the optimal applied potential as AuNPs gradually formed as isolated particles rather than agglomeration at this potential. In contrast with AuNPs, chronopotentiometry was choose for the electrodeposition of CuNPs. Applied current ranging from 0 to -350 µA with approximately 50 µA interval were employed in this experiment. It was found that at -225 µA yields the highest current from the cyclic voltammogram of 5 mM $Fe(CN)_6^{3-/4-}$ (in 0.1 M KCl), therefore this point was selected as the good condition for CuNPs modification. The deposition time in Figure 4.7 of both metals was optimized as a ratio between of AuNPs and CuNPs. The bar chart shows that the current increase with deposition time, while the opposite phenomena was observed for the peak current. However, the results were diverged after the current reaches maximum point. It happens due to the growth of nanoparticles to a larger scale and reduce the electroconductivity. It was clearly when AuNPs:CuNPs equals to 30:90 s (1:3), the highest current was achieved with peak potential shifted towards the oxidation (vs. Ag/AgCl) and was set as the appropriated deposition time. Moreover, concentrations of gold and copper ions were studied and found that at 5 mM provides the highest current signal.

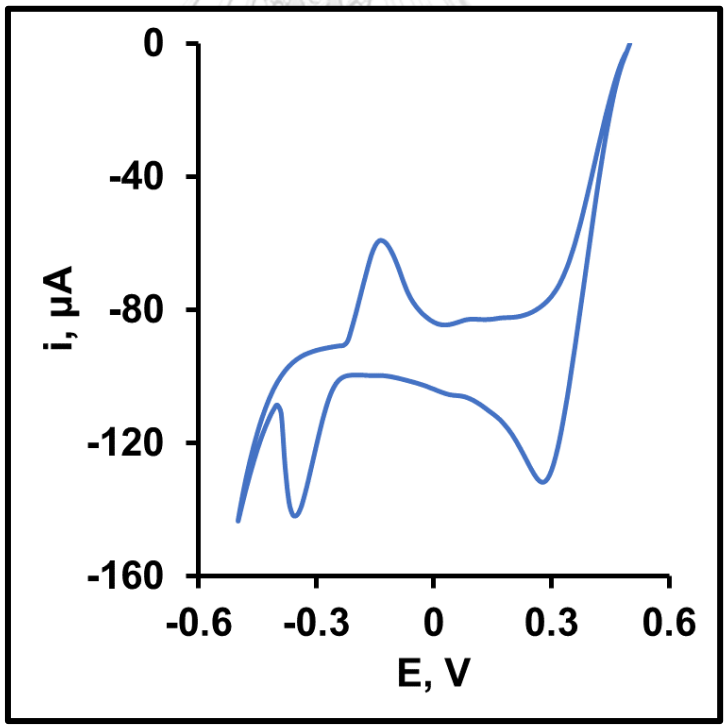

Figure 4.6 Cyclic voltammogram of 5 mM Au^{3+} in 0.2 M H_2SO_4 performed on BDD electrode with the scan rate of 0.1 V s^{-1}

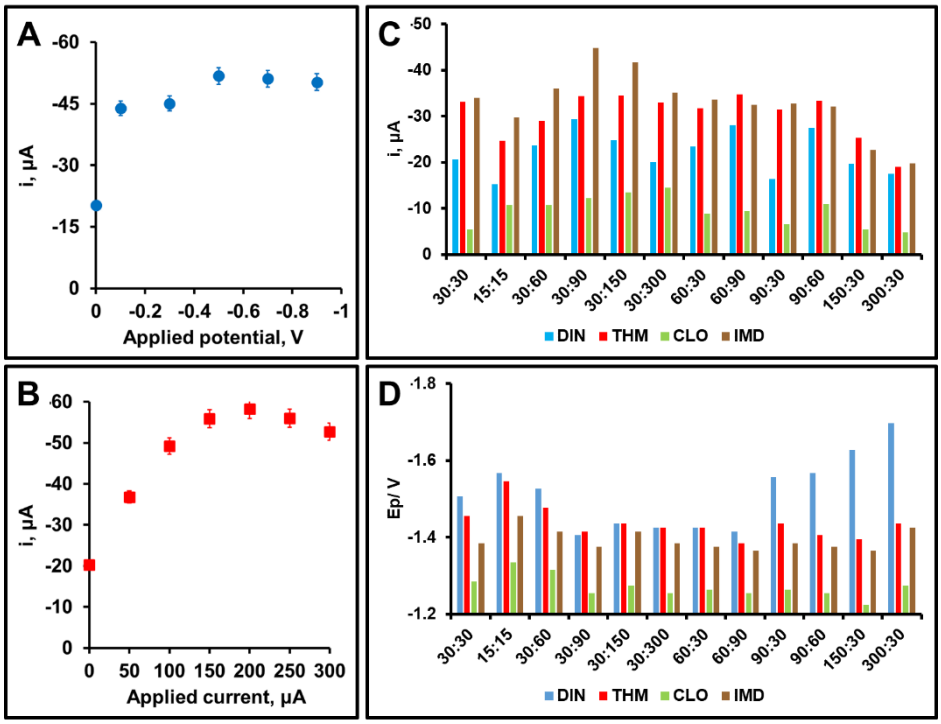

Figure 4.7 Optimization of nanoparticles electrodeposited electrode: applied potential for AuNPs (A), applies current for CuNPs (B). Plots between current signals at different deposition time (t_{AuNPs}/t_{CuNPs}, s) (C) and peak potential (D) of 5 mM DIN (blue), 4 mM THM (red), 1.25 mM CLO (green), 2 mM IMD (brown) in 90% Britton-Robinson buffer pH 7 : 10% acetonitrile.

4.1.4.3.2. u-HPLC separation and electrochemical detection

The isocratic separation of neonicotinoids in this work was done in reverse phase system using C18 materials as the analytical column. Important parameters; percent organic solvent, injection volume, and flow rate were studied so that the good resolution of the chromatogram was obtained. In this work, acetonitrile was used as the organic solvent in the mobile phase of u-HPLC and was first optimized. The higher content of acetonitrile (>10%) the peaks of CLO and IMD cannot be separated with each other, therefore percent acetonitrile of 5 to 9 were investigated. The results in Figure 4.8 show that at 7%, a good separation with R_s > 1.5 can be calculated from the last two peaks. Thus, 7% acetonitrile was chosen for other experiments. For injection volume, the parameters were 3 to 25 µL was employed. Although the higher current signals can be noticed with increasing injection volume, the peaks were broadening and R_s is lower than 1.5. The efficient parameter was yielded when 7 µL was employed for the injection of the standard analytes, thus this volume was the optimized conditions. Finally, the flow rate was evaluated together with the percent acetonitrile. The results demonstrate that

faster separation can be achieved with elevating the flow of the system; however, 1 mL min^{-1} gives more suitable separation with better resolution than highest flow rate with low content of the organic solvent. The peak width of DIN, THM, CLO, and IMD were 0.41, 0.55, 0.55, and 0.69 s, accordingly. The separation was completely with is 7.4 min which is acceptable for four compounds. From the chromatogram the optimal condition of percent acetonitrile, injection volume, and flow rate were 7%, 7μL, and 1 mL min^{-1}, respectively.

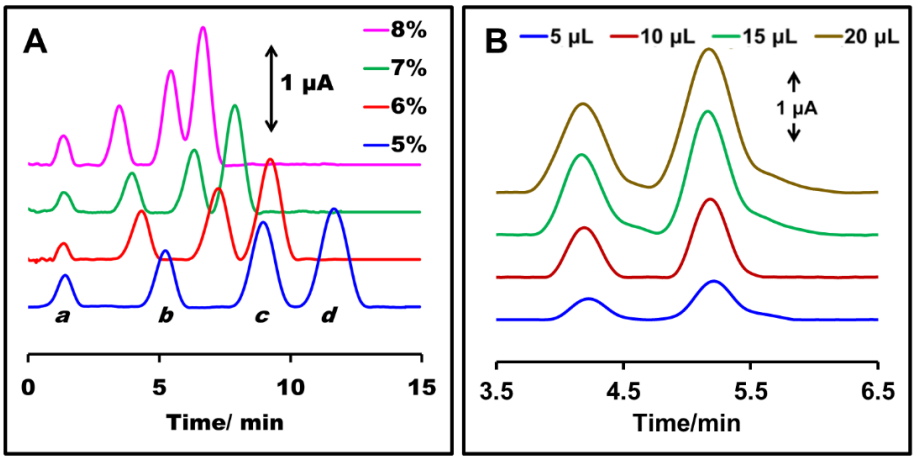

Figure 4.8 Optimization of % acetonitrile (A) and injection volume (B)

Chronoamperometry was employed as a detection technique in this study. Different applied potentials in the range of -1.0 to -2.0 V were investigated for a proper analytical purpose. The result in Figure 4.9 was the plot between the applied potential (x-axis) and signal to baseline ratio (S/B). The optimal condition was determined at the maximum ratio of S/B between current signal (S) and current of the baseline (B). The current signal of both detection potential and the baseline increase with the applied potential. Under the optimal potential, the S/B results in the best condition for the electrochemical detection, whereas other ratio shows those numbers were lower. After a careful investigation, it was found that at -1.6 V produces a superior result than other applied potential for all compounds. Thus, -1.6 V was chosen as the suitable potential for the electrochemical detection of DIN, THM, CLO, and IMD. In addition to the detection potential, pH of Britton-Robinson buffer ranging from 2 to 10 were studied and the results are displayed in Figure 4.9. pH affects the detection of neonicotinoids significantly because the dissociation of the compounds relies on the pH of the solution. It was reported that neutral to slightly basic condition was used for electrochemical detection of some neonicotinoids [131]. From the results, it agrees that moderate pH buffer provides higher current signal. Moreover, there is a report of a degradation of pesticides at higher pH [132]. Therefore, in this work a pH of 6.4 was reasonable for detection of the analytical targets and employed for the following experiments.

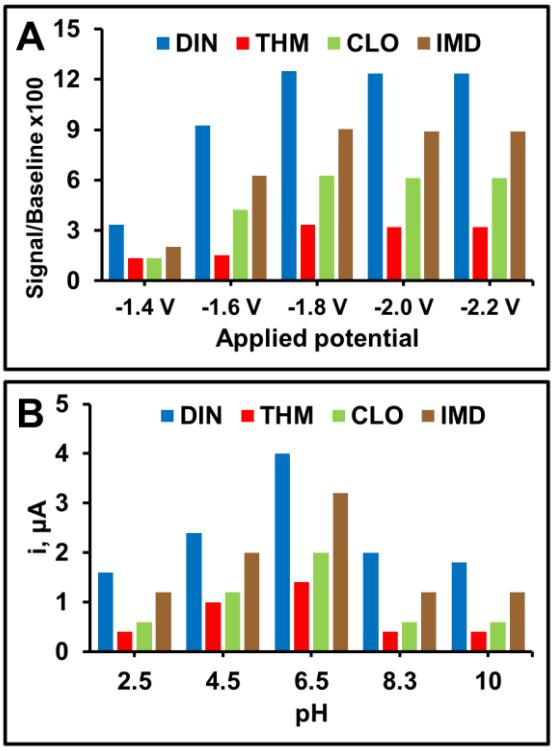

Figure 4.9 Plot between signal-to-noise and applied potential at different applied potential (A) and plot between current signals and pH (B) of 5 mM DIN (blue), THM (red), CLO (green), IMD (brown)

4.1.4.4. Analytical performance, repeatability, and reproducibility

Different neonicotinoid concentrations were injected into the u-HPLC system and detected using amperometry techniques. Figure 4.10 shows the overlaying chromatograms and the calibration plots of DIN, THM, CLO, and IMD. Table 4.1 summarizes the analytical performance of DIN, THM, CLO, and IMD. The linear range of dinotefuran and thiamethoxam is ranging from 0.004 – 1 mM, whereas 0.008 – 1 mM was obtained from clothianidin and imidacloprid, respectively with a good linearity value (r^2 > 0.99). Moreover, the calibration slopes have an excellent RSD (less than xx%) for triplicate measurements. The detection limit and the limit of quantification are calculated from $3SD_{blank}$/Slope and $10SD_{blank}$/Slope (different slope for each neonicotinoids) where SD is the standard deviation of blank (n=10). 0.75, 2.50, 1.68, and 1.09 µM is achieved for the detection limit of DIN, THM, CLO, and IMD, respectively. Literature reviews of analytical characteristics based on electrochemical detection is compared in Table 4.2. Lower detection limit of this proposed method is attributed to the outstanding electrocatalytic properties derived from the bimetallic nanoparticles modified electrode. Furthermore, the reproducibility of the modified electrode is carried out. %CV of 1.05, 0.70, and 0.24 is obtained

from the repeated measurements (n=7) of three different dinotefuran concentrations (0.04, 0.4, and 1 mM) on the same electrode. u-HPLC coupled with electrochemical detection using CuNPs/AuNPs/BDD as working electrode developed in this work shows a good performance for the determination and separation of four different insecticides.

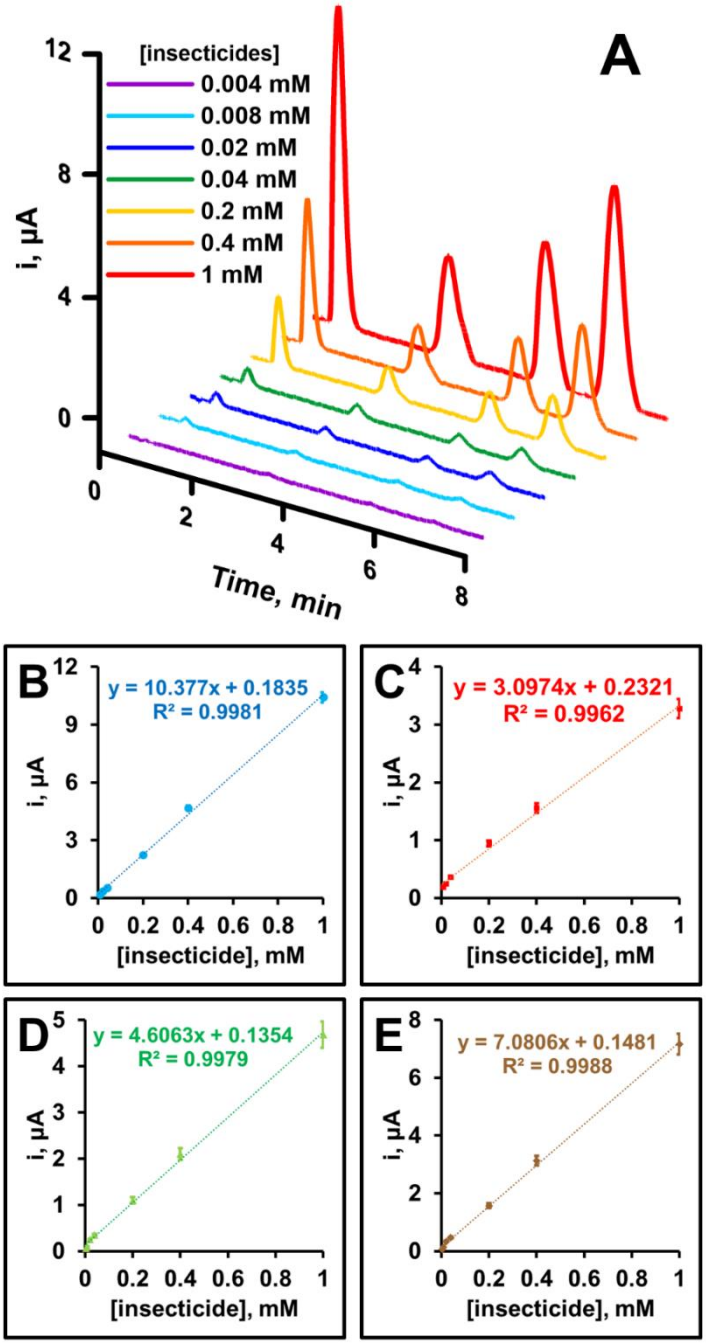

Figure 4.10 Chromatogram of nenocotinoid insecticides at different concentration (A), calibration plot of DIN (B), THM (C), CLO (E), and IMD (E)

Table 4.1 Summary of neonicotinoids analytical performance (n=3)

Analyte	Linear range(mM)	Slope (μA mM^{-1})	Intercept (μA)	LOD (μM)	LOQ (μM)
DIN	0.008-1	10.3766	0.1835	0.75	2.49
THM	0.008-1	3.0974	0.2321	2.50	8.33
CLO	0.004-1	4.6063	0.1354	1.68	5.60
IMD	0.004-1	7.0806	0.1481	1.09	3.64

Table 4.2 Comparison of analytical performance between this work and others

Modified electrode	Detection method	Linear range (mM)	LOD (μM)	Analyte	Real sample	Reference
BDD	Square wave voltammetry	0.03-0.2	8.60	Imidacloprid	Plum juice	[117]
Sputtered bismuth thick-film electrode	DPV	0-0.12	0.04-0.07	Dinotefuran, thiamethoxam, clothianidin, imidacloprid, nitenpyram	Distilled, tap, mineral, surface water	[118]
Tricresyl phosphate-based carbon paste electrode	DPV	0.015-0.166	-	thiamethoxam	River water, Actara 25 WG	[132]
Graphene oxide modified glassy carbon electrode	Square wave voltammetry	0.01-0.2	7.9-8.3	Thiamethoxam, imidacloprid	Water, honey	[133]
CuNPs/AuNPs/BDD	Amperometry coupled u-HPLC	0.004-1	0.75-2.50	Dinotefuran, thiamethoxam, clothianidin, imidacloprid	Vegetable, honey	This work

4.1.4.5. Real samples application

CuNPs/AuNPs/BDD was applied for the determination of neonicotinoids in real samples using the standard addition method. Water spinach and two honey samples were purchased from the local market and prepared for the analysis using the method described previous. The stock standard of four analytes of different concentrations (non-spiked, 0.04, 0.1, 0.2, and 0.4 mM) was spiked into the sample. From Table 4.3, this developed method provides a good precision with %RSD and %recovery in the range of 0.03-1.19 and 97.14%-101.91%, respectively. To evaluate the accuracy of the results, the identical chromatographic assay was connected to the UV-visible detector (u-HPLC-UV) and determined for the concentrations of neonicotinoids in real samples using external calibration. Two techniques including amperometry employing CuNPs/AuNPs/BDD as working electrode and UV-visible detection were compared using a paired t-test at the 95% confidence criteria for all samples. $T_{calculated}$ of the results from the developed method and u-HPLC-UV (0.1 mM) equals to 0.6068 which lower than t-value of 3.1824. From the statistic, our method agrees with the standard u-HPLC-UV without null hypothesis rejecting. Therefore, the bimetallic nanoparticles modified electrode coupled with u-HPLC developed in this work demonstrates an alternative, sensitive, and reliable approach for the practical analysis of neonicotinoids in real samples.

In this work, the stability study was investigated by injecting solutions prepared from the real samples for several days on the same and different electrode. The electrodeposition of the electrode was performed and stored at room temperature. Before the analysis, the nanoparticles modified electrode was activated by applying cyclic voltammetry for 20 cycles in 0.1 M NaOH. In case of inter-day study, the surface activation was done once and used for all measurements. The results in Table 4.4 indicate that a good stability was obtained with %recovery in the range of 97.23-102.00%. A notable stability of intra-day study is also demonstrated by this modified electrode (0.90% of %CV is achieved from the continuous analysis for three days). The results reveal that our modified electrode provide satisfactory stability throughout the long period of the experiment.

Table 4.3 Recovery data for determination of the target nenicotinoids in vegetable and honey samples at CuNPs/AuNPs/BDD electrode compare with UV-vis detection method

Samples	Spiked level (μM)	Analyte	Amount found (μM) (x ± SD)						%Recovery	
			Amperometry			UV-vis			Amperometry	UV-vis
Water spinach	40	DIN	40.74	±	0.57	40.29	±	0.31	101.85	100.72
		THM	39.61	±	0.31	39.73	±	0.10	99.01	99.32
		CLO	40.18	±	0.57	39.77	±	0.29	100.45	99.43
		IMD	40.10	±	0.35	39.91	±	0.27	100.26	99.79
	100	DIN	100.64	±	0.68	100.55	±	0.58	100.64	100.55
		THM	99.29	±	0.72	99.39	±	0.52	99.29	99.39
		CLO	100.07	±	1.02	99.95	±	0.84	100.07	99.95
		IMD	98.64	±	1.03	98.91	±	0.83	98.64	98.91
	200	DIN	200.88	±	0.52	201.41	±	1.77	100.44	100.71
		THM	201.52	±	1.12	197.87	±	1.02	100.76	98.94
		CLO	200.48	±	1.15	199.39	±	1.77	100.24	99.69
		IMD	199.29	±	0.83	199.81	±	1.07	99.64	99.91
	400	DIN	393.66	±	4.72	402.87	±	2.05	98.41	100.72
		THM	403.04	±	3.13	403.03	±	2.06	100.76	100.76
		CLO	397.51	±	4.71	399.40	±	1.98	99.38	99.85
		IMD	397.73	±	2.29	399.52	±	1.97	99.43	99.88
Kale	40	DIN	40.37	±	0.45	39.99	±	0.21	100.93	99.98
		THM	39.68	±	0.48	40.29	±	0.20	99.21	100.73
		CLO	40.54	±	0.39	39.90	±	0.16	101.36	99.75
		IMD	39.72	±	0.43	40.07	±	0.09	99.31	100.18
	100	DIN	100.06	±	0.04	100.29	±	0.19	100.06	100.29
		THM	100.04	±	0.03	100.03	±	0.07	100.04	100.03
		CLO	99.98	±	0.03	99.93	±	0.14	99.98	99.93
		IMD	99.99	±	0.04	100.06	±	0.19	99.99	100.06
	200	DIN	197.20	±	2.47	198.47	±	1.49	98.60	99.24
		THM	202.14	±	1.72	199.03	±	1.15	101.07	99.52
		CLO	199.48	±	3.03	201.28	±	0.65	99.74	100.64
		IMD	202.71	±	2.77	199.76	±	1.40	101.35	99.88
	400	DIN	399.06	±	1.87	395.88	±	1.87	99.76	98.97
		THM	396.73	±	2.39	399.61	±	1.53	99.18	99.90
		CLO	395.35	±	1.68	397.74	±	2.56	98.84	99.44
		IMD	400.01	±	2.46	400.77	±	2.47	100.00	100.19
Honey I	40	DIN	39.25	±	0.77	39.91	±	0.21	98.12	99.78
		THM	40.20	±	0.32	40.29	±	0.20	100.50	100.72

Samples	Spiked level (μM)	Analyte	Amount found (μM) (x ± SD) Amperometry				UV-vis			%Recovery Amperometry	%Recovery UV-vis
		CLO	40.76	±	0.76		39.93	±	0.21	101.91	99.82
		IMD	40.74	±	0.87		39.94	±	0.02	101.86	99.86
	100	DIN	100.04	±	0.37		99.99	±	0.39	100.04	99.99
		THM	99.73	±	0.59		99.77	±	0.84	99.73	99.77
		CLO	100.47	±	0.60		100.52	±	0.92	100.47	100.52
		IMD	100.90	±	0.43		101.46	±	0.74	100.90	101.46
	200	DIN	202.93	±	4.68		198.66	±	1.63	101.46	99.33
		THM	201.69	±	3.86		201.88	±	0.96	100.85	100.94
		CLO	194.28	±	1.54		200.74	±	1.62	97.14	100.37
		IMD	199.87	±	4.38		199.96	±	1.05	99.94	99.98
	400	DIN	400.78	±	0.91		397.02	±	2.04	100.20	99.25
		THM	400.36	±	0.71		395.67	±	3.51	100.09	98.92
		CLO	399.04	±	0.81		399.69	±	3.71	99.76	99.92
		IMD	399.22	±	0.96		402.66	±	2.82	99.80	100.66
Honey II	40	DIN	39.99	±	0.16		39.92	±	0.31	99.97	99.79
		THM	39.92	±	0.16		39.53	±	0.32	99.80	98.82
		CLO	40.23	±	0.04		40.14	±	0.25	100.57	100.36
		IMD	39.97	±	0.14		39.99	±	0.11	99.93	99.98
	100	DIN	100.04	±	0.80		100.05	±	0.96	100.04	100.05
		THM	98.63	±	0.77		98.35	±	0.96	98.63	98.35
		CLO	99.99	±	0.78		99.98	±	0.98	99.99	99.98
		IMD	99.93	±	0.06		100.06	±	0.04	99.93	100.06
	200	DIN	200.07	±	0.60		199.70	±	0.56	100.04	99.85
		THM	199.87	±	0.59		199.14	±	0.56	99.93	99.57
		CLO	200.99	±	0.13		200.25	±	0.31	100.50	100.13
		IMD	200.12	±	0.52		199.63	±	0.34	100.06	99.81
	400	DIN	397.16	±	2.87		397.16	±	2.87	99.29	99.29
		THM	394.54	±	4.13		394.54	±	4.13	98.63	98.63
		CLO	400.28	±	4.08		400.28	±	4.08	100.07	100.07
		IMD	402.55	±	2.71		402.55	±	2.71	100.64	100.64

Table 4.4 Interday and intraday study of CuNPs/AuNPs/BDD electrode for insecticides detection (n=3)

Samples	Spiked level (μM)	Analyte	Intra-day		Inter-day	
			%Recovery	%RSD	%Recovery	%RSD
Water Spinach	40	DIN	101.94	0.99	100.72	0.04
		THM	99.07	1.01	99.32	0.04
		CLO	100.52	0.47	100.81	0.04
		IMD	100.31	1.11	99.39	0.04
	100	DIN	100.69	0.96	99.52	0.10
		THM	99.35	0.03	99.85	0.10
		CLO	100.16	1.51	100.64	0.10
		IMD	98.70	0.35	99.46	0.10
	200	DIN	100.49	1.85	100.03	0.20
		THM	100.83	0.50	99.00	0.20
		CLO	100.34	0.72	100.76	0.20
		IMD	99.74	0.19	99.04	0.20
	400	DIN	98.48	0.08	99.76	0.40
		THM	100.82	0.68	99.97	0.40
		CLO	99.46	0.06	100.78	0.40
		IMD	99.52	0.85	100.83	0.40
Kale	40	DIN	101.02	1.12	99.93	0.04
		THM	99.27	1.43	99.94	0.04
		CLO	101.41	0.55	100.06	0.04
		IMD	99.38	0.72	100.79	0.04
	100	DIN	100.11	1.14	99.80	0.10
		THM	100.09	0.04	100.25	0.10
		CLO	100.04	1.95	100.39	0.10
		IMD	100.05	0.17	100.10	0.10
	200	DIN	98.68	1.67	100.00	0.20
		THM	101.13	0.60	100.14	0.20
		CLO	99.81	1.08	99.32	0.20
		IMD	101.45	0.27	99.58	0.20
	400	DIN	99.86	0.03	100.69	0.40
		THM	99.26	0.08	99.94	0.40
		CLO	98.89	0.02	99.07	0.40
		IMD	100.10	0.95	99.96	0.40
Honey I	40	DIN	98.19	1.15	99.52	0.04
		THM	100.56	1.41	100.25	0.04
		CLO	102.00	0.55	99.85	0.04

Samples	Spiked level (μM)	Analyte	Intra-day		Inter-day	
			%Recovery	%RSD	%Recovery	%RSD
		IMD	101.93	0.71	100.80	0.04
	100	DIN	100.14	1.14	99.89	0.10
		THM	99.79	0.04	99.94	0.10
		CLO	100.55	1.94	100.04	0.10
		IMD	100.95	0.17	99.85	0.10
	200	DIN	101.55	0.64	100.59	0.20
		THM	100.94	0.60	101.52	0.20
		CLO	97.23	1.11	99.42	0.20
		IMD	100.03	0.28	101.03	0.20
	400	DIN	100.25	0.03	100.47	0.40
		THM	100.15	0.08	100.04	0.40
		CLO	99.86	0.02	99.34	0.40
		IMD	99.88	0.95	98.99	0.40
Honey II	40	DIN	100.07	1.01	100.02	0.04
		THM	99.89	0.95	100.73	0.04
		CLO	100.62	0.23	99.86	0.04
		IMD	100.01	1.66	98.90	0.04
	100	DIN	100.12	1.21	100.43	0.10
		THM	98.70	0.01	100.07	0.10
		CLO	100.07	1.75	100.13	0.10
		IMD	100.01	0.41	98.43	0.10
	200	DIN	100.12	1.68	100.08	0.20
		THM	99.99	0.22	100.11	0.20
		CLO	100.56	0.43	99.92	0.20
		IMD	100.12	0.08	99.63	0.20
	400	DIN	99.36	0.12	100.22	0.40
		THM	98.69	1.01	99.88	0.39
		CLO	100.14	0.07	99.37	0.40
		IMD	100.69	0.46	98.72	0.40

4.1.5. Conclusions

Bimetallic nanoparticles modified boron-doped diamond electrode were developed for amperometric detection of four insecticides after ultra-high-performance liquid chromatography. AuNPs and CuNPs were electrodeposited homogenously according to SEM results onto the BDD surface and enhance the electroactive surface area with the additional improvement of the electrocatalytic properties towards the reduction of dinotefuran, thiamethoxam, clothianidin, and imidacloprid. A cathodic peak was observed at a potential approximately -1.6 V vs. Ag/AgCl for xx with the Britton-Robin buffer pH 6.4 (0.01 M) as a supporting electrolyte. The chromatographic method involves a reversed phase C18 as an analytical column and the separation was complete with in 8 min using 7% acetonitrile as an organic solvent. The excellent analytical performance was achieved in this work; the limit of detection for dinotefuran was calculated from $3SD_{blank}$/slope and could be as low as 0.75 mM. Moreover, the wide linear dynamic range of 0.004 – 1 mM for clothianidin and imidacloprid was obtained. This work demonstrates the practical for real sample analysis by applying the method for determination of neonicotinoids in a water spinach and honey samples. The results show exceptional recoveries in the range of 97.14-101.91%. Furthermore, this proposed method has a good reproducibility and repeatability. In conclusion, a fast, reliable, and highly sensitive analytical method is demonstrated for the determination of important insectoids used in agricultural proposes.

4.2. Capillary open tubular anion-exchange chromatography and electrochemical detection of amino acids

4.2.1. Abstract

Anion-exchange chromatography with amperometric detection of underivatized amino acid using copper electrode was studied. A facile and sensitive electrochemical detection of amino acids without complicated derivatization procedure was coupled with isocratic chromatographic separation using PA10 nanoparticles coating on sulfonated COP capillary column in alkaline solution. Two electrode systems, Cu as the working electrode and stainless-steel as the counter electrode, was used. The effects of analytical conditions including the optimal potential, the concentration of NaOH, and the choice of mobile phase for high affinity amino acids were described. Under the optimal condition (1 V applied potential, 20 mM NaOH carrier), the detection limit of serine was 20 fmol (0.42 mg L^{-1}). The linear range shows a great correlation coefficient (>0.99). Cu amperometric sensor in this work shows a good reproducibility of 5.94% over one thousand injections.

4.2.2. Introduction

Amino acids are building blocks of peptides and proteins. The structure consists of amine and carboxylic functional group connecting to the alpha carbon atom. Multiple amino acids are linked by peptide bond to form the peptides and proteins which is very specific. Each amino acid has different alkyl group that connect to alpha carbon atom. Different amino acids act as various biomarkers. For example, lysine indirectly involves in the process of turning fats into energy, lacking lysine causes slow growth and reproductive disorders [134]. Cysteine has been reported connected to depigmentation of hair, liver damage, and loss of muscle [135]. Therefore, the separation and determination of amino acids is essential.

Recent chromatographic methods of amino acids have been progressed with the advantages of technology. Most of them are focused on liquid chromatography. The separation of amino acids can be achieved using reversed-stationary phase chromatography and ion-exchange chromatography. However, the direct method is not simple because these molecules are absent of natural strong chromophore or fluorophore for photometric or fluorometric detection. Therefore, the pre- or post-column derivatization procedures are required to add the strong chromophore groups to amino acids for sensitive photometric detection. There are various derivative molecules such as ninhydrin [136], phenyl isothiocyanate [137], o-phthalaldehyde-2-mercaptoethanol [138], etc. that were purposed for sensitive determination of amino acids in chromatographic system [139-141]. However, the method that is not required derivatization process is demand because it is convenient, rapid, and simple. Currently, electrochemical detection coupled with ion-exchange chromatography is applied with sensitive direct analysis of amines and amino acids without derivatization process. For avoiding the immediate fouling of noble metal electrode, pulsed or stripping voltammetry for underivatized amino acids was frequently employed [142, 143]. The detection mechanism depends on surface-catalyzed oxidation of amine functional group on the surface of metal. On the other hand, direct anodic oxidation at constant applied potential can occur on some metal and chemical modified electrode that made from non-noble material such as copper [144], nickel [145], cobalt, etc. For copper electrode, copper oxyhydroxide in alkaline media acts as amperometric probe for underivatized amino acids detection in liquid chromatography or capillary electrophoresis [146]. In this method, there is no electrode fouling of the working electrode. Thus, the constant applied potential can be practical.

Recently, we have developed open tubular ion chromatography (OTIC) using cycloolefin polymer (COP) capillary column (19-28 μm). The column was sulfonated using mixtures of chlorosulfuric acid and glacial acetic acid, then coating with anion-exchange (AEX)

nanoparticles. Finally, AEX column was obtained and demonstrated that it can separate anions [5]. In addition, this achievement provides the possibility of the separation of another anion by changing the AEX nanoparticles that suitable with the analytes. In practical, the condition for detection on copper material agrees with the deprotonated amino acids that can be separated with AEX capillary column as well.

In this study, the facile method for amperometric determination of amino acid in alkaline condition without derivatization procedure or pulsed voltammetry after AEX chromatography was developed. Even though, the gradient elution is necessary for a complete elution of all essential amino acids, the isocratic elution for important amino acids is described. Therefore, the objectives of this study were to investigate the optimal condition for separation and quantification of important amino acids. In this work, the fast and simple, also sensitive method for determination of amino acids is demonstrated. The purposed method can be readily assembled for portable amino acids detection in the future.

4.2.3. Experimental

4.2.3.1. Reagents

All solutions were prepared from analytical reagent grade chemicals without purification and by using distilled deionized water. Sodium hydroxide pallets were purchased from Merck. Amino acids were purchased from VWR. Chlorosulfonic acid was purchased from Acros (www.acros.com). AEX latex suspensions (PA10) were received from Thermo Fisher Scientific (Dionex) (Sunnyvale, CA) as a gift.

4.2.3.2. Amperometric experiments

A DStat [147], an open-source and general-purpose potentiostat, was used for electrochemical measurements. The data acquisition was performed using DStat interface software. All voltammetry was carried out in two-electrode cell using the Cu working electrode and a stainless-steel counter electrode.

4.2.3.3. Flow injection (FIA) and chromatographic measurements

These experiments were conducted with electrochemical cell, consisting of 15-50 μm Cu copper electrode and a stainless-steel counter electrode.

Four solenoid valves (SV), PET tubes, and a circuitry equipped with Programmable System-on-Chip (PSoC) 5/S5LP (www.cypress.com) and a LabVIEW (www.ni.com) were used for FIA and chromatographic experiments.

A personal computer equipped with DStat interface allowed acquisition and processing of chromatograms. The mobile phase was purged from nitrogen, controlled by a miniature pressure controller model OEM-EP (Parker Hannifin Corp). Moreover, the eluent solution was kept in plastic bottles and sealed inside the plastic bags that filled with soda lime to minimize CO_2 dissolution.

Chromatographic separations were performed by using a AEX-COP capillary column (19-28 μm inner diameter, 150-180 cm length) prepared in our lab.

4.2.3.4. Electrode preparation

Cu (15-50 μm diameter) was used as the working electrode (WE). First, the 1.5-2 cm Cu wire was cut and inserted into polyethylene terephthalate (PET) or polyether ether ketone (PEEK) tube (370 μm outer diameter). Next, they were inserted into a stainless-steel needle (~700 μm outer diameter). Then, they were glued together with a casting resin. Finally, WE was placed in room temperature for 24 hours to completely dry the casting resin. The Cu wire was soldered to the shield cable to make connection with the DStat PCB. Prior use, the electrode was polished with sandpaper from number 6000 to 15000 respectively until the surface was smooth. The images of the electrode were obtained using digital microscope model VHX-5000 (Keyence Corp).

A counter electrode (CE) was prepared from a stainless-steel tube (18 AWG). First, the tube (2-3 cm) was cut and polished with coarse sandpaper to remove sharp edges. Next, 2 opposite holes was drilled to make the outlet of the solution. Then, it was soldered with the shield cable for connection with the DStat.

An electrochemical cell was configured from WE, CE, and the column. The WE and column was inserted from the different ends of CE and met at the outlet (2 holes that was previously drilled). Occasionally, the PET tube (1.5-2 cm) was inserted at the end of the column to ensure that the outlet of the column was centralized and aligned very well with the WE. The schematic of the electrodes and their position are shown in Figure 4.11.

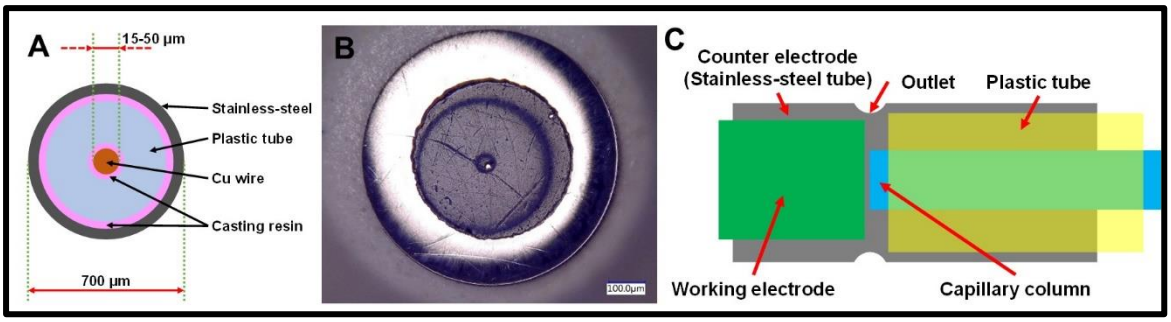

Figure 4.11 Schematic (A) and the image (B) of Cu working electrode, and the position of the electrodes at the end of the capillary column (C).

4.2.3.5. Column preparation

The column was prepared with 2 steps; sulfonation of the column, and latex coating. The procedure for polymerization and extrusion of the blank column was explained in previous publication and the instrument setup was similar to that work. COP column with 19 and 28 µm was obtained after the process. To sulfonate the column, first the COP was cut (150-180 cm). Second, N_2 was passed through for 10 minutes to thoroughly dry the column. Third, the chlorosulfonic acid in glacial acetic acid (90:10 w/w) was passed through for 5 hours. Next, the column was washed out the remaining acid with glacial acetic acid and water, each for 1 hours. Then, it was put inside the oven at 80°C while 20 mM NaOH was passing. After that the column was washed with water for 30 minutes at room temperature. Cation-exchange (CEX) column was obtained. All pressure used in these steps was 100 psi.

For coating with AEX, the CEX column was passed with PA10 nanoparticles for 2 hours using 20 psi N_2 gas. Finally, the column was washed with water and ready to use.

4.2.3.6. DStat printed circuit board preparation

The schematic and components of the board is provided by Dryden, M. D. M. and groupThe plate was pasted with solder paste at the positions of the components. The components were placed onto the specific position carefully. Then the printed circuit board (PCB) was baked inside the oven at 150°C for 2 hours. DStat PCB was obtained. The electrode position was connected with female terminator.

In order to prevent the detection with ambient noise, the rectangle metal box was used to cover the board. The box was drilled for 1-1.5 cm diameter and placed inside with insulating foam. The cable from WE and CE was passed through this hole to connect to DStat.

4.2.4. Results and discussion

4.2.4.1. Detection of amino acids on Cu electrode

From literature reviews, regarding Cu electrode in alkaline media show activity towards the oxidation of various organic molecules including carbohydrates and amines [148, 149]. Therefore, an electrochemistry of the Cu electrode as amperometric sensor for the determination of underivatized amino acids directly in the alkaline media was studied. Figure 4.12 displays the cyclic voltammogram of the Cu electrode in the presence of L-histidine in 20 mM NaOH solution. From the voltammogram, it was found that the oxidation peak at 0.32 and 0.85 V increase with the increase concentration of histidine during the anodic sweep. Moreover, the same electrochemical behavior of histidine was observed for other amino acids such as serine and proline. The potential obtained from this study was shifted (~0.3 V less) from the system using Ag/AgCl reference electrode [150]. In this work, the oxidation of Cu ($Cu \longrightarrow Cu^{2+}$) in the presence of amino acids was appeared ~0.8-1 V. From literature review, the oxidation of carbohydrates and amino acids on Cu electrode has 2 mechanisms; electrocatalytic oxidation and complexation. Vary experimental conditions such as analytes, pH differences, and potential differences can result in different mechanism [151]. Thus, it is important to investigate the mechanism of this work. For the hypothesis, the mechanism of this work was attributed to the complexation of Cu(II) by amino acids increased the dissolution of Cu from the electrode surface. This phenomenon occurred in alkaline media which is corresponding to our system as well. Moreover, the images from the digital microscope before and after the injection was investigated. The surface of Cu was etching, and curvature shape was seen on the surface of Cu as in Figure 4.13A. In addition, the distance in Figure 4.13B measured from the surface can be used as a confirmation of a loss of the working electrode surface due to the dissolution of Cu. Therefore, it can be concluded that the reaction in this work involved the complexation of amino acids with Cu(II) that Cu(s) dissolve into the solution at certain applied potential (particularly 0.8-1 V). Finally, the equation for this reaction can be described as follows

$$Cu(s) + 2HL \longrightarrow CuL_2 + 2H^+ \quad (22)$$

where L is amino acids at the amine group.

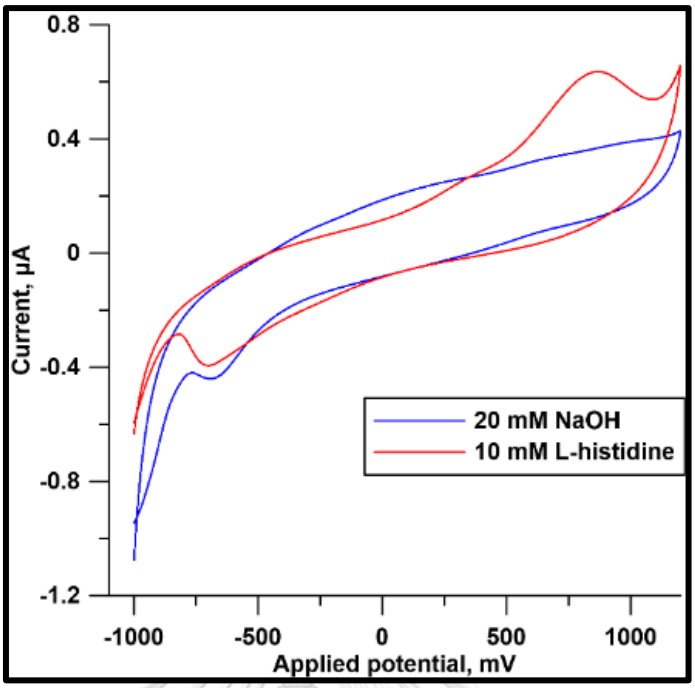

Figure 4.12 Cyclic voltammograms at Cu electrode in 20 mM NaOH solution (blue line) and in the presence of 10 mM L-histidine. Scan rate, 50 mV/s.

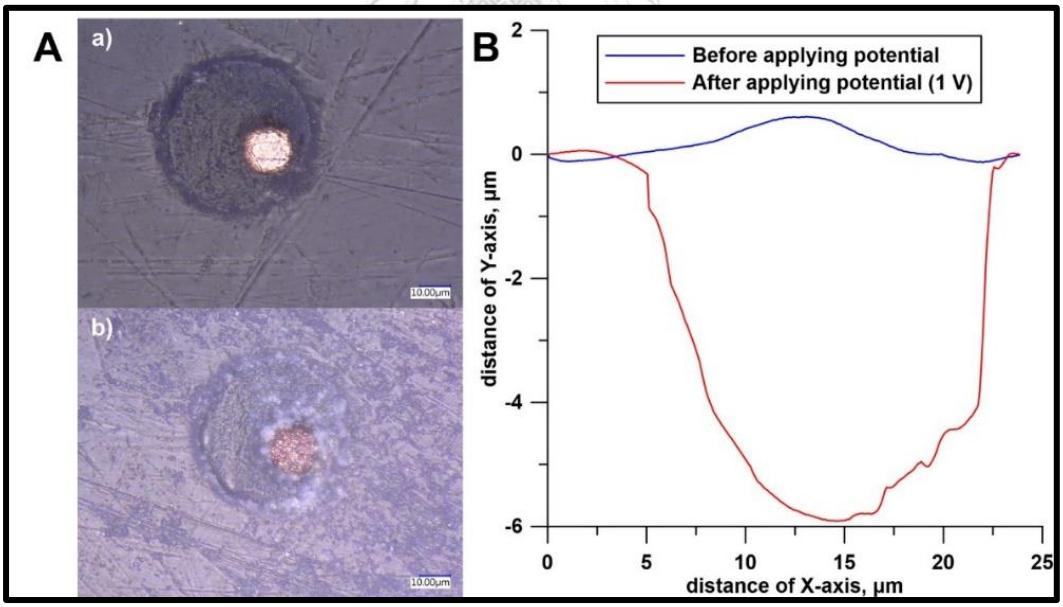

Figure 4.13 Surface of Cu electrode A) before the experiment a), and after applying potential (1 V) for hundreds of injections b). The depth of the Cu measured from the surface B). Experimental conditions were; Column: PEEK (25 µm ID, 110 cm), flow rate: 60 nL/min, injection volume: 5 nL, WE: Cu (15 µm ID), applied potential: 1 V, carrier: 20 mM NaOH, and analyte: serine (5 mM).

Considering the study described previously, it is possible to use Cu as WE for amperometric detection of amino acids in moderated alkaline solution. To optimize the applied potential, hydrodynamic voltammograms of serine, phenylalanine, and glutamate at Cu electrode at different constant applied potential (0.8-1 V with 50 mV interval) was investigated. Figure 4.14 shows the resulting plots between applied potential (V) and current (nA) obtained under flow injection conditions at 0.28 µL/min using 20 mM NaOH as carrier electrolyte. From the results, the maximum current response was observed at 0.9-1 V. Unlike a diffusion limited process, the current responses at higher potential exhibit decreased signals which is similar for all investigated amino acids. A similar behavior from other molecules in alkaline condition was observed on other metal electrodes [152] and it is in agreement with this work. Therefore, an operating potential of 1 V was chosen in the next experiments in order to achieve the best compromise of signal-to-noise ratio (S/N) for all amino acids in this work.

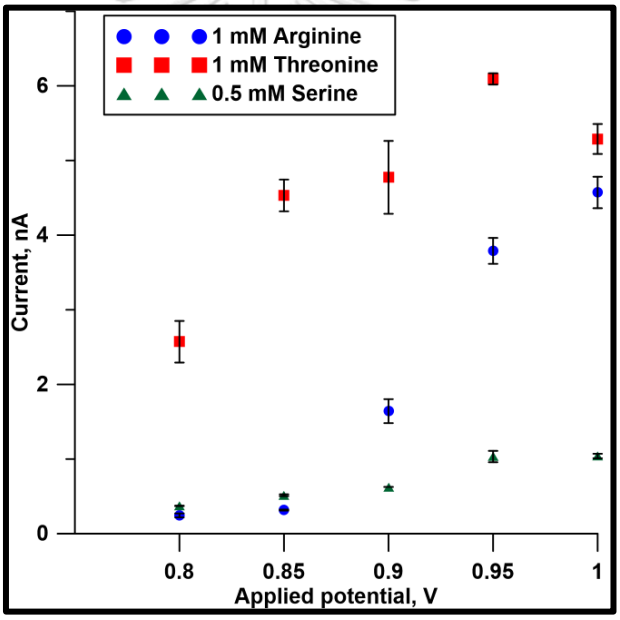

Figure 4.14 Current signal of arginine, threonine, and serine using Cu electrode at different applied potentials. Experimental conditions were; Column: PEEK (25 µm ID, 40 cm), flow rate: 0.28 µL/min, injection volume: 5 nL, WE: Cu (15 µm ID), applied potential: 0.8-1 V vs Ag/AgCl, carrier: 20 mM NaOH, and analyte: arginine (5 pmol), threonine (5 pmol), and serine (2.5 pmol).

4.2.4.2. Effect of hydroxide concentration

The interesting features of Cu or Cu modified electrode is the possibility of being an amperometric sensors for various electroactive molecules after chromatographic separation. It is notable that an oxidation of several electroactive organic compounds shows a good performance in alkaline solution. In the moderate alkaline condition, amine group of amino acids is

deprotonated and can be oxidized on the surface of the working electrode. Moreover, alkaline phase is required for the AEX chromatographic separation of weakly ionizable species such as amino acids. Thus, the hydroxide solution is suitable for a mobile phase at desired pH of chromatographic separation and a good conductivity for electrochemical detection of amino acids. To evaluate the optimal carrier electrolyte condition, the effects of various concentration of NaOH was investigated on the isocratic separation and detection of arginine, lysine, serine, isoleucine, and methionine. As can be seen in Figure 4.15 and Table 4.5, retention times of amino acids were slightly increased when increasing the concentration of NaOH. A similar behavior was observed on the metal-based electrodes separated by AEX column [153]. Hydroxide ions were important to the reaction on the surface of Cu as well. Considering the equation described previously (Equation (22)), increasing concentration of OH^- can increase the products on WE and improved the current signal of the amperometric sensor as in Figure 4.15. The optimal condition for electrochemical detection of amino acids according to the experiment was 20 mM NaOH. Then, this condition was used for the rest of the experiments.

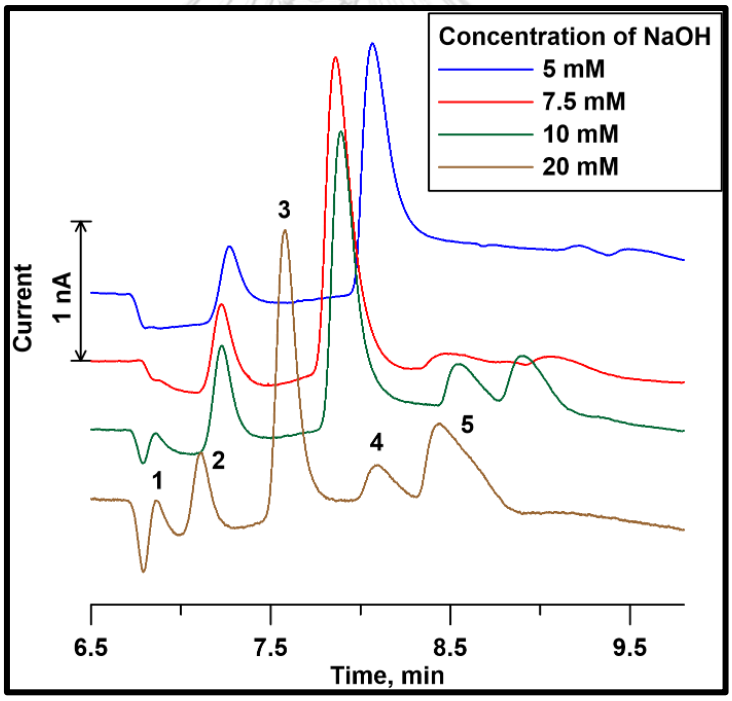

Figure 4.15 Comparison of retention time and current signal of different concentration of NaOH (mM): 5 (blue line), 7.5 (red line), 10 (green line), and 20 (brown line). Experimental conditions; Column: PA10-COP (19 µm ID, 95 cm), flow rate: 40 nL/min, injection volume: 2.5 nL, WE: Cu (50 µm ID), applied potential: 1 V, carrier: see results, and analyte (each amino acid 2.5 pmol): arginine (1), lysine (2), serine (3), isoleucine (4), and methionine (5).

Table 4.5 Influence of hydroxide concentration on the retention time (t_r) and capacity factor (k) of some amino acids separated by PA10-COP analytical column

Compound	5 mM		7.5 mM		10 mM		20 mM	
	t_r (min)	k	t_r (min)	k	t_r (min)	k	t_r (min)	k
Arginine	6.88	0.01	6.87	0.01	6.86	0.01	6.87	0.01
Lysine	7.26	0.07	7.21	0.06	7.22	0.06	7.10	0.04
Serine	8.06	0.19	7.85	0.15	7.90	0.16	7.57	0.11
Isoleucine	9.21	0.35	8.48	0.25	8.52	0.25	8.09	0.19
Methionine	9.50	0.40	9.07	0.33	8.86	0.30	8.44	0.24

In addition to the concentration of the hydroxide, the reaction was depended on a formation of Cu-amino acids complexes. Amino acids have different pI because the alkyl group is different. High pI derives from the amino acids with extra amine functional group such as arginine and lysine, while glutamate and aspartate with 2 carboxylic group have low pI. The pI affects the deprotonation of the amine group in the alkaline condition. The molecules of amino acids at amine functional group are difficult to deprotonate when increase alkalinity. Particularly, it occurs with amino acids with high pI which there is 2 amine group. Thus, the amine group that available for the complexation with Cu on the electrode depended on the pI of each amino acid. Therefore, the relationship between the optimal S/N of 22 amino acids and their isoelectric point (pI) was studied. The experiments were performed in 20 mM NaOH with 15 μm diameter Cu electrode. The concentration of each amino acid was different to provide a good S/N for data analysis. The results were shown in Figure 4.16, high pI amino acids required greater applied potential to produce a good S/N comparing with other amino acids with low and moderate pI. This effect was more obvious than the relationship between the optimal S/N and the stability constant (K) of the amino acids in different ligand configuration, shown in Figure 4.16B. Therefore, the alkalinity has a strong effect with the amperometric sensor in this work.

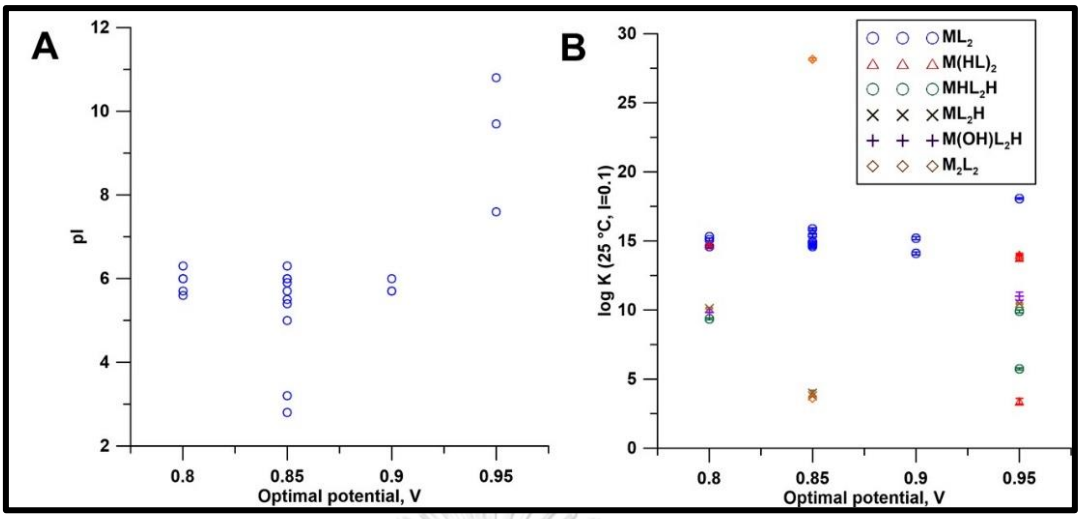

Figure 4.16 Relationship between the optimal potential (V) of several amino acids and pI (A), and stability constant (K) (B).

4.2.4.3. Liquid chromatographic measurements

A major disadvantage of Cu electrode for the amperometric detection of various amino acids is the reaction occurs approximately the same potential. This behavior hinders the advantage of the electrochemical detection feature which is the ability to separate the mixture of analytes at different potential. Therefore, the oxidation of each amino acid using constant applied potential is indistinguishable and chromatographic separation is required. The separation of amino acids using our PA10-COP AEX analytical column used 20 mM NaOH as carrier and Cu as WE for electrochemical detection. A typical chromatogram was finished within 18 minutes with a good S/N as shown in Figure 4.17A. Retention times (t_r) and capacity factor (k) of several amino acids separated and detected by amperometric sensor using Cu electrode were summarized in Table 4.6.

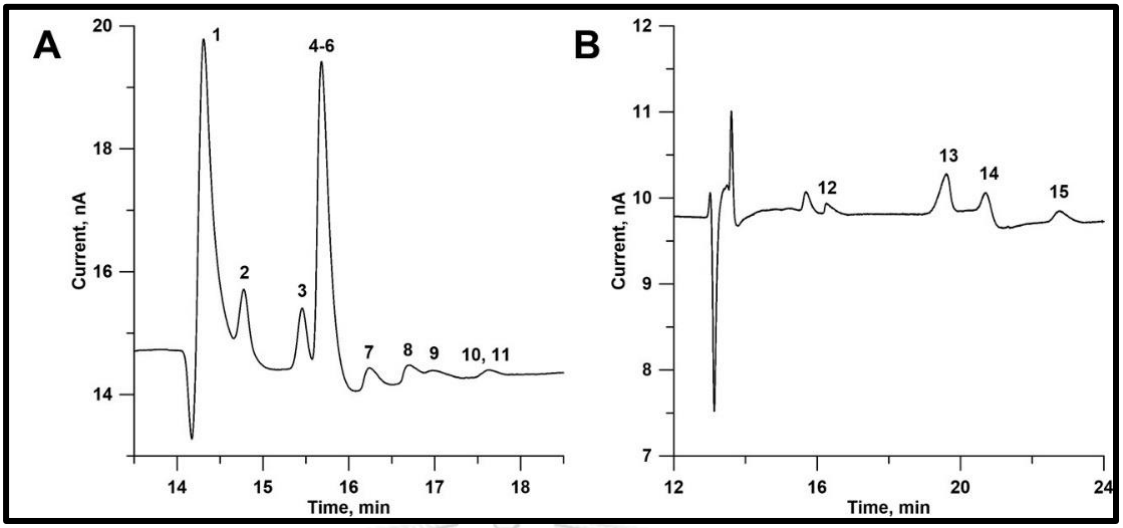

Figure 4.17 Isocratic chromatogram of a standard mixture of underivatized amino acids. Experimental conditions; Column: PA10-COP (19 µm ID, 159 cm for A) and 147 cm for B)), flow rate: 32 nL/min A), and 30 nL/min B), injection volume: 3 nL, WE: Cu (15 µm ID), applied potential: 1 V, carrier and analytes: see Table 2.

Table 4.6 Analysis of amino acids performed with PA10-COP analytical column

no	Compound	Concentration (pmol)	t_r (min)	k	eluent
1	Arginine	1.5	14.32	0.01	
2	Lysine	3	14.79	0.04	
3	Alanine	3	15.47	0.09	
4	Glycine	3			
5	Valine	1.5	15.68	0.11	20 mM NaOH
6	Serine	0.75			
7	Proline	3	16.25	0.15	
8	Isoleucine	3	16.71	0.18	
9	Leucine	3	17.05	0.20	

no	Compound	Concentration (pmol)	t_r (min)	k	eluent
10	Methionine	1.5			
			17.65	0.25	
11	Histidine	2.25			
12	Phenylalanine	3	16.24	0.24	
13	Glutamate	6	19.57	0.49	
					20 mM NaOH and 20 mM MSA
14	Aspartate	12	20.71	0.58	
15	Cystine	3	22.89	0.74	

Some amino acids such as histidine and glutamic acid have high affinity towards the stationary phase, therefore these molecules require stronger condition for the chromatographic separation. Such stronger eluents such as fluoride, bromide, nitrate, and methane sulfonate ($CH_3O_3S^-$) can interact strongly with the AEX sites of the stationary phase. Therefore, strongly-bonded amino acids are possible to elute from the analytical column. Several eluents were evaluated for the separation of histidine, phenylalanine, cystine, glutamate, and aspartate. It was found that the mixture of 20 mM NaOH and 20 mM $CH_3O_3S^-$ as an eluent can separated 5 target amino acids isocratically using our AEX chromatographic column within 23 minutes. The chromatographic peaks show a good resolution and analytical sensitivity as shown in Figure 4.17B. The analytical results were summarized in Table 4.6.

4.2.4.4. Analytical performance

For the study of linear range, the amperometric sensor was performed using serine and results are shown in Figure 4.18. The increase concentration of serine in the certain range responded linearly with the current signal with a correlative coefficient more than 0.99. Moreover, selected amino acids including serine, phenylalanine, and glutamate were used for the study of the detection limit in a simple FIA. The analytical COP column was substituted with PEEK capillary column (25 μm inner diameter with 5 nL injection volume) and used for the investigation. From the results, the detection limit of serine, phenylalanine, and glutamine were 20 fmol, 50 fmol, and 600 fmol , respectively. Thus, a very low level of amino acids can be detected with Cu by amperometric method. The performance of our developed sensor was improved from other works comprising of several inorganic analytes detection on metal-based electrode [142, 154] or biological analytes detection using enzymatic catalytic method. In

addition, our sensor was performed better than using photometric detector coupled with the pre- or post-column derivatization procedure [141, 155, 156]. The reproducibility of this amperometric sensor was calculated as the percent relative standard deviation from 1000 measurements was 5.94% demonstrating that our sensor had excellent performance.

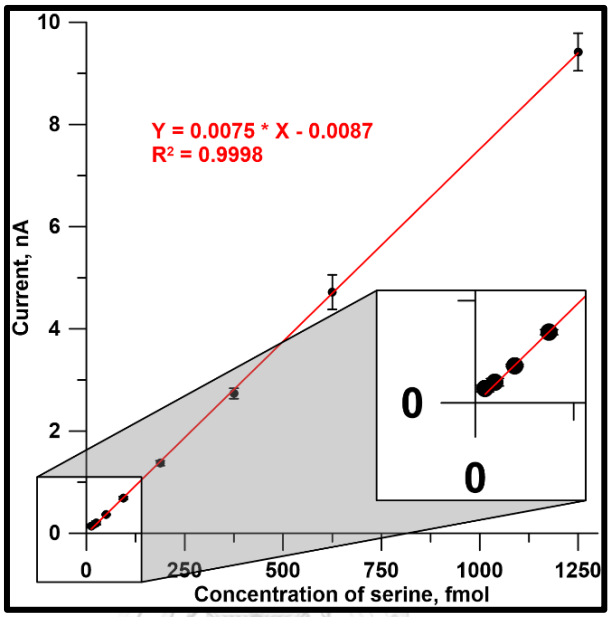

Figure 4.18 Linearity of response. Experimental conditions; Column: PA10-COP (28 µm ID, 150 cm), flow rate: 0.35 µL/min, injection volume: 2.5 nL, WE: Cu (50 µm ID), applied potential: 1 V, carrier: 20 mM NaOH, and analytes: serine 12.5-1250 fmol.

4.2.5. Conclusion

Amperometric sensors in alkaline solution after isocratic AEX chromatographic separation of several amino acids was developed. The AEX capillary column was prepared by sulfonation and coating with AEX latex PA10. Two electrode systems were used in this work; WE is Cu wire, and CE is made from stainless-steel tube. The reaction was described to be the complexation of Cu with amino acids. The concentration of NaOH and optimal potential was studied the separation and detection of amino acids. Under the best conditions, amino acids were eluted within 18-22 minutes with 20 mM NaOH. The high affinity amino acids were eluted with the mixture of 20 mM NaOH and 20 mM $CH_3O_3S^-$. The amperometric measurement was performed at 1 V with serine offering the highest current response. The detection limit was 20 fmol for serine, 50 fmol for phenylalanine, and 0.6 pmol for glutamate. Our amperometric sensor can successfully detect amino acids 1000 times with 5.94% RSD.

CHAPTER V

Conclusions and future perspective

5.1. Conclusions

Nanomaterials have interesting properties that benefits for sensing applications. Electrochemical and colorimetric methods incorporating nanoparticles/composites for environmental and biological compounds were discussed. This dissertation was categorized into PART I: lab-on-paper applications, and PART II: the development of chromatographic technique and its applications.

First, lab-on-paper applications was described. The label-free electrochemical assay for CRP was presented first. The analytical signal was derived from the resistance of the CRP/PMPC-SH complex on the surface of the electrode. PMPC-SH contains a specific functional group for capturing CRP selectively and thiol-group that interacts with AuNPs using S-Au bond. The electrode was assembled with PAD to store all chemicals for all-in-one device. The analytical assay was successfully used for evaluation the concentration of CRP from the serum samples. Finally, PAD with colorimetric assay was developed for sensing of Pi from soil samples. The detection mechanism relies on the aggregation/anti-aggregation capability of MS-AgNPls and the competitive complexation of MS-AgNPls and Pi for Eu^{3+}. The changing of purple color (aggregation) to red color (anti-aggregation) indicates the presence of Pi in the sample. A simple PAD for Pi detection was demonstrated for on-site analysis by different users. In conclusion, lab-on-paper coupled with electrochemical and colorimetric method establish portable and disposable devices for the analysis of an environmental compound and a biomarker.

Second, the chromatographic technique for separation and electrochemical detection of neonicotinoid insecticide was demonstrated. Bimetallic nanoparticles of CuNPs and AuNPs electrodeposited BDDE improve the detection through the catalytic property of AuNPs and affinity between copper and nitro-functional group of neonicotinoids. A new highly conductive materials was achieved. Individual peaks of each neonicotinoid were obtained after inject sample into u-HPLC system. The combination of the electrochemical analysis with u-HPLC are highly sensitive and rapid for insecticide identification and detection with an excellent reproducibility. Similarly, OTIC coupled amperometry was purposed for amino acids. OTIC employed AEX nanoparticles functionalized capillary column for separation of essential amino acids using ion-exchange principle. The electrochemical detection was performed by oxidation of copper electrode to Cu^{2+} and the formation between Cu and amine complex. Highly sensitive method

was achieved with detection limits in less than fmol. This part demonstrates successful applications for lab-on-column for the analysis of food and amino acids.

5.1. Future perspective

The significant methods including lab-on-column and lab-on-paper together with electrochemistry and colorimetry lead to novel chemical/biosensors. Nanoparticles were employed for their excellent optical and electronic features which significantly improve the performance of the analytical tools. The developed devices demonstrate that they are accessible and portable. However, majority of the procedures have been reported in publications rather than practical applications. After further validation for on-site analysis, nanoparticles-based sensors are interesting maneuver that will affect the analytical detection in the future.

REFERENCES

1. Murray, E., et al., *A colorimetric method for use within portable test kits for nitrate determination in various water matrices.* Analytical Methods, 2017. **9**(4): p. 680-687.
2. Wikipedia contributors, N., " Wikipedia, The Free Encyclopedia, https://en.wikipedia.org/w/index.php?title=Nanoparticle&oldid=689128532 (accessed November 9, 2015).
3. Tian, K., M. Prestgard, and A. Tiwari, *A review of recent advances in nonenzymatic glucose sensors.* Materials Science and Engineering: C, 2014. **41**: p. 100-118.
4. Christian, G.D., P.K. Dasgupta, and K.A. Schug, *Analytical Chemistry*. 2013: Wiley.
5. Huang, W., et al., *Functionalized Cycloolefin Polymer Capillaries for Open Tubular Ion Chromatography.* Analytical Chemistry, 2016. **88**(24): p. 12013-12020.
6. Pepys, M.B. and G.M. Hirschfield, *C-reactive protein: a critical update.* The Journal of Clinical Investigation, 2003. **111**(12): p. 1805-1812.
7. Steel, D.M. and A.S. Whitehead, *The major acute phase reactants: C-reactive protein, serum amyloid P component and serum amyloid A protein.* Immunology Today, 1994. **15**(2): p. 81-88.
8. Buckley, D.I., et al., *C-reactive protein as a risk factor for coronary heart disease: A systematic review and meta-analyses for the u.s. preventive services task force.* Annals of Internal Medicine, 2009. **151**(7): p. 483-495.
9. Pepys, M.B., et al., *Targeting C-reactive protein for the treatment of cardiovascular disease.* Nature, 2006. **440**: p. 1217.
10. Shrivastava, A.K., et al., *C-reactive protein, inflammation and coronary heart disease.* The Egyptian Heart Journal, 2015. **67**(2): p. 89-97.

11. Casas, J.P., et al., *C-reactive protein and coronary heart disease: a critical review.* Journal of Internal Medicine, 2008. **264**(4): p. 295-314.

12. Şişman, A.R., et al., *Comparison and evaluation of two C-reactive protein assays based on particle-enhanced immunoturbidimetry.* Journal of Clinical Laboratory Analysis, 2007. **21**(2): p. 71-76.

13. Chikkaveeraiah, B.V., et al., *Electrochemical Immunosensors for Detection of Cancer Protein Biomarkers.* ACS Nano, 2012. **6**(8): p. 6546-6561.

14. Albareda-Sirvent, M., A. Merkoçi, and S. Alegret, *Configurations used in the design of screen-printed enzymatic biosensors. A review.* Sensors and Actuators B: Chemical, 2000. **69**(1): p. 153-163.

15. Hernández-Santos, D., M.B. González-García, and A.C. García, *Metal-Nanoparticles Based Electroanalysis.* Electroanalysis, 2002. **14**(18): p. 1225-1235.

16. Agüí, L., et al., *Electrochemical determination of homocysteine at a gold nanoparticle-modified electrode.* Talanta, 2007. **74**(3): p. 412-420.

17. Rattanarat, P., et al., *A Microfluidic Paper-Based Analytical Device for Rapid Quantification of Particulate Chromium*. Vol. 800C. 2013. 50-55.

18. Rattanarat, P., et al., *Multilayer Paper-Based Device for Colorimetric and Electrochemical Quantification of Metals*. Vol. 86. 2014.

19. Panraksa, Y., et al., *Paper-based amperometric sensor for determination of acetylcholinesterase using screen-printed graphene electrode*. Vol. 178. 2017.

20. Ruecha, N., et al., *Novel paper-based cholesterol biosensor using graphene/polyvinylpyrrolidone/polyaniline nanocomposite*. Vol. 52C. 2013. 13-19.

21. Thompson, D., M.B. Pepys, and S.P. Wood, *The physiological structure of human C-reactive protein and its complex with phosphocholine.* Structure, 1999. **7**(2): p. 169-177.

22. Volanakis, J.E. and K.W.A. Wirtz, *Interaction of C-reactive protein with artificial*

phosphatidylcholine bilayers. Nature, 1979. **281**: p. 155.

23. Wu, J.-G., et al., *Critical Study of the Recognition between C-Reactive Protein and Surface-Immobilized Phosphorylcholine by Quartz Crystal Microbalance with Dissipation.* Langmuir, 2018. **34**(3): p. 943-951.

24. Goda, T., et al., *Biomimetic Interfaces Reveal Activation Dynamics of C-Reactive Protein in Local Microenvironments.* Advanced Healthcare Materials, 2014. **3**(11): p. 1733-1738.

25. Shimada, T., et al., *Biomolecular recognition on nanowire surfaces modified by the self-assembled monolayer.* Lab on a Chip, 2018. **18**(21): p. 3225-3229.

26. Goda, T., et al., *Poly(3,4-ethylenedioxythiophene) Bearing Phosphorylcholine Groups for Metal-Free, Antibody-Free, and Low-Impedance Biosensors Specific for C-Reactive Protein.* ACS Applied Materials & Interfaces, 2015. **7**(49): p. 27440-27448.

27. Kitayama, Y. and T. Takeuchi, *Localized Surface Plasmon Resonance Nanosensing of C-Reactive Protein with Poly(2-methacryloyloxyethyl phosphorylcholine)-Grafted Gold Nanoparticles Prepared by Surface-Initiated Atom Transfer Radical Polymerization.* Analytical Chemistry, 2014. **86**(11): p. 5587-5594.

28. Iwasaki, S., H. Kawasaki, and Y. Iwasaki, *Label-Free Specific Detection and Collection of C-Reactive Protein Using Zwitterionic Phosphorylcholine-Polymer-Protected Magnetic Nanoparticles.* Langmuir, 2019. **35**(5): p. 1749-1755.

29. Bhuchar, N., et al., *Detailed study of the reversible addition–fragmentation chain transfer polymerization and co-polymerization of 2-methacryloyloxyethyl phosphorylcholine.* Polymer Chemistry, 2011. **2**(3): p. 632-639.

30. Ma, Q., et al., *Fabrication of cell outer membrane mimetic polymer brush on polysulfone surface via RAFT technique.* Applied Surface Science, 2012. **258**(24): p. 9711-9717.

31. Jampasa, S., et al., *Electrochemically reduced graphene oxide-modified screen-*

printed carbon electrodes for a simple and highly sensitive electrochemical detection of synthetic colorants in beverages. Talanta, 2016. **160**: p. 113-124.

32. Katz, E. and I. Willner, *Probing Biomolecular Interactions at Conductive and Semiconductive Surfaces by Impedance Spectroscopy: Routes to Impedimetric Immunosensors, DNA-Sensors, and Enzyme Biosensors.* Electroanalysis, 2003. **15**(11): p. 913-947.

33. Bard, A.J., et al., *Electrochemical methods: fundamentals and applications*. Vol. 2. 1980: wiley New York.

34. Boonyasit, Y., O. Chailapakul, and W. Laiwattanapaisal, *A Folding Affinity Paper-Based Electrochemical Impedance Device for Cardiovascular Risk Assessment*. 2018.

35. Christopeit, T., T. Gossas, and U.H. Danielson, *Characterization of Ca2+ and phosphocholine interactions with C-reactive protein using a surface plasmon resonance biosensor.* Analytical Biochemistry, 2009. **391**(1): p. 39-44.

36. Kim, E., et al., *C-Reactive protein-directed immobilization of phosphocholine ligands on a solid surface.* Chemical Communications, 2011. **47**(43): p. 11900-11902.

37. Mi, L.Z., H.W. Wang, and S.F. Sui, *Interaction of rabbit C-reactive protein with phospholipid monolayers studied by microfluorescence film balance with an externally applied electric field.* Biophysical Journal, 1997. **73**(1): p. 446-451.

38. Suresh, M.V., S.K. Singh, and A. Agrawal, *Interaction of Calcium-bound C-reactive Protein with Fibronectin Is Controlled by pH: IN VIVO IMPLICATIONS.* The Journal of biological chemistry, 2004. **279**(50): p. 10.1074/jbc.M409054200.

39. Volanakis, J.E., *Human C-reactive protein: expression, structure, and function.* Molecular Immunology, 2001. **38**(2): p. 189-197.

40. Kong, B., Y. Kim, and I. Choi, *pH-Dependent Stability of Self-Assembled Monolayers on Gold.* Bulletin of the Korean Chemical Society, 2008. **29**(9): p. 1843-1846.

41. Hutt, D.A. and G.J. Leggett, *Functionalization of Hydroxyl and Carboxylic Acid Terminated Self-Assembled Monolayers.* Langmuir, 1997. **13**(10): p. 2740-2748.

42. Lin, C.-Y., et al., *Colorimetric Sensing of Silver(I) and Mercury(II) Ions Based on an Assembly of Tween 20-Stabilized Gold Nanoparticles.* Analytical Chemistry, 2010. **82**(16): p. 6830-6837.

43. Boonkaew, S., et al., *An origami paper-based electrochemical immunoassay for the C-reactive protein using a screen-printed carbon electrode modified with graphene and gold nanoparticles*. Vol. 186. 2019.

44. Jampasa, S., et al., *Electrochemical detection of c-reactive protein based on anthraquinone-labeled antibody using a screen-printed graphene electrode.* Talanta, 2018. **183**: p. 311-319.

45. Ishihara, K., et al., *Novel polymer biomaterials and interfaces inspired from cell membrane functions.* Biochimica et Biophysica Acta (BBA) - General Subjects, 2011. **1810**(3): p. 268-275.

46. Iwasaki, Y. and K. Ishihara, *Phosphorylcholine-containing polymers for biomedical applications.* Analytical and Bioanalytical Chemistry, 2005. **381**(3): p. 534-546.

47. Iwasaki, Y. and K. Ishihara, *Cell membrane-inspired phospholipid polymers for developing medical devices with excellent biointerfaces.* Science and technology of advanced materials, 2012. **13**(6): p. 064101.

48. AQUILINA, J.A. and C.V. ROBINSON, *Investigating interactions of the pentraxins serum amyloid P component and C-reactive protein by mass spectrometry.* Biochemical Journal, 2003. **375**(2): p. 323-328.

49. Emsley, J., et al., *Structure of pentameric human serum amyloid P component.* Nature, 1994. **367**: p. 338.

50. Heegaard, N.H.H., X. He, and L.G. Blomberg, *Binding of Ca2+, Mg2+, and heparin by human serum amyloid P component in affinity capillary electrophoresis.* ELECTROPHORESIS, 2006. **27**(13): p. 2609-2615.

51. Bannister, W.H., *The biological chemistry of the elements: The inorganic chemistry of life: By J J R Fraústo da Silva and R J P Williams. pp 561. Clarendon Press, Oxford. 1991. £60 ISBN 0-19-855598-9.* Biochemical Education, 1992. **20**(1): p. 62-63.

52. Musso, C.G., *Magnesium metabolism in health and disease.* International Urology and Nephrology, 2009. **41**(2): p. 357-362.

53. Ong, C.N., H.Y. Ong, and L.H. Chua, *Determination of copper and zinc in serum and whole blood by ion chromatography.* Analytical Biochemistry, 1988. **173**(1): p. 64-69.

54. Blizniukov, O.P., et al., *Effect of Calcium Ions on Hydrodynamic Properties of Pentameric and Decameric C-Reactive Protein in Solution.* Molecular Biology, 2003. **37**(6): p. 912-919.

55. Smith, D.R., et al., *Phosphorus losses from monitored fields with conservation practices in the Lake Erie Basin, USA.* AMBIO, 2015. **44**(2): p. 319-331.

56. Trichet, P., et al., *Fifty years of fertilization experiments on Pinus pinaster in Southwest France: The importance of phosphorus as a fertilizer.* Forest Science, 2009. **55**(5): p. 390-402.

57. Howarth Robert, W., et al., *Nitrogen fixation in freshwater, estuarine, and marine ecosystems. 1. Rates and importance1.* Limnology and Oceanography, 1988. **33**(4part2): p. 669-687.

58. Foyer, C. and C. Spencer, *The relationship between phosphate status and photosynthesis in leaves.* Planta, 1986. **167**(3): p. 369-375.

59. Fredeen, A.L., I.M. Rao, and N. Terry, *Influence of Phosphorus Nutrition on Growth and Carbon Partitioning in <em>Glycine max</em&gt.* Plant Physiology, 1989. **89**(1): p. 225.

60. Usuda, H. and K. Shimogawara, *Phosphate Deficiency in Maize. I. Leaf Phosphate Status, Growth, Photosynthesis and Carbon Partitioning.* Plant and Cell Physiology, 1991. **32**(4): p. 497-504.

61. Carpenter, S.R., *Phosphorus control is critical to mitigating eutrophication.* Proceedings of the National Academy of Sciences of the United States of America, 2008. **105**(32): p. 11039-11040.

62. Cheng, W.-L., et al., *Activated Nickel Platform for Electrochemical Sensing of Phosphate.* Analytical Chemistry, 2010. **82**(3): p. 1157-1161.

63. Cosnier, S., et al., *A Bienzyme Electrode (Alkaline Phosphatase-Polyphenol Oxidase) for the Amperometric Determination of Phosphate.* Analytical Chemistry, 1998. **70**(18): p. 3952-3956.

64. Li, C.M., et al., *Optical investigations on ATP-induced aggregation of positive-charged gold nanoparticles.* Talanta, 2010. **81**(4): p. 1339-1345.

65. Udnan, Y., et al., *Evaluation of on-line preconcentration and flow-injection amperometry for phosphate determination in fresh and marine waters.* Talanta, 2005. **66**(2): p. 461-466.

66. Martinez, A.W., et al., *Diagnostics for the Developing World: Microfluidic Paper-Based Analytical Devices.* Analytical Chemistry, 2010. **82**(1): p. 3-10.

67. Arduini, F., et al., *Electrochemical biosensors based on nanomodified screen-printed electrodes: Recent applications in clinical analysis.* TrAC Trends in Analytical Chemistry, 2016. **79**: p. 114-126.

68. Zhang, Q., T. Liu, and J. Qin, *A microfluidic-based device for study of transendothelial invasion of tumor aggregates in realtime.* Lab on a Chip, 2012. **12**(16): p. 2837-2842.

69. Chen, W., et al., *A Simple Paper-Based Colorimetric Device for Rapid Mercury(II) Assay.* Scientific Reports, 2016. **6**: p. 31948.

70. Wang, X., et al., *Paper-Based Sensor Chip for Heavy Metal Ion Detection by SWSV*. Vol. 9. 2018. 150.

71. Martinez, A.W., S.T. Phillips, and G.M. Whitesides, *Three-dimensional microfluidic devices fabricated in layered paper and tape.* Proceedings of the National

Academy of Sciences, 2008. **105**(50): p. 19606.

72. Maxwell, E.J., A.D. Mazzeo, and G.M. Whitesides, *Paper-based electroanalytical devices for accessible diagnostic testing.* MRS Bulletin, 2013. **38**(4): p. 309-314.

73. Hu, D., et al., *Highly selective fluorescent sensors for Hg2+ based on bovine serum albumin-capped gold nanoclusters.* Analyst, 2010. **135**(6): p. 1411-1416.

74. Ju, J. and W. Chen, *Synthesis of highly fluorescent nitrogen-doped graphene quantum dots for sensitive, label-free detection of Fe (III) in aqueous media.* Biosensors and Bioelectronics, 2014. **58**: p. 219-225.

75. Chi, T.T., et al., *Photothermal optical coherence tomography based on the localized surface plasmon resonance of Au nanoring.* Optics Express, 2014. **22**(10): p. 11754-11769.

76. Wang, S., et al., *Label-free colorimetric sensing of copper(ii) ions based on accelerating decomposition of H2O2 using gold nanorods as an indicator.* Analyst, 2013. **138**(7): p. 2080-2084.

77. Chen, Z., et al., *Application of triangular silver nanoplates for colorimetric detection of H2O2.* Sensors and Actuators B: Chemical, 2015. **220**: p. 314-317.

78. Kelly, K.L., et al., *The Optical Properties of Metal Nanoparticles: The Influence of Size, Shape, and Dielectric Environment.* The Journal of Physical Chemistry B, 2003. **107**(3): p. 668-677.

79. Lou, T., et al., *A simple and sensitive colorimetric method for detection of mercury ions based on anti-aggregation of gold nanoparticles.* Analytical Methods, 2012. **4**(2): p. 488-491.

80. Xu, H., et al., *Hg 2+-mediated aggregation of gold nanoparticles for colorimetric screening of biothiols.* Analyst, 2012. **137**(4): p. 924-931.

81. Na Rae, K., et al., *Surface modification of oleylamine-capped Ag–Cu nanoparticles to fabricate low-temperature-sinterable Ag–Cu nanoink.* Nanotechnology, 2016. **27**(34): p. 345706.

82. Gukowsky Joshua, C., et al., *Cysteamine-Modified Gold Nanoparticles as a Colorimetric Sensor for the Rapid Detection of Gentamicin.* Journal of Food Science, 2018. **83**(6): p. 1631-1638.

83. Jin, Y., et al., *Efficient bacterial capture with amino acid modified magnetic nanoparticles.* Water Research, 2014. **50**: p. 124-134.

84. Pope, S.J.A., et al., *Self-assembly of luminescent ternary complexes between seven-coordinate lanthanide(III) complexes and chromophore bearing carboxylates and phosphonates.* Dalton Transactions, 2006(23): p. 2907-2912.

85. Parnklang, T., et al., *H2O2-triggered shape transformation of silver nanospheres to nanoprisms with controllable longitudinal LSPR wavelengths*. Vol. 3. 2013.

86. Liu, S., et al., *Synthesis of monodisperse Au, Ag, and Au-Ag alloy nanoparticles with tunable size and surface plasmon resonance frequency.* Chemistry of Materials, 2011. **23**(18): p. 4098-4101.

87. Sarangi, S.N., A.M.P. Hussain, and S.N. Sahu, *Strong UV absorption and emission from L-cysteine capped monodispersed gold nanoparticles.* Applied Physics Letters, 2009. **95**(7): p. 073109.

88. Li, H., et al., *Highly sensitive and selective tryptophan colorimetric sensor based on 4,4-bipyridine-functionalized silver nanoparticles.* Sensors and Actuators, B: Chemical, 2010. **145**(1): p. 194-199.

89. Zhang, Q., et al., *A Systematic Study of the Synthesis of Silver Nanoplates: Is Citrate a "Magic" Reagent?* Journal of the American Chemical Society, 2011. **133**(46): p. 18931-18939.

90. Adhikari, B. and A. Banerjee, *Facile synthesis of water-soluble fluorescent silver nanoclusters and HgII sensing.* Chemistry of Materials, 2010. **22**(15): p. 4364-4371.

91. Le Guével, X., et al., *Highly fluorescent silver nanoclusters stabilized by glutathione: A promising fluorescent label for bioimaging.* Nano Research, 2012. **5**(6): p. 379-387.

92. Sudeep, P.K., S.T.S. Joseph, and K.G. Thomas, *Selective detection of cysteine and glutathione using gold nanorods.* Journal of the American Chemical Society, 2005. **127**(18): p. 6516-6517.

93. Gao, X., et al., *Colorimetric detection of iron ions (III) based on the highly sensitive plasmonic response of the N-acetyl-l-cysteine-stabilized silver nanoparticles.* Analytica Chimica Acta, 2015. **879**: p. 118-125.

94. Kim, T., et al., *Control of Gold Nanoparticle Aggregates by Manipulation of Interparticle Interaction.* Langmuir, 2005. **21**(21): p. 9524-9528.

95. Liu, W., et al., *A specific colorimetric probe for phosphate detection based on anti-aggregation of gold nanoparticles.* Sensors and Actuators B: Chemical, 2013. **176**: p. 927-931.

96. Debruyne, I., *Inorganic phosphate determination: Colorimetric assay based on the formation of a rhodamine B-phosphomolybdate complex.* Analytical Biochemistry, 1983. **130**(2): p. 454-460.

97. Han Min, S. and H. Kim Dong, *Naked-Eye Detection of Phosphate Ions in Water at Physiological pH: A Remarkably Selective and Easy-To-Assemble Colorimetric Phosphate-Sensing Probe.* Angewandte Chemie International Edition, 2002. **41**(20): p. 3809-3811.

98. Holman, W.I.M., *A new technique for the determination of phosphorus by the molybdenum blue method.* Biochemical Journal, 1943. **37**(2): p. 256-259.

99. Zhao, H.X., et al., *Highly selective detection of phosphate in very complicated matrixes with an off–on fluorescent probe of europium-adjusted carbon dots.* Chemical Communications, 2011. **47**(9): p. 2604-2606.

100. Jeschke, P. and R. Nauen, *Neonicotinoids—from zero to hero in insecticide chemistry.* Pest Management Science, 2008. **64**(11): p. 1084-1098.

101. Goulson, D., *REVIEW: An overview of the environmental risks posed by neonicotinoid insecticides.* Journal of Applied Ecology, 2013. **50**(4): p. 977-987.

102. Jeschke, P., et al., *Overview of the Status and Global Strategy for Neonicotinoids.* Journal of Agricultural and Food Chemistry, 2011. **59**(7): p. 2897-2908.

103. Godfray, H.C.J., et al., *A restatement of the natural science evidence base concerning neonicotinoid insecticides and insect pollinators.* Proceedings of the Royal Society B: Biological Sciences, 2014. **281**(1786): p. 20140558.

104. Authority, E.F.S. *EFSA identifies risks to bees from neonicotinoids*. 2013 [cited 2019; Available from: http://www.efsa.europa.eu/en/press/news/130116.htm?wtrl= 01.

105. *COMMISSION IMPLEMENTING REGULATION (EU) No 485/2013 of 24 May 2013 amending Implementing Regulation (EU) No 540/2011, as regards the conditions of approval of the active substances clothianidin, thiamethoxam and imidacloprid, and prohibiting the use and sale of seeds treated with plant protection products containing those active substances*. 2013.

106. *REGULATION (EC) No 396/2005 OF THE EUROPEAN PARLIAMENT AND OF THE COUNCIL of 23 February 2005 on maximum residue levels of pesticides in or on food and feed of plant and animal origin and amending Council Directive 91/414/EEC*. 2012.

107. Faundation, T.J.F.c.R. *The Japanese Positive List System for Agricultural Chemical Residues in Foods (Enforcement on May 29, 2006)*. 2006 [cited 2019; Available from: https://www.ffcr.or.jp/en/zanryu/the-japanese-positive/the-japanese-positive-list-system-for-agricultural-chemical-residues-in-foods-enforcement-on-may-29-.html.

108. Navalón, A., et al., *Determination of Imidacloprid in Vegetable Samples by Gas Chromatography–Mass Spectrometry.* Analyst, 1997. **122**(6): p. 579-581.

109. Botitsi, H., A. Economou, and D. Tsipi, *Development and validation of a multi-residue method for the determination of pesticides in processed fruits and vegetables using liquid chromatography–electrospray ionization tandem mass*

spectrometry. Analytical and Bioanalytical Chemistry, 2007. **389**(6): p. 1685-1695.

110. Sánchez-Hernández, L., et al., *Capillary electrophoresis–mass spectrometry as a new approach to analyze neonicotinoid insecticides.* Journal of Chromatography A, 2014. **1359**: p. 317-324.

111. Honeychurch, K.C. and J.P. Hart, *Screen-printed electrochemical sensors for monitoring metal pollutants.* TrAC Trends in Analytical Chemistry, 2003. **22**(7): p. 456-469.

112. Wang, J., *Electrochemical detection for microscale analytical systems: a review.* Talanta, 2002. **56**(2): p. 223-231.

113. Liu, S., et al., *Simultaneous Determination of Seven Neonicotinoid Pesticide Residues in Food by Ultraperformance Liquid Chromatography Tandem Mass Spectrometry.* Journal of Agricultural and Food Chemistry, 2010. **58**(6): p. 3271-3278.

114. Hupert, M., et al., *Conductive diamond thin-films in electrochemistry.* Diamond and Related Materials, 2003. **12**(10): p. 1940-1949.

115. Medeiros, R.A., et al., *Simultaneous voltammetric determination of synthetic colorants in food using a cathodically pretreated boron-doped diamond electrode.* Talanta, 2012. **97**: p. 291-297.

116. Salazar-Banda, G.R., et al., *On the changing electrochemical behaviour of boron-doped diamond surfaces with time after cathodic pre-treatments.* Electrochimica Acta, 2006. **51**(22): p. 4612-4619.

117. Ben Brahim, M., et al., *Electrochemical behavior and analytical detection of Imidacloprid insecticide on a BDD electrode using square-wave voltammetric method.* Chinese Chemical Letters, 2016. **27**(5): p. 666-672.

118. Lezi, N. and A. Economou, *Voltammetric Determination of Neonicotinoid Pesticides at Disposable Screen-Printed Sensors Featuring a Sputtered Bismuth Electrode.* Electroanalysis, 2015. **27**(10): p. 2313-2321.

119. Pungjunun, K., et al., *Anodic stripping voltammetric determination of total arsenic using a gold nanoparticle-modified boron-doped diamond electrode on a paper-based device.* Microchimica Acta, 2018. **185**(7): p. 324.

120. Nantaphol, S., et al., *Bimetallic Pt–Au nanocatalysts electrochemically deposited on boron-doped diamond electrodes for nonenzymatic glucose detection.* Biosensors and Bioelectronics, 2017. **98**: p. 76-82.

121. Yang, J., et al., *A highly sensitive non-enzymatic glucose sensor based on a simple two-step electrodeposition of cupric oxide (CuO) nanoparticles onto multi-walled carbon nanotube arrays.* Talanta, 2010. **82**(1): p. 25-33.

122. Hutton, L.A., et al., *Electrodeposition of Nickel Hydroxide Nanoparticles on Boron-Doped Diamond Electrodes for Oxidative Electrocatalysis.* The Journal of Physical Chemistry C, 2011. **115**(5): p. 1649-1658.

123. Mavrokefalos, C.K., et al., *Electrochemical aspects of Pt–Cu and Cu modified boron-doped diamond.* physica status solidi (a), 2015. **212**(11): p. 2559-2567.

124. Mavrokefalos, C.K., et al., *Electrochemically modified boron-doped diamond electrode with Pd and Pd-Sn nanoparticles for ethanol electrooxidation.* Electrochimica Acta, 2017. **243**: p. 310-319.

125. Navalón, A., et al., *Differential-pulse polarographic determination of the insecticide imidacloprid in commercial formulations.* Microchimica Acta, 1999. **130**(4): p. 261-265.

126. Guiberteau, A., et al., *Study and determination of the pesticide Imidacloprid by square wave adsorptive stripping voltammetry.* Talanta, 2001. **53**(5): p. 943-949.

127. Smarzewska, S., S. Skrzypek, and W. Ciesielski, *Voltammetric Determination of Proguanil in Malarone and Spiked Urine with a Renewable Silver Amalgam Film Electrode.* Electroanalysis, 2012. **24**(10): p. 1966-1972.

128. Guzsvany, V.J., et al., *Voltammetric determination of imidacloprid and thiamethoxam.* JOURNAL-SERBIAN CHEMICAL SOCIETY, 2005. **70**(5): p. 735.

129. Guzsvány, V., et al., *Rapid Differential Pulse Polarographic Determination of Thiamethoxam in Commercial Formulations and some Real Samples.* Microchimica Acta, 2006. **154**(3): p. 321-328.

130. Bandžuchová, L., et al., *Voltammetric method for sensitive determination of herbicide picloram in environmental and biological samples using boron-doped diamond film electrode.* Electrochimica Acta, 2013. **111**: p. 242-249.

131. Guzsvány, V., et al., *Bismuth modified carbon-based electrodes for the determination of selected neonicotinoid insecticides.* Molecules, 2011. **16**(6): p. 4451-4466.

132. Papp, Z.J., et al., *Voltammetric determination of the neonicotinoid insecticide thiamethoxam using a tricresyl phosphate-based carbon paste electrode.* J. Serb. Chem. Soc, 2010. **75**: p. 681-687.

133. Urbanová, V., et al., *A facile graphene oxide based sensor for electrochemical detection of neonicotinoids.* Biosensors and Bioelectronics, 2017. **89**: p. 532-537.

134. Zhou, Y., Z. Yang, and M. Xu, *Colorimetric detection of lysine using gold nanoparticles aggregation.* Analytical Methods, 2012. **4**(9): p. 2711-2714.

135. Duan, L., et al., *Highly selective fluorescent chemosensor with red shift for cysteine in buffer solution and its bioimage: symmetrical naphthalimide aldehyde.* Tetrahedron Letters, 2008. **49**(47): p. 6624-6627.

136. Friedman, M. and C.W. Sigel, *A Kinetic Study of the Ninhydrin Reaction*.* Biochemistry, 1966. **5**(2): p. 478-485.

137. Zheng, G., et al., *A novel method for detecting amino acids derivatized with phenyl isothiocyanate by high-performance liquid chromatography–electrospray ionization mass spectrometry.* International Journal of Mass Spectrometry, 2015. **392**: p. 1-6.

138. Dorresteijn, R.C., et al., *Determination of amino acids using o-phthalaldehyde-2-mercaptoethanol derivatization effect of reaction conditions.* Journal of Chromatography A, 1996. **724**(1): p. 159-167.

139. Heems, D., et al., *Fully automated precolumn derivatization, on-line dialysis and high-performance liquid chromatographic analysis of amino acids in food, beverages and feedstuff.* Journal of Chromatography A, 1998. **798**(1): p. 9-17.

140. Krause, I., et al., *Simultaneous determination of amino acids and biogenic amines by reversed-phase high-performance liquid chromatography of the dabsyl derivatives.* Journal of Chromatography A, 1995. **715**(1): p. 67-79.

141. Schuster, R., *Determination of amino acids in biological, pharmaceutical, plant and food samples by automated precolumn derivatization and high-performance liquid chromatography.* Journal of Chromatography B: Biomedical Sciences and Applications, 1988. **431**: p. 271-284.

142. Clarke, A.P., et al., *An Integrated Amperometry Waveform for the Direct, Sensitive Detection of Amino Acids and Amino Sugars Following Anion-Exchange Chromatography.* Analytical Chemistry, 1999. **71**(14): p. 2774-2781.

143. Welch, L.E., et al., *Comparison of pulsed coulometric detection and potential-sweep-pulsed coulometric detection for underivatized amino acids in liquid chromatography.* Analytical Chemistry, 1989. **61**(6): p. 555-559.

144. Kok, W.T., U.A.T. Brinkman, and R.W. Frei, *Amperometric detection of amino acids in high-performance liquid chromatography with a copper electrode.* Journal of Chromatography A, 1983. **256**: p. 17-26.

145. Kafil, J.B. and C.O. Huber, *A nickel oxide amperometric detector in the chromatographic separation of amino acids.* Analytica Chimica Acta, 1985. **175**: p. 275-280.

146. Ye, J. and R.P. Baldwin, *Determination of Amino Acids and Peptides by Capillary Electrophoresis and Electrochemical Detection at a Copper Electrode.* Analytical Chemistry, 1994. **66**(17): p. 2669-2674.

147. Dryden, M.D.M. and A.R. Wheeler, *DStat: A Versatile, Open-Source Potentiostat for Electroanalysis and Integration.* PLOS ONE, 2015. **10**(10): p. e0140349.

148. Casella, I.G. and M. Gatta, *Anodic electrodeposition of copper oxide/hydroxide*

films by alkaline solutions containing cuprous cyanide ions. Journal of Electroanalytical Chemistry, 2000. **494**(1): p. 12-20.

149. Casella, I.G., M. Gatta, and E. Desimoni, *Determination of histamine by high-pH anion-exchange chromatography with electrochemical detection.* Food Chemistry, 2001. **73**(3): p. 367-372.

150. Prabhu, S.V. and R.P. Baldwin, *Constant potential amperometric detection of carbohydrates at a copper-based chemically modified electrode.* Analytical Chemistry, 1989. **61**(8): p. 852-856.

151. Luo, P., F. Zhang, and R.P. Baldwin, *Constant-potential amperometric detection of underivatized amino acids and peptides at a copper electrode.* Analytical Chemistry, 1991. **63**(17): p. 1702-1707.

152. Nguyen, H.D., et al., *Amperometric detection of carbohydrates based on the glassy carbon electrode modified with gold nano-flake layer.* Analytical Chemistry Research, 2015. **5**: p. 14-20.

153. Casella, I.G., M. Gatta, and T.R.I. Cataldi, *Amperometric determination of underivatized amino acids at a nickel-modified gold electrode by anion-exchange chromatography.* Journal of Chromatography A, 2000. **878**(1): p. 57-67.

154. Zhou, J. and M. Lunte Susan, *Direct determination of amino acids by capillary electrophoresis/electrochemistry using a copper microelectrode and zwitterionic buffers.* ELECTROPHORESIS, 2005. **16**(1): p. 498-503.

155. Björklund, J., et al., *Automated amino acid determination by high-performance liquid chromatography with 2-(9-anthryl)ethyl chloroformate as precolumn reagent.* Journal of Chromatography A, 1998. **798**(1): p. 1-8.

156. Carducci, C., et al., *Automated method for the measurement of amino acids in urine by high-performance liquid chromatography.* Journal of Chromatography A, 1996. **729**(1): p. 173-180.

VITA

NAME	Chanika Pinyorospathum
DATE OF BIRTH	19 October 1990
PLACE OF BIRTH	Phitsanulok
INSTITUTIONS ATTENDED	1998-2008 Sarasas Witaed Suksa School 2009-2012 King Mongkut's University of Technology Thonburi
HOME ADDRESS	1957 Chumchon Phanit Alley, Talat, Phra Pradaeng District, Samut Prakan 10130
PUBLICATION	Yakoh, A., et al., Biomedical probes based on inorganic nanoparticles for electrochemical and optical spectroscopy applications. Sensors (Switzerland), 2015. 15(9): p. 21427-21477. Pinyorospathum, C., et al., Colorimetric sensor for determination of phosphate ions using anti-aggregation of 2-mercaptoethanesulfonate-modified silver nanoplates and europium ions. Sensors and Actuators, B: Chemical, 2019: p. 226-232.